The Dissertation Committee for Ki Youl Yoon
Certifies that this is the approved version of the following dissertation:

The Design and Control of Stability and Magnetic Properties of Imaging Nanoparticles

Committee:

Keith P. Johnston, Supervisor

Steven L. Bryant

Thomas E. Milner

Chun Huh

Rodney S. Ruoff

Paulo J. Ferreira

The Design and Control of Stability and Magnetic Properties of Imaging Nanoparticles

by

Ki Youl Yoon, B.S.; M.S.

Dissertation

Presented to the Faculty of the Graduate School of

The University of Texas at Austin

in Partial Fulfillment

of the Requirements

for the Degree of

Doctor of Philosophy

The University of Texas at Austin

December 2012

Acknowledgements

I would like to thank my supervisor Dr. Johnston for their support, patience and encouragement in my Ph.D. degree. I am grateful for the amazing research opportunities he has given me. Also, this dissertation would not be possible but for the scientific contributions from many other collaborators. First, I also would like to extend my appreciation to my other committee members: Dr. Huh, Dr. Bryant, Dr. Milner, Dr. Ruoff, and Dr. Ferreira, for their support and useful suggestion and comments in the dissertation and the final defense.

I would also like to express my gratitude to my former advisor, Dr. Taeghwan Hyeon, whose passion and education philosophy certainly provided me to establish my stance as a researcher.

I also share my thanks to all of my collaborators over several years: Beth M. Neilson and Dr. Bielawski for various types of synthesizing polymer. Dr. SeungYup Ryoo for PS-OCT experiments. Dr. Haiyang Yu for core-flood experiments with nanoparticle dispersion. Dr. Mohammad Mehrmohammadi for pMMUS experiments with iron oxide nanoclusters.

I thank my fellow graduate students as well as former students and post-doc in Johnston group: Dr. Csaba Kotsmar, Dr. Hitesh Bagaria, Dr. Daniel Slanac, Dr. Leo Ma, Zheng Xue, Avinash Murthy, Ameya Borwankar, Bobby Stover, Aileen Dinin, Josh Laber, Yunshen Chen, William Hardin, Andrew Worthen, Amro Elhag.

I would also like to express my friends outside of the lab who made my graduate school experience memorable. I thank Dr. Seihyun Choi, Dr. Tae Hyun Yoo, Dr. Seok Koo Kim, Dr. Sung kuk Kim, Dr. Jae Young Lee, Dr. Hyungchul Ham, Dr. Sangtaek Jung, Dr. Young Nam Kim, Dr. Young Jae Yoo, Dr. Byoung Joon Ko, Dr. Sangheon Lee, Taihyun Kang, Joon Hee Cho, Dr. Bonil Koo, Dr. Kyunghaeng Lee, Yongjin Lee, Eunsu Paek, Jong Suk Kim, Summi Lee, Dr. Cheulhee Jung, Dr. Kyungeun Kwon, Hee Jeung Oh, Minjung Kim, Jiwon Lee, and Jungup Park for their friendship and encouragement during my graduate studies.

I would like to thank all of the undergraduate students who helped me gain a deeper understanding of science through their scientific curiosity and contributions: Jae Ho Lee, Wonjae Lee, Grace Ji Hyun Kim, Wonjin Yun.

Also, this research is supported by the Advanced Energy Consortium (BP America Inc., Baker Hughes Inc., Conoco-Phillips, Halliburton Energy Services Inc., Marathon Oil Corp., Occidental Oil and Gas, Petrobras, Schlumberger, Shell, and Total).

Lastly, I would like to thank all of my family for all the love and support during my graduate school life. I wish thank my parents, elder brother, elder sister, brother-in-law, sister-in-law, three nephews have believed in and support me. Their faith and support have been a solid foundation enabling me to achieve all of my accomplishments. I give them both my deepest thanks and love.

The Design and Control of Stability and Magnetic Properties of Imaging Nanoparticles

Publication No._____

Ki Youl Yoon, Ph.D.

The University of Texas at Austin, 2012

Supervisors: Keith P. Johnston

There is significant interest in applying nanoparticle (NP) science to subsurface reservoirs to facilitate oil and gas recovery, image subsurface reservoirs, aid sequestration of CO_2 and benefit environmental remediation. Imaging nanoparticles have been designed with long-term dispersion stability in brine and minimal retention in reservoir rock and with preferential adsorption at oil-water interfaces. Polymer-stabilized nanoparticles provide sufficient electrostatic repulsion for high colloidal stability, as characterized by the zeta potential. The small size of the clusters, superparamagnetic properties, and high salt tolerance are highly beneficial in various applications including magnetomotive and electromagnetic imaging and mapping of petroleum reservoirs.

Superparamagnetic nanoclusters may be used in imaging in biomedicine and in mapping of petroleum reservoirs, by generating either ultrasonic or acoustic signals with oscillating magnetic motion. For a given magnetization per weight of iron oxide, nanoclusters with sub ~100 nm diameters experience a much larger magnetic force than

that of the primary sub- 10 nm primary particles. Aqueous dispersions of 0.1-0.2 wt% superparamagnetic iron oxide nanoclusters were stabilized with citric acid, poly(acrylic acid) (PAA), or poly(styrene sulfonate-*alt*-maleic acid) (PSS-*alt*-MA) on the particle surface, with a high loading of ~90% iron oxide. For nanoclusters with only 12% (w/w) PSS-*alt*-MA electrosteric stabilization was sufficient even in 8 wt% NaCl. Both PAA and PSS-*alt*-MA were used to stabilize nanoclusters with controlled size during synthesis in aqueous media. To obtain a permanent coating on the surface of clusters cross-linking of the polymer for different cross-linking densities was applied. In this general and highly flexible approach, iron oxide nanoparticles may be formed with an adsorbed polymer stabilizer, which is then permanently bound to the surface via cross-linking.

To investigate interfacial activity of nanoparticles, oil-in-water emulsions were stabilized with iron oxide nanoclusters or graphene oxide platelets. In each case, the stabilization was achieved by designing the hydrophilic/hydrophobic nature of surface coating. For oil/water emulsions, the droplet size was as low as ~1 micron diameter, and strongly shear-thinning rheology was observed. A series of sub-100 nm superparamagnetic iron oxide nanoparticles with amphiphilic poly(acrylic acid-*b*-butylacrylate), (PAA-*b*-PBA) copolymer shells was synthesized to investigate the effect of the polymer structure on the interfacial tension for nanoparticles adsorbed at the dodecane-water interface. Large reductions in interfacial tension of up to 27.6 mN/m were obtained for a 0.27 wt% nanoparticle concentration indicating significant nanoparticle adsorption and interaction with the oil and water molecules at the interface. The adsorption energy of the polymer-coated nanoparticles at the dodecane/water interface was determined from the interfacial tension and nanoparticle radius, and analyzed in terms of the structure of the polymer stabilizer. Furthermore, oil-in-water emulsions stabilized with graphene oxide nanoplatelets were found to remain stable for

several months even at high salinity (up to 5 wt% NaCl, for pH = 2 to 10). The droplet sizes were as small as ~1 μm with a low nanoplatelet concentration of 0.2 wt%.

Table of Contents

List of Tables

List of Figures

Chapter 1: Introduction

1.1 MOTIVATION

Magnetic nanoparticles (MNP) in aqueous media are widely used in biomedical applications including drug delivery systems, affinity purification, *in vitro* cell separation, and biomedical imaging.[1] For both biological and oil recovery applications, the long-term stability of nanoparticle dispersions is a key requirement to carry out their desired functions. This is because, due to the van der Waals attraction between particles, they tend to aggregate and become unstable. To counteract the van der Waals attraction, a variety of surface coatings are applied to the particles to provide electrostatic repulsion and entropic repulsion, thereby stabilizing the nanoparticle dispersions. The attractive magnetic interactions between ferromagnetic nanoparticles are a major challenge for colloidal stabilization. These interactions may be avoided with superparamagnetic nanoparticles, which do not have a magnetic moment in the absence of an applied magnetic field. Iron oxide (IO) nanocrystals smaller than ~15 nm in diameter are often superparamagnetic. [1d, 2]

Recently, we proposed that aqueous magnetic nanoparticle dispersions may be utilized as imaging agents for detection and visualization of oil/water interfaces in oil reservoirs.[3] The motion of MNPs in a magnetic field generates acoustic waves from which the oil saturation of the reservoir can be estimated.[4] In this application, the particles may be designed to be superparamagnetic to enhance colloidal stability, resistant to aggregation at high salinities (salt tolerant), and on the order of 100 nm to be small

enough for transport through porous rock. The activity of nanoparticles at the oil-water interface is a function of the interfacial properties of the stabilizers on the particle surface.[5] Since PAA is highly hydrophilic, it is only weakly active at an oil-water interface [6] and thus provides only modest interfacial activity when coated on a NP surface. For subsurface applications, the stabilizer must also be designed to provide high colloidal stability of the NPs in aqueous media with high salt content. The stabilizer must also be designed for weak adsorption of the NPs on the rock surfaces such that the nanoparticles may be transported through the porous formation.

A major objective of this thesis research is to develop an optimum strategy to synthesize iron oxide nanoparticles and apply surface coatings, to maintain long-term dispersion stability; provide the capability for transport a long distance through the oil reservoir; and with superparamagnetism. The magnetic force on a particle is proportional to the magnetization and the particle volume. Whereas the large volume of a 100 nm particle is accordingly desirable, iron oxide particles of this size are typically ferromagnetic, and thus require large amounts of higher molecular weight stabilizer to overcome the magnetic attraction. However, an excess of stabilizer lowers the magnetic fraction of the particles and thus the magnetic force. A novel strategy to overcome this limitation is to form 100 nm superparamagentic clusters of adjacent sub-15 nm primary particles.[1e, 3c, 7] Even with very small spacings between these primary particles, the spins on neighboring particles are usually not close enough to influence the magnetization per mass of iron.[8] In essence, the magnetization/mass remains relatively constant relative to individual primary particles, whereas the large volume leads to a strong magnetic force.

The cluster size, however, cannot be too large, as it will then no longer permeate through the porous reservoir rock.

Various strategies have been utilized to tailor permanent coatings for iron oxide NPs including covalent linkages, as well as adsorption followed by cross linking. Arkles et al. [9] used silylating agents such as 3-aminopropyltrimethoxysilane or *p*-aminophenyl trimethoxysilane to covalently bind molecules with the desired functionalities to metal oxide surfaces. De Palma et al. [10] used triethoxysilanes to covalently attach a variety of functional groups to iron oxide, where the weight fraction of coating in case of water dispersible particles amounts to above 40 %. Gamma-ray induced polymerization of a surfactant bilayer on IO NP surface was carried out by Shen et al. [11] to prevent desorption of the secondary surfactant layer upon dilution with water. The stability of a dextran coating on NP surfaces *in vivo* has been demonstrated with crosslinked iron oxide nanoparticles (CLIO).[12] Dresco et al.[13] reported an inverse microemulsion method to synthesize cross-linked polymer-coated iron oxide nanoparticles. Lee et al. [14] used a polyethylene glycol (PEG)-silane co-polymer to covalently bind the PEG on IO NP surfaces. Kawano et al. [15] used precipitation polymerization to synthesize silica-coated nanorods core and cross-linked poly(*N*-isopropylacrylamide) (PNIPAM) shells on the surface of Au nanocrystals. Polymer nanospheres with cross-linked shells were synthesized following self-assembly of amphiphilic poly(acrylic acid)- poly (methyl acrylate) (PAA-*b*-PMA)[16] and polystyrene-*b*-poly(acrylic acid) (PS-*b*-PAA) copolymers.[17] The carboxylic groups in the PAA segments, comprising the shells of micelles, were cross-linked by amidation using several di- and multiamino linkers. In this

study we used a similar procedure, in which PAA molecules were cross-linked on the surface of IO NPs using the diamino linker hexanediamine.

PAA, a slightly surface active biocompatible polymer[6] has been used to coat MNPs and to aid bioadhesion.[18] PAA has also been used to modify the surface properties in order to transfer oleic acid-coated IO particles from toluene to water.[19] The carboxylate functionalities on PAA form relatively strong complexes with the Fe atoms of the particle surface through bidentate bonding.[18b] Recently Janus magnetic core NPs have been synthesized which are coated on one side with PAA and on the other side by polystyrene sodium sulfonate (PSSNa) or poly(*N*-isopropyl acrylamide).[20] The magnetic cores were synthesized in organic solvent and the PAA coating was polymerized onto the surface of the particles by atom-transfer radical polymerization. Graft polymerization has also been applied to coat IO NPs with PAA.[18f] To achieve stronger binding of the PAA-coating on MNPs, the polymer was covalently attached directly to the IO surface via carbodiimide activation of the carboxylic functionality on PAA.[21] Formation of NP clusters by using PAA [18b, 22] and PAA-based co-polymers [23] as stabilizer have been reported elsewhere, but these studies did not use crosslinking. Iron oxide nanoparticles dispersions in 5 M NaCl have been stabilized with adsorbed random copolymers of acrylic acid, styrenesulfonic acid, and vinylsulfonic acid.[23a] However, adsorbed polymers may be susceptible to desorption at dilute conditions, as a function of the binding strength.

Electrostatic interactions between surface modified nanoparticles in solution influence the behavior of many dynamic phenomena including aggregation, coagulation, coalescence, and flocculation. Interactions between nanoparticles and rock surfaces can

lead to adsorption, adhesion and deposition. An increase in the surface charge of nanoparticles with charged polymers[5c,24] provides electrosteric repulsions between nanoparticles to inhibit aggregation, and between nanoparticles and rock surfaces to inhibit attachment. The interactions between particles are described by the Derjaguin [25] and Verwey and Overbeek[26] known as the DLVO theory. The force and energy of interactions between plates and spherical particles may be determined in the DLVO theory with modification by the simple Gouy,[27] Chapman,[28] and Stern[29] double-layer model based on the continuous Poisson- Boltzmann equation.

1.2 OBJECTIVES

The main objective of this research is to design magnetic nanoparticles that can be effectively employed for imaging of subsurface oil reservoirs, which generally present harsh conditions, such as high salinity and high temperature. To meet the objective, we investigated ways to coat the nanoparticles with commercially available or synthesized polymers to have high colloidal stability and low adsorption on reservoir rock surfaces. We have developed polymer-stabilized nanoparticles to maximize flexibility for technical success of particles that can be economic for practical application. The nanoparticles need to be low cost for large-volume production based on laboratory scale concepts developed in this thesis. To explore the design and properties of polymer-stabilized nanoparticles, we adsorb different types of polymers on iron oxide magnetic nanoparticles which have optimal size and magnetic properties, and then characterize the nanoparticle colloidal properties. This approach increases throughput in

nanoparticle/coating design by over an order of magnitude relative to synthesis of nanoparticles in the presence of polymer, to meet the multiple goals needed for imaging and transport. Furthermore, the polymers may be adsorbed on any type of nanoparticle core in addition to iron oxide magnetic particles. Our novel, permanent coating strategy is achieved by the formation of a loosely crosslinked polymer network that wraps around the nanoparticles.

Our objective is to design, synthesize, and characterize the polymer-coated magnetic nanoparticles with strong magnetic properties in order to: (i) maximize dispersion stability at high salt content and high temperature, and (ii) minimize particle adsorption to the rock surfaces. Our results with a commercial sulfonated polymer coating, poly(styrenesulfonate-alt-maleic acid), indicate that the addition of sulfonated component promotes dispersion stability at high NaCl concentration and high divalent-ion content. The carboxylate-containing components [acrylic acid (AA) and maleic acid (MA)] allow for adsorption of the polymer to the iron oxide surface, while the sulfonated components [vinylsulfonate(VS), styrenesulfonate (SS), and 2-acrylamido-2-methylpropanesulfonate (AMPS)) promote salt stability via electrosteric stabilization.

In the case of only electrostatically stabilized nanoparticles, changes in ionic strength and ionic composition can change the screening distance for the double layer, which modifies the electrostatic and electosteric interactions between particles or between particles and rock surfaces. Thus, high salinities have a significant effect on the nanoparticle stability (resistance to aggregation) and mobility in the subsurface reservoir30. In the case of polymer coated nanoparticles, the electrosteric repulsion

rendered by the polymer chains greatly enhances the stability between nanoparticles and between nanoparticles and rock surfaces. Electrosteric repulsions tend to be quite strong and long-ranged even at high ionic strengths as the steric forces and large number of charged groups on the polymers oppose the van der Waals attraction between the particles[31]. Both electrostatic and electrosteric repulsions can help to prevent nanoparticle aggregation and their attachment on solid surfaces as well.[32]

Overall, the combined use of commercial copolymers in conjunction with newly synthesized polymers will enable tuning of nanoparticle properties through efficient design and synthesis of coatings. We found that a limited class of polymers will tolerate high salinity, and a select few of them further tolerate both high salinity and high temperature conditions. Our approach allows rapid screening of various types of polymer coatings that stabilize nanoparticles in dispersions and minimize interactions with rock surfaces. For development of various novel upstream applications of nanoparticles, therefore, we offer the ability to efficiently synthesize and supply the nanoparticles that meet the specific oil reservoir conditions.

1.3 DISSERTATION OUTLINE

Chapter 2 of the dissertation reported iron oxide nanoparticles, in the form of sub-100 nm clusters, which were synthesized in the presence of poly(acrylic acid) (PAA) or poly(styrene sulfonate-*alt*-maleic acid) (PSS-*alt*-MA) to provide electrosteric stabilization. To stabilize the polymer on the magnetic nanoparticle surface, the polymer was cross-linked for a range of cross-link densities. Without the cross-linking reaction,

over half of the polymer desorbed from the particle surfaces upon dilution of the nanoparticles, for iron oxide concentrations down to 0.014 wt%. With cross-linking, the desorption was reduced markedly. In the case of nanoclusters with only 12% (w/w) PSS-alt-MA electrosteric stabilization was sufficient even in 8 wt% NaCl. Chapter 2 was a collaboration with significant contributions from a post-doctoral student Csaba Kotsmar and myself. I contributed to all aspects of this study including writing of the manuscript.

Chapter 3 presented superparamagnetic nanoclusters for imaging in biomedicine and for mapping of subsurface reservoirs, by either ultrasonic or acoustic signals with oscillating magnetic motion. For a given magnetization per weight of iron oxide, nanoclusters with diameters from 20 to 100 nm experience a much larger magnetic force than that of the primary sub- 10 nm primary particles. Aqueous dispersions of 0.1 wt% superparamagnetic iron oxide nanoclusters were stable for months even with high salt concentrations up to 4 wt% at pH 6 and pH 8. Chapter 3 was mainly a collaboration with Dr. Csaba Kotsmar, and myself. Dr. Haiyang Yu did the work with the sandstone core-flood experiments. Dr. Seung Yup Ryoo did phase-sensitive optical coherence tomography (PS-OCT) experiments with iron oxide nanoparticle dispersions. Dr. Csaba Kotsmar took the primary role in writing the manuscript. My contributions were for the design of the magnetic nanoparticles and the non-acoustic characterization procedures.

Chapter 4 introduced A series of sub-100 nm superparamagnetic iron oxide nanoparticles with amphiphilic poly(acrylic acid-*b*-butylacrylate; PAA-*b*-PBA) copolymer shells adsorbed on their surfaces. Large reductions in interfacial tension were measured between the oil and water molecules at the interface with nanoparticle

concentrations of 0.27 wt%. Furthermore, the formation and stabilization of oil droplets on the order of 10 μm in water with low nanoparticle concentrations was explained in terms of the high interfacial activity of the particles. Chapter 4 was a collaboration with Dr. Zicheng Li and myself. Dr. Zicheng Li synthesized the block copolymers and characterized the block copolymer stabilizers used in this study. I contributed to all aspects of this study. Also I took the lead role in the writing of the manuscript.

Chapter 5 presented oil-in-water emulsions stabilized with graphene oxide nanoplatelets that remained stable for several months even at high salinity (up to 5 wt% NaCl, for pH = 2 to 10). The droplet sizes were as small as ~1 μm with a low nanoplatelet concentration of 0.2 wt%. Stable emulsions could also be formed even for nanoplatelet concentrations down to 0.001 wt%. The remarkable stability of emulsions even at high salinity may be attributed to the high anion density at the platelet edges. Chapter 5 was a collaboration with Dr. Sung Jin An and myself. Dr. Sung Jin An synthesized the grapheme oxide materials. I contributed to all aspects of this study and took the lead in writing the manuscript.

Chapter 6 reported a facile synthetic approach for preparing water-soluble Fe3O4 nanoparticle clusters with tunable size distribution and magnetic properties. We demonstrate the contrast enhancement in a newly-designed ultrasound-based cellular and molecular imaging modality, pulsed magneto-motive ultrasound (pMMUS) imaging. With these nanoparticles clusters consisting of large primary particles, pMMUS signals were enhanced significantly, which is essential for further development of in vivo pMMUS imaging. Chapter 6 was a collaboration with Dr. Mohammad Mehrmohammadi

and myself. Dr. Mohammad Mehrmohammadi did pulsed magneto-motive ultrasound (pMMUS) imaging experiment with iron oxide nanoparticle dispersion. I contributed to all aspects of design and synthesis of nanoparticles. Also, I took the lead role in the writing of the manuscript.

1.4 REFERENCES

1. (a) Gupta, A. K.; Gupta, M., Synthesis and surface engineering of iron oxide nanoparticles for biomedical applications. *Biomaterials* **2005,** *26*, 3995–4021; (b) Oh, J.; Feldman, M. D.; Kim, J.; Condit, C.; Emelianov, S.; Milner, T. E., Detection of magnetic nanoparticles in tissue using magneto-motive ultrasound. *Nanotechnology* **2006,** *17* (16), 4183-4190; (c) Lattuada, M.; Hatton, T. A., Preparation and Controlled Self-Assembly of Janus Magnetic Nanoparticles. *Journal of the American Chemical Society* **2007,** *129* (42), 12878-12889; (d) Lu, A.-H.; Salabas, E. L.; Schueth, F., Magnetic nanoparticles: synthesis, protection, functionalization and application. *Angew. Chem. Int. Ed.* **2007,** *46*, 1222-1244; (e) Ma, L. L.; Feldman, M. D.; Tam, J. M.; Paranjape, A. S.; Cheruku, K. K.; Larson, T. A.; Tam, J. O.; Ingram, D. R.; Paramita, V.; Villard, J. W.; Clarke, G. D.; Jenkins, J. T.; Asmis, R.; Sokolov, K.; Chandrasekar, B.; Milner, T. E.; Johnston, K. P., Small multifunctional nanoclusters (Nanoroses) for targeted cellular imaging and therapy. *ACS Nano* **2009,** *3*, 2686-2696; (f) Satarkar, N. S.; Biswal, D.; Hilt, J. Z., Hydrogel nanocomposites: a review of applications as remote controlled biomaterials. *Soft Matter* **2010,** *6*, 2364–2371; (g) Mehrmohammadi, M.; Yoon, K. Y.; Qu, M.; Johnston, K.; Emelianov, S. Y., Enhanced pulsed magneto-motive ultrasound imaging using superparamagnetic nanoclusters. *Nanotechnology* **2011,** *22*, 045502.

2. Wu, W.; He, Q.; Jiang, C., Magnetic iron oxide nanoparticles: synthesis and surface functionalization strategies. *Nanoscale Research Letters* **2008,** *3*, 397-415.

3. (a) Yu, H.; Kotsmar, C.; Yoon, K. Y.; Ingram, D. R.; Johnston, K. P.; Bryant, S. L.; Huh, C., Transport and retention of aqueous dispersions of paramagnetic nanoparticles in reservoir rocks. *17th SPE Improved Oil Recovery Symposium Tulsa, OK* **2010,** *SPE 129887*; (b) Prodanovic, M.; Ryoo, S.; Rahmani, A. R.; Kuranov, R.; Kotsmar, C.; Milner, T. E.; Johnston, K. P.; Bryant, S. L.; Huh, C., Effects of magnetic field on the motion of multiphase fluids containing paramagnetic particles in porous media. *17th SPE Improved Oil Recovery Symposium Tulsa, OK* **2010,** *SPE 129850*; (c) Ingram, D. R.; Kotsmar, C.; Yoon, K. Y.; Shao, S.; Huh, C.; Bryant, S. L.; Milner, T.; Johnston, k. P., Superparamagnetic nanoclusters coated with oleic acid bilayers for stabilization of emulsions of water and oil at low loncentration. *J. Colloid Interface Sci.* **2010,** *351*, 225-232; (d) Prakash, A.; Zhu, H.; Jones, C. J.; Benoit, D. N.; Ellsworth, A. Z.; Bryant, E. L.; Colvin, V. L., Bylayers as Phase Transfer Agents for Nanocrystals Prepared in Nonpolar Solvents. *ACS Nano* **2009,** *3*, 2139-2146.

4. Ryoo, S.; Rahmani, A. R.; Yoon, K. Y.; Prodanovic, M.; Kotsmar, C.; Milner, T. E.; Johnston, K. P.; Bryant, S. L.; Huh, C., Theoretical and experimental investigation of the motion of multiphase fluids containing paramagnetic nanoparticles in porous media. *SPE Annual Meeting, Florence, Italy* **2010,** *SPE 134879*.

5. (a) Lan, Q.; Liu, C.; Yang, F.; Liu, S.; Xu, J.; Sun, D., Synthesis of bilayer oleic acid-coated Fe3O4 nanoparticles and their application in pH-responsive Pickering emulsions. *J. Colloid Interface Sci.* **2007,** *310*, 260-269; (b) Binks, B. P.; Kirkland, M., Interfacial structure of solid-stabilised emulsions studied by scanning electron microscopy. *Phys. Chem. Chem. Phys.* **2002,** *4*, 3727-3733; (c) Saleh, N.; Phenrat, T.; Sirk, K.; Dufour, B.; Ok, J.; Sarbu, T.; Matyjaszewski, K.; Tilton, R. D.; Lowry, G. V., Adsorbed Triblock Copolymers Deliver Reactive Iron Nanoparticles to the Oil/Water Interface. *Nano Letters* **2005,** *5* (12), 2489-2494; (d) Melle, S.; Lask, M.; Fuller, G. G., Pickering emulsions with controllable stability. *Langmuir* **2005,** *21*, 2158-2162.

6. Ishimuro, Y.; Ueberreiter, K., The surface tension of poly(acrylic acid) in aqueous solution. *Coll. Polym. Sci.* **1980,** *258*, 928-931.

7. (a) Moeser, G. D.; Roach, K. A.; Green, W. H.; Laibinis, P. E.; Hatton, T. A., High-gradient magnetic separation of coated magnetic nanoparticles. *AIChE Journal* **2004,** *50*, 2835-2848; (b) Ditsch, A. P.; Lindemann, S.; Laibnis, P. E.; Wang, D. I. C.; Hatton, T. A., High-gradient magnetic separation of magnetic nanoclusters. *Ind. Eng. Chem. Res.* **2005,** *44*, 6824-6836; (c) Gerber, R.; Birss, R. R., *High Gradient Magnetic Separation*. Research Studies Press: London, 1983.

8. (a) Ditsch, A.; Lindenmann, S.; Laibinis, P. E.; Wang, D. I. C.; Hatton, T. A., High-gradient magnetic separation of magnetic nanoclusters. *Ind. Eng. Chem. Res.* **2005,** *44*, 6824-6836; (b) Ma, L. L.; Feldman, M. D.; Tam, J. M.; Paranjape, A. S.; Cheruku, K. K.; Larson, T. A.; Tam, J. O.; Ingram, D. R.; Paramita, V.; Villard, J. W.; Jenkins, J. T.; Wang, T.; Clarke, G. D.; Asmis, R.; Sokolov, K.; Chandrasekar, B.; Milner, T. E.; Johnston, K. P., Small multifunctional nanoclusters (Nanoroses) for targeted cellular imaging and therapy. *ACS Nano* **2009,** *3*, 2686-2696.

9. Arkles, B., Tailoring surfaces with silanes. *Chem. Tech.* **1977,** *7*, 766-770.

10. De Palma, R.; Peeters, S.; Van Bael, M. J.; Van den Rul, H.; Bonroy, K.; Laureyn, W.; Mullens, J.; Borghs, G.; Maes, G., Silane Ligand Exchange to Make Hydrophobic Nanoparticles Water-Dispersible. *Chem. Mater.* **2007,** *19*, 1821-1831.

11. Shen, L.; Stachowiak, A.; Hatton, A. T.; Laibnis, P. E., Polymerization of olefin-terminated surfactant bilayers on magnetic fluid nanoparticles. *Langmuir* **2000,** *16*, 9907-9911.

12. (a) Wang, Y.-X. J.; Hussain, S. M.; Krestin, G. P., Superparamagnetic iron oxide contrast agents: physicochemical characteristics and applications in MR imaging. *Eur. Radiol.* **2001,** *11*, 2319-2331; (b) Wunderbaldinger, P.; Josephson, L.; Weissleder, R.,

Crosslinked iron oxide (CLIO): a new platform for the development of targeted MR contrast agents. *Acad. Radiol.* **2002,** *Suppl 2* (S), 304-306.

13. Dresco, P. A.; Zaitsev, V. S.; Gambino, R. J.; Chu, B., Preparation and Properties of Magnetite and Polymer Magnetite Nanoparticles. *Langmuir* **1999,** *15*, 1945-1951.

14. Lee, H.; Yu, M. K.; Park, S.; Moon, S.; Min, J. J.; Jeong, Y. Y.; Kang, H.-W.; Jon, S., Thermally cross-linked superparamagnetic iron oxide nanoparticles: synthesis and application as a dual imaging probe for cancer in vivo. *J. Am. Chem. Soc.* **2007,** *129*, 12739-12745.

15. Kawano, T.; Niidome, Y.; Mori, T.; Katayama, Y.; Niidome, T., PNIPAM Gel-Coated Gold Nanorods for Targeted Delivery Responding to a Near-Infrared Laser. *Bioconjugate Chem.* **2009,** *20*, 209–212.

16. Turner, J. L.; Pan, D.; Plummer, R.; Chen, Z.; Whittaker, A. K.; Wooley, K. L., Synthesis of gadolinium-labeled shell-crosslinked nanoparticles for magnetic resonance imaging applications *Adv. Funct. Mater.* **2005,** *15*, 1248-1254.

17. Huang, H.; Kowalewski, T.; Remsen, E. E.; Gertzmann, R.; Wooley, K. L., Hydrogel-coated glassy nanospheres: a novel method for the synthesis of shell cross-linked knedels. *J. Am. Chem. Soc.* **1997,** *119*, 11635-11659.

18. (a) Arbab, A. S.; Bashaw, L. A.; Miller, B. R.; Jordan, E. K.; Lewis, B. K.; Kalish, H.; Frank, J. A., Characterization of biophysical and metabolic properties of cells labeled with superparamagnetic iron oxide nanoparticles and transfection agent for cellular MR imaging. *Radiology* **2003,** *229*, 838-846; (b) Lin, C.-L.; Lee, C.-F.; Chiu, W.-Y., Preparation and properties of poly(acrylic acid) oligomer stabilized superparamagnetic ferrofluid. *J. Colloid Interf. Sci.* **2005,** *291*, 411-420; (c) Santra, S.; Kaittanis, C.; Grimm, J.; Perez, M., Drug/dye-loaded, multifunctional iron oxide nanoparticles for combined targeted cancer therapy and dual optical/magnetic resonance

imaging. *Small* **2009,** *5* (16), 1862-1868; (d) Chanteau, B.; Fresnais, J.; Berret, J.-F., Electrosteric enhanced stability of functional sub-10 nm cerium and iron oxide particles in cell culture medium. *Langmuir* **2009,** *25* (16), 9064-9070; (e) Gu, B.; Mehlhorn, T. L.; Liang, L.; McCarthy, J. F., Competitive adsorption, displacement, and transport of organic matter on iron oxide: I. Competitive adsorption. *Geochimica et Cosmochimica Acta* **1996,** *60* (11), 1943-1950; (f) Hong, R. Y.; Pan, T. T.; Han, Y. P.; Zhang, S. Z.; Li, H. Z.; Ding, J., Graft polymerization synthesis and application of magnetic Fe3O4/polyacrylic acid composite nanoparticles. *J. Appl. Polym. Sci.* **2007,** *106*, 1439-1447.

19. Zhang, T.; Ge, J.; Hu, Y.; Yin, Y., A general approach for transferring hydrophobic nanocrystals into water. *Nano Letters* **2007,** *7* (10), 3203-3207.

20. Isojima, T.; Lattuada, M.; Vander Sande, J. B.; Hatton, A. T., Reversible Clustering of pH- and Temperature-Responsive Janus Magnetic Nanoparticles. *ACS Nano* **2008,** *2* (9), 1799-1806.

21. (a) Chen, D.-H.; Huang, S.-H., Fast separation of bromelain by polyacrylic acid-bound iron oxide magnetic nanoparticles. *Process Biochemistry* **2004,** *39*, 2207-2211; (b) Liao, M.-H.; Chen, D.-H., Preparation and characterization of a novel magnetic nano-adsorbent. *J. Mater. Chem.* **2002,** *12*, 3654-3659.

22. Ge, J.; Hu, Y.; Biasini, M.; Beyermann, W. P.; Yin, Y., Superparamagnetic magnetite colloidal nanocrystal clusters. *Angew. Chem. Int. Ed.* **2007,** *46*, 4342-4345.

23. (a) Ditsch, A.; Laibinis, P. E.; Wang, D. I. C.; Hatton, T. A., Controlled Clustering and Enhanced Stability of Polymer-Coated Magnetic Nanoparticles. *Langmuir* **2005,** *21* (13), 6006-6018; (b) Sondjaja, R.; Hatton, A. T.; Tam, M. K. C., Clustering of magnetic nanoparticles using a double hydrophilic block copolymer, poly(ethylene oxide)-b-poly(acrylic acid). *J. Magn. Magn. Mat.* **2009,** *321*, 2393-2397.

24. Rosen, M. J., Surfactants and Interfacial Phenomena; Wiley-Interscience: New York, 2002.

25. Derjaguin, B. V., *Trans. Faraday Sot.,* **1940,** (36), 203.

26. Vervey, E. J. W.; and Overbeek, J. T. G., Theory ofthe Stability of Lyophobic Colloids.Elsevier, Amsterdam, New York, 1948.

27. Gouy, G., *J. Physique* **1910,** *9*, 457.

28. Chapman, D. L., *Philos. Mag.* **1913,** *25*, 475.

29. Stern, *Z. Electrochem.* **1924,** *30*, 508.

30. (a) Kretzschmar, R.; Sticher, H., Transport of humic-coated iron oxide colloids in a sandy soil: Influence of Ca2+and trace metals. *Environ. Sci. Technol.* **1997,** *31*, 3497–3504; (b) Nyer, E. K.; Vance, D. B., Nano-scale iron for dehalogenation. *Ground Water Monit. Rem.* **2001,** *21*, 41–46; (c) Elimelech, M., Particle deposition on ideal collectors from dilute flowing suspensions: Mathematical formulation, numerical solution, and simulations. *Sep. Technol.* **1994,** *4*, 186–212; (d) Liu, D.; Johnson, P. R.; , a. E., M., Colloid deposition dynamics in flow-through porous media: Role of electrolyte concentration. *Environ. Sci. Technol.* **1995,** *29*, 2963–2973.

31. (a) Biesheuvel, P. M., Ionizable polyelectrolyte brushes: Brush height and electrosteric interaction. *J. Colloid Interface Sci.* **2004,** *275*, 97–106; (b) Pincus, P., Colloid stabilization with grafted polyelectrolytes. *Macromolecules* **1991,** *24*, 2912–2919.

32. Phenrat, T.; Saleh, N.; Sirk, K.; Kim, H.-J.; Tilton, R. D.; and Lowry, G. V., Stabilization of aqueous nanoscale zerovalent iron dispersions by anionic polyelectrolytes: adsorbed anionic polyelectrolyte layer properties and their effect on aggregation and sedimentation. *J. Nanopart. Res.* **2008,** *10*, 795-814.

Chapter 2: Stabilization of Superparamagnetic Iron Oxide Nanoclusters in Concentrated Brine with Crosslinked Polymer Shells

Iron oxide nanoparticles, in the form of sub-100 nm clusters, were synthesized in the presence of poly(acrylic acid) (PAA) or poly(styrene sulfonate-alt-maleic acid) (PSS-*alt*-MA) to provide electrosteric stabilization. The superparamagnetic nanoclusters were characterized using a superconducting quantum interference device (SQUID), transmission electron microscopy (TEM), dynamic light scattering (DLS), thermogravimetric analysis (TGA), and zeta potential measurements. To anchor the polymer shell on the nanoparticle surface, the polymer was cross-linked for a range of cross-link densities. For nanoclusters with only 12% (w/w) PSS-*alt*-MA electrosteric stabilization was sufficient even in 8 wt% NaCl. For PAA, the cross-linked polymer shell was essentially permanent and did not desorb even upon dilution of the nanoparticles, for iron oxide concentrations down to 0.014 wt%. Without cross-linking, over half of the polymer desorbed from the particle surfaces. This general approach of adsorption of polymer stabilizers onto nanoparticles followed by cross-linking may be utilized for a wide variety of cross-linkable polymers without the need to form covalent bonds between the nanoparticles and polymer stabilizer. Thus, this cross-linking approach offers is an efficient and inexpensive method for stabilization nanoparticles for large scale applications, including electromagnetic imaging of subsurface reservoirs, even with high salinities.

2.1 INTRODUCTION

Magnetic nanoparticles in aqueous media are widely used in biomedical applications including drug delivery systems, affinity purification, *in vitro* cell separation, and biomedical imaging.[1] Colloidal stabilization of the magnetic nanoparticles against attractive magnetic dipole–dipole interactions and van der Waals forces may be achieved with polymeric stabilizers on the particle surface. The attractive magnetic interactions may be avoided with superparamagnetic nanoparticles, which do not have a magnetic moment in the absence of an applied magnetic field. Magnetite nanoparticles (MNPs) smaller than ~15 nm in diameter are often superparamagnetic, and have been stabilized with a variety of ligands.[1d, 2]

Recently, we proposed that aqueous magnetite nanoparticles dispersions may be utilized as imaging agents for detection and visualization of residual oil in oil reservoirs, which may have salinities up to 8% NaCl.[3] The nanoparticles are designed to adsorb at the the interface of residual oil and brine, as a function of the interfacial properties of the stabilizers on the particle surface.[4] The motion of magnetite nanoparticles at this interface caused by a magnetic field generates acoustic waves from which the oil saturation of the reservoir (~ pH 8) can be estimated.[5] In this application, the particles may be designed to be superparamagnetic (no permanent magnetic dipole) to enhance colloidal stability, resistant to colloidal aggregation at high salinities (salt tolerant), and to be small enough (~100 nm) for transport through porous rock. A negative surface charge on the nanoparticles is beneficial for repulsion from negatively charged minerals such as sandstone and limestone to minimize adsorption and facilitate transport.[6]

The magnetic force on a particle is proportional to the magnetization and the particle volume. Whereas the large volume of a 100 nm nanoclusters would be desirable, Magnetite nanoparticles of this size are typically ferromagnetic, and thus require large amounts of stabilizer to overcome the magnetic attraction. An excess of stabilizer lowers the magnetic fraction of the particles and thus the magnetic force. A strategy to overcome this limitation is to form 100 nm superparamagentic clusters of adjacent sub-15 nm primary particles.[1e, 3c, 7] Even with very small spacings between these primary particles, the spins on neighboring particles are usually not close enough to influence the magnetization per mass of iron.[1e] In essence, the magnetization/volume remains relatively constant relative to individual primary particles, whereas the large volume leads to a strong magnetic force.

Various strategies have been utilized to covalently attach stabilizers to iron oxide nanoparticles including silylating agents,[8-9] and gamma-ray induced polymerization.[10] Graft polymerization has been applied to coat iron oxide nanoparticles with PAA. [11] PAA has been covalently attached directly to the iron oxide surface via carbodiimide activation of the carboxylic functionality.[12] An alternative is to adsorb a polymer to the surface of iron oxide particles and then crosslink the polymer to prevent subsequent desorption. The carboxylate functionalities on PAA and poly(maleic acid) form relatively strong complexes with the Fe atoms of the particle surface through bidentate bonding.[13] A stable cross-linked dextran stabilizer on nanoparticle surfaces *in vivo* has been demonstrated for iron oxide nanoparticles (CLIO).[14] Dresco et al. [15] reported an inverse microemulsion method to synthesize cross-linked polymer-coated Magnetite nanoparticles. Lee et al. [16]

used a PEG-silane co-polymer to covalently bind the PEG on iron oxide nanoparticle surfaces. Polymer nanospheres with cross-linked shells were synthesized following self assembly of amphiphilic poly(acrylic acid)- poly (methyl acrylate) PAA-*b*-PMA [17] and polystyrene-*b*-poly(acrylic acid) (PS-*b*-PAA) copolymers.[18,19] PAA has also been used to modify the surface properties in order to transfer oleic acid-coated iron oxide nanoparticles from toluene to water.[20]

Synthesis of nanoparticle clusters by using PAA[13, 21] and PAA-based co-polymers [22] as stabilizer have been reported elsewhere, but these studies did not use polymer cross-linking. Iron oxide nanoparticles dispersions in 5 M NaCl have been stabilized with adsorbed random copolymers of acrylic acid, styrenesulfonic acid, and vinylsulfonic acid. [22a] However, adsorbed polymers may be susceptible to desorption at dilute conditions, as a function of the binding strength.

The objective of the present study is to synthesize sub-100 nm superparamagnetic iron oxide nanoclusters with controlled size, high magnetization, and colloidal stability, provided by copolymers that are later cross-linked. PAA or PSS-*alt*-MA were adsorbed to the nanocluster surface during synthesis, without the need for covalent attachment. During hydrolysis and condensation of the iron oxide precursors, the polymer stabilized the primary particles during nucleation and growth and mediated aggregation of the particles to form nanoclusters. For iron oxide nanoclusters stabilized with cross-linked PSS-*alt*-MA, the surface charge on the particles was sufficient even at high salinities up to 8 wt% NaCl at certain pH values to provide electrosteric stabilization. TGA experiments showed that the polymer stabilizer remains on the surface of the clusters

even after extensive dilution to a concentration of 0.014 wt% for various ratios of cross-linking agent to iron oxide. This technique is highly general and can be applied to a wide range of readily available and inexpensive copolymers that adsorb on iron oxide, as the cross-linking step is independent of the nanoparticle synthesis step. The large volume of the nanoclusters, relative to the primary nanoparticles, in addition to the small mass of the cross-linked polymer stabilizer, less than 15% by weight, provide for a large magnetic force on the particles, which is of benefit in magnetomotive imaging. The cross-linked stabilizer provides a secondary potential benefit, as the addition of a hydropobic cross-linking agent is shown to improve the interfacial activity of the nanoclusters at the oil/water interface.

2.2 EXPERIMENTAL SECTION

2.2.1 Materials

Ferrous chloride tetrahydrate ($FeCl_2 \cdot 4H_2O$; MW=198.81 g; catalog number: I90-500), ferric chloride hexahydrate ($FeCl_3 \cdot 6H_2O$; MW=270.32 g; catalog number: I88-100), ammonium hydroxide (NH4OH, 28% catalog number: A669-212), poly(acrylic acid, sodium salt) (PAA, MW=5100, catalog number: 447013-100G) and sodium chloride (NaCl, MW=58.44 g; catalog number: S671-3) were purchased from Fisher Scientific, USA. Poly(4-styrenesulfonic acid:maleic acid, sodium salt) (PSS-*alt*-MA MW=20,000, catalog number: 434566) was purchased from Sigma-Aldrich. 1,6-hexanediamine (MW=116.21 g; catalog number: 124-09-4) was purchased from Acros Organics, USA. 1-ethyl-3-(3-dimethylamino-propyl)carbodiimide hydrochloride (EDC, MW=191.7 g;

catalog number: D1601) was purchased from TCA America. Hydrochloric Acid (HCl; MW=36.46 g; catalog number: UN1789) and sodium hydroxide (NaOH; MW=40 g; catalog number: UN1823) were purchased from EM Science, Germany. Dialysis tubing (Spectra/Por® 6; 50,000 MWCO; lot number 3246779) was purchased from Spectrum Laboratories, Inc., USA.

2.2.2 Nanoparticle synthesis and nanocluster formation

The IO NPs were prepared by coprecipitation of Fe(II) and Fe(III) chlorides in an alkaline solution [23]. Briefly, in a three-necked flask $FeCl_2$ and $FeCl_3$ (1:2 molar ratio) and 0.75 g of PAA or 1 g of PSS-*alt*-MA were dissolved in 40 mL DI water and the solution was magnetically stirred for 30 minutes under nitrogen atmosphere. The mixture was heated to 90 ^{o}C while stirring and 8 ml of 30 wt % NH_4OH solution was injected to the reaction mixture to nucleate the iron oxide NPs. The reaction was further stirred and heated for 2 hours and then cooled to room temperature. To remove the excess PAA that was not adsorbed to the nanoparticle surfaces, the dispersions were ultra-centrifuged (SORVALL RC 6+, Thermo Scientific) at 10000 rpm for 40 minutes, the supernatant was discarded and the sediment was re-dispersed in 20 ml DI water by probe sonication. The final dispersion contained ~1 wt% Fe by flame atomic absorption spectroscopy (FAAS), and the pH value was around 9. Prior to crosslinking, the dispersions were diluted with DI water to reach final 0.1 wt% Fe, which corresponds to 0.14 wt% iron oxide concentrations. The pH was adjusted to the desired values by using NaOH or HCl and NaCl was added to adjust the salinity.

2.2.3 Cross-linking of polymer stabilizer on iron oxide surface

To a 100 ml dispersion of PAA or PSS-*alt*-MA coated iron oxide particles, containing 0.14 wt% iron oxide (based on iron amount from FAAS), 1-10 mg/mL aqueous solution of 1,6-hexanediamine was added drop-wise in over 5 minutes with magnetic stirring. The concentration of the added 1,6-hexanediamine solution was varied to adjust the cross-link density. The change in the volume of the reaction mixture was below 3 % upon adding the cross-linking reagents. The reaction mixture was stirred for additional 2 h at room temperature. Then 10 mg/mL aqueous solution of EDC was added and the mixture was further stirred 20 h at room temperature before transferring to the dialysis tubing, and dialyzed against DI water for 3 days to remove the unreacted reagents. The volume increase in the dispersion upon addition of all the reagents was negligible relative to the initial volume.

The nominal or "theoretical" crosslinking ratios were calculated based on the stoichiometry of the carboxylic acids groups of PAA or PSS-*alt*-MA on the iron oxide surface to that of the cross-linker 1,6-hexanediamine. The number of carboxylic groups on the iron oxide surface was calculated from TGA data. The theoretical stoichiometry employed to achieve 100% nominal cross-linking would be 2:1 for carboxylic acid units : 1,6-hexanediamine, to achieve 50% the stoichiometry would be 4:1, to achieve 25% the stochiometry would be 8:1 and the lowest applied cross-linking density 12.5% cross-linking would be 16:1. The actual cross-linking will be well below the theoretical value, particularly as the degree of cross-linking increases.[24]

2.2.4 Particle dilution process

20 ml of 0.14 wt% PAA-coated iron oxide dispersion was diluted to 200 ml by using DI water and equilibrated for one day. The dispersion was centrifuged at 14,000 rpm for 20 minutes which caused the settling of the particles. The supernatant was discarded and the pellet was redispersed in 200 ml DI water by probe sonication and another day was allowed for the system to reach equilibrium. The dispersion was centrifuged again at 14,000 rpm for 20 minutes and the pellet was dried for TGA analysis.

2.2.5 Materials Characterization

Dynamic light scattering (DLS) analysis was performed on a custom-built apparatus, and the data were analyzed using a digital autocorrelator (Brookhaven BI-9000AT) and a non-negative least-squares (NNLS) routine (Brookhaven 9KDLSW32).[25] The scattering angle was 90º. The dispersion concentration for the measurements was approximately 0.05 mg/mL iron oxide which gave a measured count rate of approximately 200 kcps. Measurements were made over a period of 2 min at least three times on each sample.

Zeta potential measurements were performed in triplicate on a ZetaPlus dynamic light scattering apparatus (Brookhaven Instruments) at 90° scattering angle and temperature of 25 °C.

Transmission electron microscopy (TEM) was used to observe the morphology of nanoclusters. The experiments were performed on a FEI TECNAI G2 F20 X-TWIN TEM

using a high-angle annular dark field detector. The samples were prepared using a "flash-freezing" technique, in which a 200 mesh carbon-coated copper TEM grids were cooled using liquid nitrogen and then dipped into dilute aqueous nanocluster dispersion. [26] The sample was immediately dried using a Virtis Advantage Tray Lyophilizer (Virtis Company, Gardiner, NY) with 2 hours of primary drying at -40 ^{o}C followed by a 12 hour ramp to +25 ^{o}C and then 2 hours of secondary drying at 25 ^{o}C. In this manner the aggregation of NPs caused by capillary forces during drying of the liquid on the TEM grid could be avoided.

Thermo gravimetric analysis (TGA) was used to determine the mass of stabilizer on the iron oxide nanoclusters. The experiments were performed using a Mettler Toledo TGA/DSC 1 STAR^e system equipped with a gas controller (GC 200) and a temperature set at 22°C (Julabo). The powder samples were held at 100°C for 120 minutes to remove the remaining water in the sample and then heated at a constant rate of 20 °C/min from 100°C to 800 °C and held at 800°C for 30 minutes. The loss in mass after heating indicated the organic component of the particles.

Flame atomic absorption spectroscopy (FAAS) was used to determine the iron concentration in the dispersion by using a GBC 908AA flame atomic absorption spectrometer (GBC Scientific Equipment Pty Ltd). All measurements were conducted at 242.8 nm using an air-acetylene flame.

Superconducting quantum interference device or SQUID magnetometer (Quantum Design MPMS) was used to measure the normalized saturation magnetization of the particles at 300 K.

2.3 RESULTS AND DISCUSSION

2.3.1 Aqueous dispersion of PAA or PSS-alt-MA coated iron oxide nanoparticle

The Fe_3O_4 content of the PAA or PSS-*alt*-MA coated iron oxide nanoparticle aqueous dispersions was determined by flame atomic absorption spectroscopy (FAAS). The PAA and PSS-*alt*-MA coated iron oxide particles in dispersion at pH 8 were studied with TEM and DLS before cross-linking. The iron oxide nanocrystals spontaneously aggregated to form flocculated clusters, as shown in the transmission electron microscopy (TEM) images (Figure 2.1).

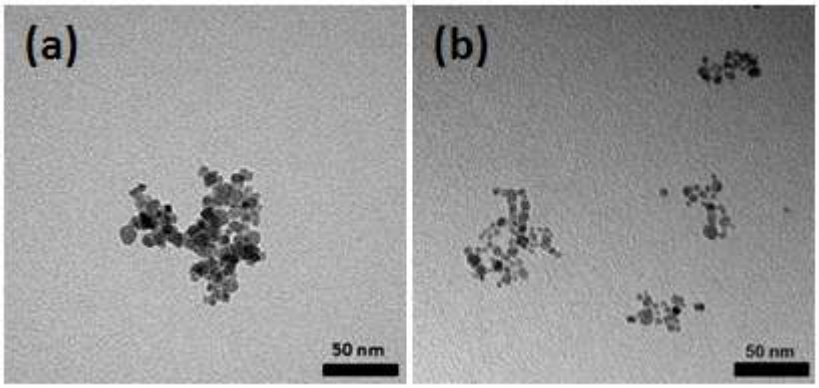

Figure 2.1 TEM images of (a) PAA-coated iron oxide nanoclusters (b) PSS-*alt*-MA-coated iron oxide nanoclusters, in before cross-linking.

VDW and electrostatic interactions govern the formation of clusters from the primary particles. Despite the negative surface charge of the particles in the alkali

medium (~pH12), VDW attraction overcomes the electrostatic repulsion.[27] The adsorption of the carboxylate ions in the copolymer to the surface of the iron oxide nanoparticles provides a sufficient polymer steric layer to stabilize the clusters against excessive growth. At the end of the reaction and after centrifugation to remove excess reagents, probe sonication was used to redisperse the clusters. The 40-150 nm diameter clusters were composed of small primary crystals with sizes of 3–10 nm. During the preparation of the TEM samples it is possible that the clusters underwent changes, despite the "flash-freezing" technique, such that their appearance may be perturbed from the morphology in the dispersion. To determine the hydrodynamic diameter of the clusters in-situ, DLS was utilized. The volume distribution of the NPs is given in the histograms shown in Figure 2.2 for NP dispersions at pH 8 to show the reproducibility in size for a single reaction. The peaks can be observed between 40 and 150 nm indicating the process of cluster formation was controllable at these conditions. The average diameter value of the clusters was 83 nm for PAA-coated iron oxide nanoclusters and 44 nm for PSS-*alt*-MA-coated iron oxide nanoclusters (Table 2.1). The sizes of the nanoclusters by TEM were in agreement with the DLS values. At this pH, the dispersed clusters are stabilized electrosterically by the negative surface charge of the PAA molecules. The point of zero charge (PZC) of PAA molecules is ~ pH5.5. [28] The high negative values of zeta potential for PAA-coated iron oxide nanoclusters (-39.7 mV) and PSS-*alt*-MA-coated iron oxide nanoclusters (-48.6 mV), (Table 2.1) quantify the strong charge that provides electrostatic repulsion. Similar zeta potentials were reported in the literature for PAA-coated iron oxide nanoparticles. [13, 29]

Table 2.1 Zeta potential and average hydrodynamic diameters of PAA or PSS-*alt*-MA coated iron oxide nanoparticles with different cross-linking densities for an iron oxide concentration of 0.14 wt. % at pH8

Cross-linking (%)	Hydrodynamic diameter (DLS) [nm]	Zeta potential [mV]
PSS-*alt*-MA before cross-linking	44 ± 9	-48.6 ± 4.7
PAA before cross-linking	83 ± 2	-39.7 ± 1.5
PAA, 12.5% cross-linking	69 ± 17	-48.6 ± 1.1
PAA, 25% cross-linking	126 ± 9	-44.3 ± 2.2
PAA, 50% cross-linking	77 ± 16	-47.1 ± 2.2
PAA, 100% cross-linking	91 ± 1	-38.3 ± 3.0

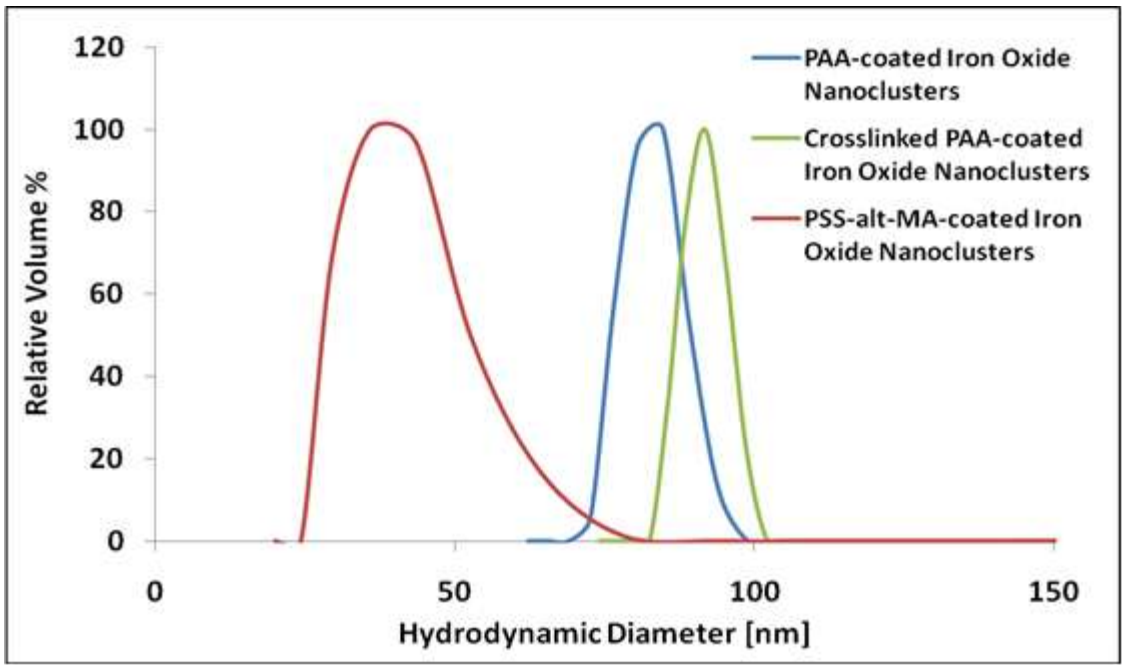

Figure 2.2 Volume fraction based distributions of PAA and PSS-alt-MA coated iron oxide nanoclusters at pH8, before cross-linking.and after 100 % cross-linking.

2.3.2 Thermal stability of PAA or PSS-alt-MA coated iron oxide nanoparticle

TGA analysis of PAA-coated nanoparticles shows initially 14.3 % weight loss from the mass of the PAA stabilizer, as shown in Table 2.2. The major weight loss occured at temperatures between 200 and 550 °C as observed by Zhang et al. [20] for PAA-coated iron oxide nanoparticles. Chen et al. [12a] attached 180000 g/mol PAA molecules covalently to iron oxide surface by using carbodiimide and observed around 12 wt% loss with TGA.

Table 2.2 TGA analysis of PAA-coated iron oxide nanoparticles with different cross-linking densities, before and after particle dilution process.

Particle type	Coating (initial) [wt%]	Coating after dilution [wt%]
PAA-coated IO, no cross-linking	14	6
PAA-coated IO, 12.5% cross-linking	16	12
PAA-coated IO, 25% cross-linking	20	13
PAA-coated IO, 50% cross-linking	19	17
PAA-coated IO, 100% cross-linking	14	13

2.3.3 The mechanism of cluster formation with PAA or PSS-alt-MA coated iron oxide nanoparticle

The mechanism of cluster formation of iron oxide nanoparticles in this study has been described in detail in numerous studies. The formation of clusters of the nucleating individual nanocrystals, is governed by a balance of van der Waals (VDW) and electrostatic interactions. A variety of methods have been developed to form clusters of nanoparticles in either one step in the presence of the final stabilizer [13, 21] or multiple steps. In the multiple step method, the individual nanoparticles are synthesized and stabilized in dispersion with the first stabilizer. Then a second stabilizer is used in a subsequent step to cause the primary particles for form clusters.[30] In this case, since the nanoparticles were nucleated in presence of PAA, the PAA influenced the stabilization of both the primary particles and the nanoclusters in one step. The carboxylate groups of PAA coordinate strongly with the iron cations. The polymer chains extend into the

aqueous solution and provide electrosteric stabilization of the particles.[21] Additionally, PAA can enable clustering of primary nanoparticles by bridging between two or more nanoparticles upon adsorption on the particle surfaces. Lin et al. [13] observed formation of 150-400 nm sized clusters, upon synthesis with high concentrations of PAA. After sonication the cluster sizes decreased to 10-40 nm. Ge et al. [21] controlled the size of PAA-coated iron oxide nanoclusters between 30 and 180 nm by varying the amount of NaOH added during the particle synthesis. The sizes of the individual nanocrystals ranged from 6 to10 nm. The PAA-coated clusters were highly dispersible in water even after washing 3 times with a water-ethanol mixture. Santra et al. [29a] synthesized 90 nm PAA-coated iron oxide particles. They reported individual 8 nm sized particles with an approximately 40 nm thick PAA shell, based on TEM measurements. In each of these studies as well as the current study, the PAA provided electrosteric stabilization of the iron oxide nanoclusters, often in the presence of free PAA in the solution. However, in most previous studies the dispersions were not diluted to determine if the PAA desorbs from the nanoparticle surface.

2.3.4 Magnetic properties of PAA or PSS-alt-MA coated iron oxide nanoparticle

The iron oxide crystals exhibited superparamagnetism, without hysteresis in the magnetization curve (Figure 2.3). The figure shows the magnetization of the iron oxide nanoparticles in emu/g Fe at 300 K up to 50000 Oersted (Oe). The saturation magnetization was ~90 emu/g Fe, which approaches the theoretical magnetization value for magnetite (92–100 emu/g).[22b] Thus, the primary nanoparticles were highly crystalline

and sufficiently large that the surface stabilizer did not lower the magnetization significantly. Furthermore, the primary nanoparticles were sufficiently far apart that the magnetization per g Fe in the nanoclusters approached the maximum value for primary nanoparticles. Thus magnetic coupling was not observed between the primary nanoparticles.

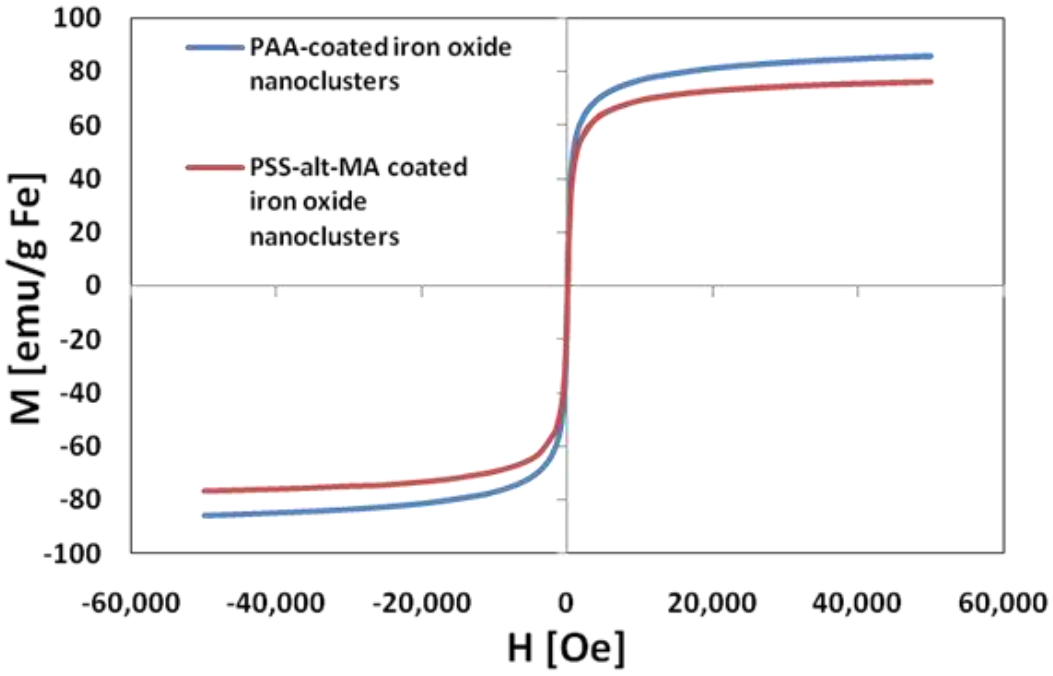

Figure 2.3 Magnetization (M) of iron oxide NPs coated with PAA or PSS-*alt*-MA stabilizer in emu/g units for Fe vs. magnetic field (H) at 300 K and pH8 without crosslinking. The samples are the same as in Figure 2.2.

2.3.5 Iron oxide nanoparticle with cross-linked polymer shell

The nanoparticle dispersions were diluted to Fe concentration of 0.01 wt% (see above section “Particle dilution process”) in DI water to determine if the adsorbed PAA

remained on the surface. As shown in Table 2.2 for the diluted PAA-coated particles with TGA measurements, the weight loss was only 6.3 wt% PAA indicating a loss of more than half of the PAA. Here the coordination of the carboxylate functionalities of the Fe cations was not strong enough to balance the favorable hydration of the polymer in bulk water at low concentration, as well as the gain in conformational entropy. There may have been a distribution of binding energies of PAA chains to the surface depending upon the number of carboxylate groups attached to Fe ions. The same technique was used to analyze the binding of the PAA to the nanoparticle surface for the various cross-linked samples, both before and after dilution with DI water. The case of 100 % nominal (theoretical) cross-linking corresponds to a PAA:hexanediamine ratio of 2:1. The number of carboxylic groups on the iron oxide surface was calculated from TGA of the non-cross-linked nanoparticles. TGA data at all 4 nominal cross-linking densities before and after washing the particles with DI water are presented in Table 2.2. For the three lowest cross-link densities, the initial weight loss went up a small amount as as result of the unremoved cross-linking reagents. However, in each case, the weight of the PAA stabilizer after dilution was high from 12 to 16.6%, indicating that the cross-linking prevented desorption of the polymer from the iron oxide surface. The successful binding of the polymer to the surface stands out in contrast with the case without cross-linking where the PAA amount dropped from 14.3 wt% to 6.3 wt%. All the dispersions were stable against settling after dilution for at least 4 weeks. The TGA results indicate that the cross-linking of a simple adsorbed polymer on an iron oxide surface leads to an electrosteric shell that is resistant to desorption at a very low concentration of iron oxide

down to 0.014 wt%. The cross-linking reaction complements the synthesis of a stable aqueous dispersion of sub-100 nm iron oxide nanoclusters.

DLS and zeta potential measurements on the PAA-coated iron oxide nanoparticles with different cross-linking densities, before dilution in pH 8 dispersions are presented in Table 1. The results show that the sizes of the clusters ranging from 69 to 126 nm do not change significantly with the cross-linking reaction. The average size of the clusters without cross-linking was 83 nm and even with the highest, 100 % nominal cross-linking density the measured value was just slightly higher: 91 nm. The zeta potential data were also similar at different cross-linking densities; the values varied between -38.3 and -48.6 mV. A clear trend was not observed between the nominal cross-link density and zeta potential, perhaps because of the variation in PAA amount. However, the greatest removal of charge was observed with the largest cross-link density as expected. The mesh size of the cross-linked gel is well below the size of the nanoclusters, which prohibits diffusion of the iron oxide nanoclusteres through the gel stabilizer at each of the cross-link densities.

2.3.6 The colloidal stability of crosslinked PSS-alt-MA-coated iron oxide nanoparticles

The stability of crosslinked PSS-*alt*-MA-coated iron oxide nanoparticles dispersed in water or NaCl brine up to 8 wt% NaCl was determined at a concentration of 0.27 wt%. From pH 8 to 10, the nanoparticles in the dispersions did not settle over 24 hrs with 8 wt% NaCl concentration. (Figure 2.4) At pH 6, we observed modest aggregation

of the nanoparticles at the bottom. Here the carboxylate groups may not be as negatively charged and bind more weakly to the Fe cations. Furthermore, the salt reduces the thickness of the diffuse electric double layer and weakens electrostatic repulsion.

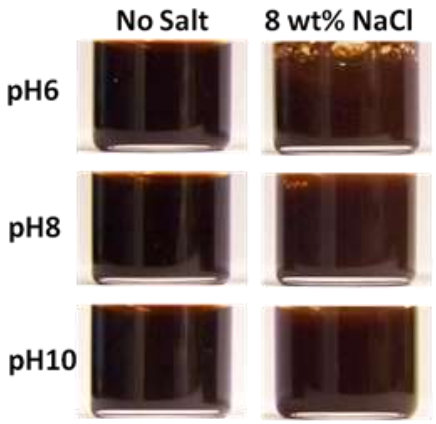

Figure 2.4 Photographs of PSS-*alt*-MA coated iron oxide nanoparticle dispersions after 1day at pH 6,8, and 10 with 8 wt% NaCl.

The effect of adding salt on the hydrodynamic diameter of the nanoclusters was studied by dynamic light scattering (DLS) at pH 8, as shown in Figure 2.5. Without added salt, the hydrodynamic diameter was ~ 100 nm. With added salt up to 8 wt% NaCl, the size decreased monotonically from 85 to 71 nm. It is straightforward to show that contraction of the polymer in the shell with added salt, as seen previously for high molecular weight polymer (~200,000)[22a, 31] would not account for much of this decrease in size. The hydrodynamic diameter of PSS-*alt*-MA was ~2 nm measured by without salt. Thus any contraction with added salt would be minimial. The most likely reason for the decrease in hydrodynamic diameter is a reduction in electrostatic repulsion with a

decrease in the charge on the primary particles within the cluster with added salt. Consequently, the attractive van der waals interactions are strengthened relative to electrostatic repulsion forces and the clusters contract.[31] For the porous nanoclusters, the effective Hamaker constant is significantly smaller than for the case of solid iron oxide, resulting in weaker van der Waals attraction. The viscosity of the aqueous solvent increases from 1.02 to 1.09 cP at 5 wt% NaCl, which would have a small effect on the hydrodynamic diameter calculated with the Stokes-Einstein equation from the diffusion coefficient measured by DLS.[32] In summary, these results indicate that PSS-alt-MA provides sufficient steric and electrostatic repulsion to overcome the van der Waals attraction between clusters even at 8 wt% NaCl.

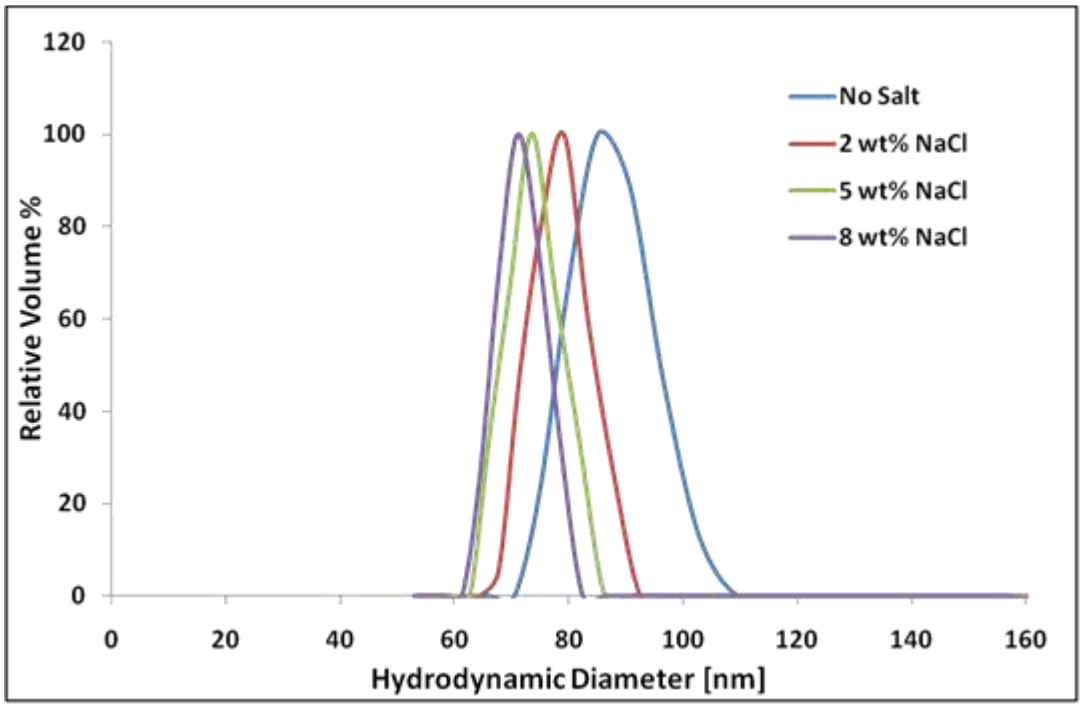

Figure 2.5 Volume fraction based distributions of crosslinked PSS-*alt*-MA coated iron oxide nanoclusters at pH8, with varying NaCl concentrations.

Random copolymers of acrylic acid, styrenesulfonic acid, and vinylsulfonic acid were used to synthesize and stabilize iron oxide clusters at different pH values and salinities by Ditsch et al.[22a] The nanoparticles were prepared by co-precipitation in the presence of a primary polymer stabilizer in the solution during the synthesizing step. A secondary polymer was added to completely coat the vacant iron oxide surface sites and achieve stable nanoparticle dispersions for up to 5 M NaCl concentrations. In this study, the polymer levels were 15-30 wt% according to TGA, in contrast with the smaller polymer levels in our study, which are beneficial for maximizing the magnetic coupling with the field. Another difference in the studies is the crosslinking of the shell in the current study.

2.3.7 The interfacial activity of the nanoparticles

The interfacial activity of the nanoparticles was examined by studies of emulsion stability. Emulsions of dodecane and water were formed with 0.14 wt% dispersions (in water) of non-cross-linked, 25 % and 100 % cross-linked PAA-coated nanoparticles at pH8 without salt and with 1 wt% NaCl content (Figure 2.6). Photographs of the emulsions were taken immediately after their formation by probe sonication and 1 day after. Micrographs of the particle-stabilized emulsions (Figure 2.6 a, b, c, d) are presented in Figure 2.7. All the emulsions formed with dodecane had a curvature of oil in water (O/W), based on electrical conductivity measurements, as was expected for hydrophilic particles with high negative surface charge.[33] In the case of non-cross-linked particles, without salt, after probe sonication the entire volume of the oil and water were emulsified

(Figure 2.6a). The brown-colored emulsion had droplet sizes of 10-50 μm (Figure 2.7a) and completely separated after 1 day. The oil underwent creaming, and the hydrophilic nanoparticles ended up in the aqueous phase. Similarly, the emulsion from the particle dispersion with 25 % cross-linking density (Figure 2.6b), where the droplet sizes also ranged between 10 and 50 μm (Figure 2.7b), almost completely resolved after 1 day with some emulsion droplets remaining wall of the vial. Upon adding 1 wt% NaCl to the dispersions, no emulsions formed with non-cross-linked and 25 % cross-linked nanoparticles. Without added salt, 100 % cross-linked particles formed emulsions (Figure 2.6c) with smaller droplets than in the above cases, around 3-15 μm (Figure 2.7c). The smaller oil droplets, compared to the aforementioned ones, produced a lighter brown color. This emulsion also almost completely resolved in 1 day, however some remaining droplets could be observed. After adding 1 wt% NaCl to this dispersion, an emulsion formed (Figure 2.6d) with droplet sizes of 10-60 μm (Figure 2.7d). The color of this emulsion was similar to that of the emulsions stabilized with non-cross-linked and 25 % cross-linked nanoparticles without salt (Figures 2.6a and b), consistent with the similar drop sizes. These bigger oil droplets did not mask the color of the iron oxide to the degree observed for the emulsion with smaller droplet sizes (Figure 2.6c). After 1 day the emulsion stabilized by 100 % cross-linked PAA-coated IO particles with 1 wt% NaCl (Figure 2.6d) was partially resolved. Approximately 60% of the total volume was still emulsion with darker brown color, suggesting growth in the emulsion droplet size. The lower aqueous phase was clear, indicating that the iron oxide particles left this phase and remained adsorbed at the oil/water interface. The emulsion stability is enhanced by strong

adsorption of particles to oil/water interfaces. [34] The low concentration of iron oxide in the lower aqueous phase, indicates a very high interfacial activity of the nanoparticles to coat the large volume of the emulsion droplets. Also, our nanoclusters are porous and consequently occupy a larger area than if they were solid. Thus a smaller mass of nanoclusters is required to cover the oil/water interface and stabilize an emulsion relative to solid particles.

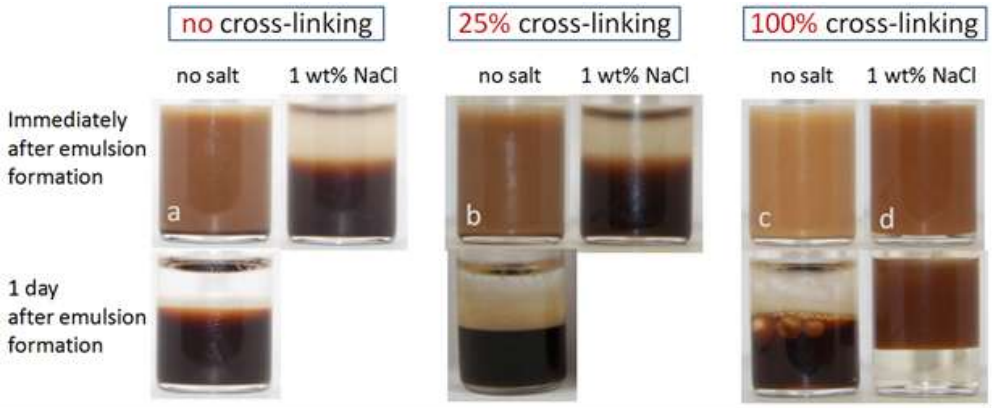

Figure 2.6 Emulsions formed with equal volume fractions of dodecane and aqueous dispersion of 0.14 wt% PAA-coated iron oxide particles with different cross-linking densities at pH8 without salt and with 1 wt% NaCl content. The photos were taken immediately after emulsion formation and after 1 day. The degree of crosslinking is based on the feed amount of crosslinking agent.

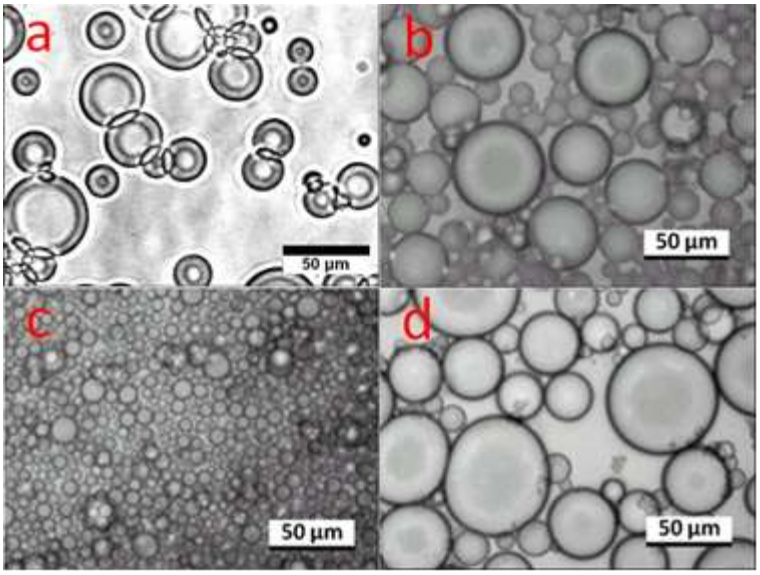

Figure 2.7 Optical micrographs of emulsions formed at conditions in Figure 4. **a**: no cross-linking, no salt; **b**: 25% cross-linking, no salt; **c**: 100% cross-linking, no salt; **d**: 100% cross-linking, 1 wt% NaCl.

The change in interfacial activity indicates that the incorporation of the cross-linking agent in the stabilizer enhances the hydrophobicity of the particles. Higher cross-linking density results in more hydrophobic clusters. The fact that the emulsions without salt did not break completely after 1 day in case of 25 % and 100 % cross-linked particles suggest the more hydrophobic character of the particles compared to the non-cross-linked ones. Without cross-linking the particles were too hydrophilic and did not favor the interface strongly enough to provide stabilization after 1 day. The smaller droplet size in case of the emulsion formed without salt from the dispersion of 100 % cross-linked nanoparticles (Figure 2.6c) also suggests enhanced hydrophobicity. For the 100% nominal cross-linking, the salt drove these less hydrophilic nanoparticles out of the water

phase to the oil-water interface, where they stabilized the emulsion. Thus, the less hydrophilic polymer stabilizer has some characteristics of a copolymer of PAA with a hydrophobic monomer. [4c, 35]

2.4 CONCLUSIONS

The formation of ~100 nm nanoclusters with adsorbed PAA or PSS-*alt*-MA followed by cross-linking leads to permanent polymer shells that pr colloidal stabilization. With the large cluster size and relatively thin polymer shell, the magnetic fraction in the nanocomposite is high, which is important for achieving a strong force on the particle with an external magnetic field. The mesh size of the cross-linked polymer stabilizer shell was well below the size of the nanoclusters, which prohibits diffusion of the iron oxide nanoclusters through the shell at each of the cross-link densities. The cross-linking of adsorbed polymer on the surface of iron oxide nanoparticles provides a shell that is resistant to desorption at a very low concentration down to 0.014 wt%. The lack of desorption is shown by TGA for a wide variety of nominal cross-link densities. The cross-linking produces only a minor perturbation on the thickness of the polymer shell, unlike the case for silylation and other surface modification chemistries, which may result in thick shells that greatly reduce the magnetic fraction of the composite particle. After cross-linking, the zeta potential remains highly negative, and consequently, electrosteric stabilization of the PSS-*alt*-MA-coated nanoparticle dispersions is observed even in 8 wt% NaCl at pH 8. The cross-linking agent, 1,6-hexanediamine, is incorporated in the stabilizer and enhances the hydrophobicity, and thus the activity of the clusters at

the oil/water interface. This synthetic approach is quite general and may be applied to a wide variety of cross-linkable polymer that adsorb on the nanoparticle surface, as has been demonstrated previously for dextran,[14] In this adsorption/cross-linking approach, it is not necessary to use expensive specialty polymers with reactive terminal functional groups. The separation of the synthesis into two steps, the first for formation of iron oxide nanoclusters with an adsorbed polymer stabilizer and second for cross-linking of the stabilizer offers great flexibility for the design of stable dispersions. This cross-linking approach offers important benefits for the formation of inexpensive polymer shells on nanoparticles for large scale applications including magnetomotive imaging of subsurface reservoirs.

2.5 REFERENCES

1. (a) Gupta, A. K.; Gupta, M., Synthesis and surface engineering of iron oxide nanoparticles for biomedical applications. Biomaterials 2005, 26, 3995–4021; (b) Oh, J.; Feldman, M. D.; Kim, J.; Condit, C.; Emelianov, S.; Milner, T. E., Detection of magnetic nanoparticles in tissue using magneto-motive ultrasound. Nanotechnology 2006, 17 (16), 4183-4190; (c) Lattuada, M.; Hatton, T. A., Preparation and Controlled Self-Assembly of Janus Magnetic Nanoparticles. Journal of the American Chemical Society 2007, 129 (42), 12878-12889; (d) Lu, A.-H.; Salabas, E. L.; Schueth, F., Magnetic nanoparticles: synthesis, protection, functionalization and application. Angew. Chem. Int. Ed. 2007, 46, 1222-1244; (e) Ma, L. L.; Feldman, M. D.; Tam, J. M.; Paranjape, A. S.; Cheruku, K. K.; Larson, T. A.; Tam, J. O.; Ingram, D. R.; Paramita, V.; Villard, J. W.; Clarke, G. D.; Jenkins, J. T.; Asmis, R.; Sokolov, K.; Chandrasekar, B.; Milner, T. E.; Johnston, K. P., Small multifunctional nanoclusters (Nanoroses) for targeted cellular imaging and therapy.

ACS Nano 2009, 3, 2686-2696; (f) Satarkar, N. S.; Biswal, D.; Hilt, J. Z., Hydrogel nanocomposites: a review of applications as remote controlled biomaterials. Soft Matter 2010, 6, 2364–2371; (g) Mehrmohammadi, M.; Yoon, K. Y.; Qu, M.; Johnston, K.; Emelianov, S. Y., Enhanced pulsed magneto-motive ultrasound imaging using superparamagnetic nanoclusters. Nanotechnology 2011, 22, 045502.

2. Wu, W.; He, Q.; Jiang, C., Magnetic iron oxide nanoparticles: synthesis and surface functionalization strategies. Nanoscale Research Letters 2008, 3, 397-415.

3. (a) Yu, H.; Kotsmar, C.; Yoon, K. Y.; Ingram, D. R.; Johnston, K. P.; Bryant, S. L.; Huh, C., Transport and retention of aqueous dispersions of paramagnetic nanoparticles in reservoir rocks. 17th SPE Improved Oil Recovery Symposium Tulsa, OK 2010, SPE 129887; (b) Prodanovic, M.; Ryoo, S.; Rahmani, A. R.; Kuranov, R.; Kotsmar, C.; Milner, T. E.; Johnston, K. P.; Bryant, S. L.; Huh, C., Effects of magnetic field on the motion of multiphase fluids containing paramagnetic particles in porous media. 17th SPE Improved Oil Recovery Symposium Tulsa, OK 2010, SPE 129850; (c) Ingram, D. R.; Kotsmar, C.; Yoon, K. Y.; Shao, S.; Huh, C.; Bryant, S. L.; Milner, T.; Johnston, k. P., Superparamagnetic nanoclusters coated with oleic acid bilayers for stabilization of emulsions of water and oil at low loncentration. J. Colloid Interface Sci. 2010, 351, 225-232; (d) Prakash, A.; Zhu, H.; Jones, C. J.; Benoit, D. N.; Ellsworth, A. Z.; Bryant, E. L.; Colvin, V. L., Bylayers as Phase Transfer Agents for Nanocrystals Prepared in Nonpolar Solvents. ACS Nano 2009, 3, 2139-2146.

4. (a) Lan, Q.; Liu, C.; Yang, F.; Liu, S.; Xu, J.; Sun, D., Synthesis of bilayer oleic acid-coated Fe3O4 nanoparticles and their application in pH-responsive Pickering emulsions. J. Colloid Interface Sci. 2007, 310, 260-269; (b) Binks, B. P.; Kirkland, M., Interfacial structure of solid-stabilised emulsions studied by scanning electron microscopy. Phys. Chem. Chem. Phys. 2002, 4, 3727-3733; (c) Saleh, N.; Phenrat, T.; Sirk, K.; Dufour, B.; Ok, J.; Sarbu, T.; Matyjaszewski, K.; Tilton, R. D.; Lowry, G. V., Adsorbed Triblock Copolymers Deliver Reactive Iron Nanoparticles to the Oil/Water

Interface. Nano Letters 2005, 5 (12), 2489-2494; (d) Melle, S.; Lask, M.; Fuller, G. G., Pickering emulsions with controllable stability. Langmuir 2005, 21, 2158-2162.

5. Ryoo, S.; Rahmani, A. R.; Yoon, K. Y.; Prodanovic, M.; Kotsmar, C.; Milner, T. E.; Johnston, K. P.; Bryant, S. L.; Huh, C., Theoretical and experimental investigation of the motion of multiphase fluids containing paramagnetic nanoparticles in porous media. SPE Annual Meeting, Florence, Italy 2010, SPE 134879.

6. (a) Rodriguez, E.; Roberts, M. R.; Yu, H.; Huh, C.; Bryant, S. L., Enhanced migration of surface-treated nanoparticles in sedimentary rocks. SPE Annual Technical Conference and Exhibition, New Orleans, LA, USA 2009, SPE 124418; (b) Golas, P. L.; Lowry, G. V.; Matyjaszewski, K.; Tilton, R. D., Comparative Study of Polymeric Stabilizers for Magnetite Nanoparticles Using ATRP. Langmuir 2010, 26, 16890–16900; (c) Saleh, N.; Kim, H.-J.; Phenrat, T.; Matyjaszewski, K.; Tilton, R. D.; Lowry, G. V., Ionic strength and composition affect the mobility of surface-modified Fe0 nanoparticles in water-saturated sand columns. Environ. Sci. Technol. 2008, 42, 3349-3355.

7. (a) Moeser, G. D.; Roach, K. A.; Green, W. H.; Laibinis, P. E.; Hatton, T. A., High-gradient magnetic separation of coated magnetic nanoparticles. AIChE Journal 2004, 50, 2835-2848; (b) Ditsch, A. P.; Lindemann, S.; Laibnis, P. E.; Wang, D. I. C.; Hatton, T. A., High-gradient magnetic separation of magnetic nanoclusters. Ind. Eng. Chem. Res. 2005, 44, 6824-6836; (c) Gerber, R.; Birss, R. R., High Gradient Magnetic Separation. Research Studies Press: London, 1983.

8. Arkles, B., Tailoring surfaces with silanes. Chem. Tech. 1977, 7, 766-770.

9. De Palma, R.; Peeters, S.; Van Bael, M. J.; Van den Rul, H.; Bonroy, K.; Laureyn, W.; Mullens, J.; Borghs, G.; Maes, G., Silane Ligand Exchange to Make Hydrophobic Nanoparticles Water-Dispersible. Chem. Mater. 2007, 19, 1821-1831.

10. Shen, L.; Stachowiak, A.; Hatton, A. T.; Laibnis, P. E., Polymerization of olefin-terminated surfactant bilayers on magnetic fluid nanoparticles. Langmuir 2000, 16, 9907-9911.

11. Hong, R. Y.; Pan, T. T.; Han, Y. P.; Zhang, S. Z.; Li, H. Z.; Ding, J., Graft polymerization synthesis and application of magnetic Fe3O4/polyacrylic acid composite nanoparticles. J. Appl. Polym. Sci. 2007, 106, 1439-1447.

12. (a) Chen, D.-H.; Huang, S.-H., Fast separation of bromelain by polyacrylic acid-bound iron oxide magnetic nanoparticles. Process Biochemistry 2004, 39, 2207-2211; (b) Liao, M.-H.; Chen, D.-H., Preparation and characterization of a novel magnetic nano-adsorbent. J. Mater. Chem. 2002, 12, 3654-3659.

13. Lin, C.-L.; Lee, C.-F.; Chiu, W.-Y., Preparation and properties of poly(acrylic acid) oligomer stabilized superparamagnetic ferrofluid. J. Colloid Interf. Sci. 2005, 291, 411-420.

14. (a) Wang, Y.-X. J.; Hussain, S. M.; Krestin, G. P., Superparamagnetic iron oxide contrast agents: physicochemical characteristics and applications in MR imaging. Eur. Radiol. 2001, 11, 2319-2331; (b) Wunderbaldinger, P.; Josephson, L.; Weissleder, R., Crosslinked iron oxide (CLIO): a new platform for the development of targeted MR contrast agents. Acad. Radiol. 2002, Suppl 2 (S), 304-306.

15. Dresco, P. A.; Zaitsev, V. S.; Gambino, R. J.; Chu, B., Preparation and Properties of Magnetite and Polymer Magnetite Nanoparticles. Langmuir 1999, 15, 1945-1951.

16. Lee, H.; Yu, M. K.; Park, S.; Moon, S.; Min, J. J.; Jeong, Y. Y.; Kang, H.-W.; Jon, S., Thermally cross-linked superparamagnetic iron oxide nanoparticles: synthesis and application as a dual imaging probe for cancer in vivo. J. Am. Chem. Soc. 2007, 129, 12739-12745.

17. Turner, J. L.; Pan, D.; Plummer, R.; Chen, Z.; Whittaker, A. K.; Wooley, K. L., Synthesis of gadolinium-labeled shell-crosslinked nanoparticles for magnetic resonance imaging applications Adv. Funct. Mater. 2005, 15, 1248-1254.

18. Huang, H.; Kowalewski, T.; Remsen, E. E.; Gertzmann, R.; Wooley, K. L., Hydrogel-coated glassy nanospheres: a novel method for the synthesis of shell cross-linked knedels. J. Am. Chem. Soc. 1997, 119, 11635-11659.

19. Kim, B.-S.; Taton, A., Multicomponent Nanoparticles via Self-Assembly with Cross-Linked Block Copolymer Surfactants. Langmuir 2007, 23, 2198-2202.

20. Zhang, T.; Ge, J.; Hu, Y.; Yin, Y., A general approach for transferring hydrophobic nanocrystals into water. Nano Letters 2007, 7 (10), 3203-3207.

21. Ge, J.; Hu, Y.; Biasini, M.; Beyermann, W. P.; Yin, Y., Superparamagnetic magnetite colloidal nanocrystal clusters. Angew. Chem. Int. Ed. 2007, 46, 4342-4345.

22. (a) Ditsch, A.; Laibinis, P. E.; Wang, D. I. C.; Hatton, T. A., Controlled Clustering and Enhanced Stability of Polymer-Coated Magnetic Nanoparticles. Langmuir 2005, 21 (13), 6006-6018; (b) Sondjaja, R.; Hatton, A. T.; Tam, M. K. C., Clustering of magnetic nanoparticles using a double hydrophilic block copolymer, poly(ethylene oxide)-b-poly(acrylic acid). J. Magn. Magn. Mat. 2009, 321, 2393-2397.

23. (a) Massart, R., Preparation of aqueous magnetic liquids in alkaline and acidic media. IEEE Trans. Magn. 1981, 17, 1247-1248; (b) Lyon, J. L.; Fleming, D. A.; Stone, M. B.; Schiffer, P.; Williams, M. E., Synthesis of Fe oxide core/Au shell nanoparticles by iterative hydroxylamine seeding. Nano Letters 2004, 4, 719-723.; (c) Sahoo, Y.; Goodarzi, A.; Swihart, M. T.; Ohulchanskyy, T. Y.; Kaur, N.; Furlani, E. P.; Prasad, P. N., Aqueous ferrofluid of magnetite nanoparticles: fluorescence labeling and magnetophoretic control. J. Phys. Chem. B 2005, 109, 3879–3885; (d) Massart, R.;

Dubois, E.; Cabuil, V.; Hasmonay, E., Preparation and properties of monodisperse magnetic fluids. Journal of Magnetism and Magnetic Materials 1995, 149, 1-5.

24. Peppas, N. A.; Bures, P.; Leobandung, W.; Ichikawa, H., Hydrogels in pharmaceutical formulations. European Journal of Pharmaceutics and Biopharmaceutics 2000, 50, 27-46.

25. Ryoo, W.; Webber, S. E.; Johnston, K. P., Water-in-Carbon Dioxide Microemulsions with Methylated Branched Hydrocarbon Surfactants. Ind. Eng. Chem. Res. 2003, 42, 6348-6358.

26. Tam, J. M.; Murthy, A. K.; Ingram, D. R.; Nguyen, R.; Sokolov, K. V.; P., J. K., Kinetic assembly of near-IR active gold nanoclusters using weakly adsorbing polymers to control size. Langmuir 2010, 26, 8988-8999.

27. Hiemenz, P. C.; Rajagopalan, R.; Editors, Principles of Colloid and Surface Chemistry, Third Edition, Revised and Expanded. Marcel Dekker Inc.: New York, 1997; p 688 pp.

28. Sehgal, A.; Lalatonne, Y.; Berret, J.-F.; Morvan, M., Precipitation-redispersion of cerium oxide nanoparticles with poly(acrylic acid): towards stable dispersions. Langmuir 2005, 21, 9359-9364.

29. (a) Santra, S.; Kaittanis, C.; Grimm, J.; Perez, M., Drug/dye-loaded, multifunctional iron oxide nanoparticles for combined targeted cancer therapy and dual optical/magnetic resonance imaging. Small 2009, 5 (16), 1862-1868; (b) Mak, S.-Y.; Chen, D.-H., Binding and sulfonation of poly(acrylic acid) on iron oxide nanoparticles: a novel, magnetic, strong acid cation nano-adsorbent. Macromol. Rapid. Commun. 2005, 26, 1567-1571.

30. (a) Euliss, L. E.; Grancharov, S. G.; O'Brien, S.; Deming, T. J.; Stucky, G. D.; Murray, C. B.; Held, G. A., Cooperative assembly of magnetic nanoparticles and block

copolypeptides in aqueous media. nano Letters 2003, 3, 1489-1493; (b) Kim, B.-S.; Qiu, J.-M.; Wang, J.-P.; Taton, T. A., Magnetomicelles: composite nanostructures from magnetic nanoparticles and cross-linked amphiphilic block copolymers. Nano Letters 2005, 5, 1987-1991; (c) Zheng, W.; Gao, F.; Gu, H., Magnetic polymer nanospheres with high and uniform magnetite content. J. Magn. Magn. Mater. 2005, 288, 403-410.

31. Fritz, G.; Schadler, V.; Willenbacher, N.; Wagner, N. J., Electrosteric Stabilization of Colloidal Dispersions. Langmuir 2002, 18, 6381-6390.

32. Reith, D.; Muller, B.; Muller-Plathe, F.; Wiegand, S., How does the chain extension of poly „acrylic acid… scale in aqueous solution? A combined study with light scattering and computer simulation. Journal of Chemical Physics 2002, 116, 9100-9106.

33. Binks, B. P.; Lumsdon, S. O., Transitional phase inversion of solid-stabilized emulsions using particle mixtures. Langmuir 2000, 16, 3748-3756.

34. Binks, B. P., Particles as surfactantssimilarities and differences. Current Opinion in Colloid and Interface Science 2002, 7, 21-41.

35. Wan, S.; Zheng, Y.; Liu, Y.; Yan, H.; Liu, K., Fe3O4 Nanoparticles coated with homopolymers of glycerol mono(meth)acrylate and their block copolymers. J. Mater. Chem. 2005, 15, 3424-3430.

Chapter 3: Stable Citrate Coated Iron Oxide Superparamagnetic Nanoclusters at High Salinity

Superparamagnetic nanoclusters may be used in imaging in biomedicine and in mapping of petroleum reservoirs, by generating either ultrasonic or acoustic signals with oscillating magnetic motion. For a given magnetization per weight of iron oxide, nanoclusters with diameters from 20 to 100 nm experience a much larger magnetic force than that of the primary sub- 10 nm primary particles. Aqueous dispersions of 0.1 wt% superparamagnetic iron oxide nanoclusters were stabilized with citric acid on the particle surface, with a high loading of 90% iron oxide. The dispersions were stable for months even with high salt concentrations up to 4 wt% at pH6 and pH8 based on the hydrodynamic diameter from dynamic light scattering. The citrate ligands provide electrostatic repulsion, as characterized by the zeta potential. The small size of the clusters, superparamagnetic properties, and high salt tolerance are highly beneficial in various applications including mapping of petroleum reservoirs with magnetomotive techniques.

3.1 INTRODUCTION

Iron oxide nanoparticles (NPs) consisting of magnetite (Fe_3O_4) or maghemite (γ-Fe_2O_3) have been studied extensively for applictions in many fields including microelectronics and biomedical imaging.[1,2] Nanoparticles may be utilized for mobility

control in improved oil recovery[3], and CO_2-enhanced oil recovery/CO_2 sequestration.[4] Recently, we have proposed that aqueous magnetic nanoparticle dispersions may be used as imaging agents for the detection and visualization of various phases and interfaces in oil reservoirs, by generation acoustic waves via motion of the nanoparticles in a magnetic field[5]. In this application, the particles should be superparamagnetic, salt tolerant, and small enough for transport through porous rock with pores on the order of 10 μm, or in some cases even smaller pores. In contrast, it can be difficult to prevent aggregation of ferromagnetic NPs as a result of magnetic forces. The high salinities in oil reservoirs can make it challenging to stabilize the nanoparticles against aggregation.

In a magnetic field the force (F_m) acting on a magnetic particle depends on the volume of the particle V_p and the magnetic field gradient according to [6]

$$F_m = -\mu_0 V_P M_P \nabla H \qquad (1)$$

where M_P is its magnetization in a given field (H) and μ_0 is the permeability of free space.[7] Ditsch et al. [7] and Moeser et al. [8] captured magnetic nanoclusters 50 nm or larger with a high-gradient magnetic separation (HGMS)[9] technique, given the large values of V_p and M_p.

For magnetic iron oxide NPs formed by co-precipitation of Fe-salts in alkaline solution[10], the typical size of the nucleated primary particles ranges between 3 and 10 nm. To stabilize the particles in the dispersion, various surface coatings including polymers[7], surfactants[11] or small polar molecules including citric acid (CA)[12] have been used.

Phillipse et al. observed formation of clusters from iron oxide NPs immediately after nucleation by co-precipitation of iron-salts in pH 13 tetramethylammonium hydroxide (TMAOH) solution. SAXS experiments showed 26 nm clusters formed from ~ 10 nm primary particles.[13] Ditsch et al. used random copolymers of acrylic acid, styrenesulfonic acid, and vinylsulfonic acid to coat iron oxide to control the size of the resulting nanoclusters. By choosing two different polymers to coat the particles, approximately 74 nm sized stable clusters could be formed [7]. Berret et al. [14] were able to control clustering of maghemite (γ-Fe_2O_3) by using poly(trimethylammonium ethylacrylate methyl sulfate)-*b*-poly-acrylamide), with different molecular weights. The size of the clusters observed by dynamic light scattering and transmission electron microscopy ranged from 20 to 200 nm. Kinetically controlled, near-IR active, gold-coated iron oxide nanoclusters were synthesized from a dispersion of iron oxide nanoparticles, and utilized for biomedical applications. [15]

In contrast with polymeric stabilizers, small ligands including the citrate ion may be used to stabilize iron oxide NPs in aqueous dispersions with very thin stabilizing shells. Here, the mass fraction of inorganic iron oxide relative to the total mass can be much larger. Two of the carboxylate functionalities chemisorb to the Fe atoms.[12b, 12d] Above around pH4, the negatively charge surface provides electrostatic stabilization.[12a] To our knowledge the effect of salinity on dispersions of citrate-coated iron oxide NPs has not been reported.

Increasing the salt concentration can lead to loss of steric or electrostatic stabilization and result in aggregation of nanoparticle dispersions.[16] The salt reduces the

thickness of the diffuse electric double layer and weakens electrostatic repulsion.[17] For pharmaceutical nanoparticles stabilized with PEO/PPO/PEO triblock copolymer, the addition of 0.25 M Na_2SO_4 lowered the solvation of the PEO groups, leading to flocculation near the phase boundary for the polymer.[16] However, iron oxide NPs stabilized with amphiphilic copolymers containing polyethylene glycol (PEG) were stable in up to 2 M NaCl solutions.[18] For iron oxide NPs stabilized with an adsorbed oleic acid bilayer, aggregation and sedimentation occurred above 250 mM NaCl.[19] Ditsch et al. [7] produced dispersions of iron oxide with extremely high salt tolerance (5M NaCl) by using random copolymers of acrylic acid, styrenesulfonic acid, and vinylsulfonic acid. Transport of zerovalent iron nanoparticles through porous media in solutions with various Na^+ and Ca^{2+} concentrations was studied by Saleh et al.[20] The NPs were coated with poly(methacrylic acid)-*b*-(methyl methacrylate)-*b*-(styrene sulfonate) triblock copolymer (PMAA-PMMA-PSS), with polyaspartate and with sodium dodecyl benzene sulfonate (SBDS). It was found that the PMAA-PMMA-PSS-coated particles were the most resistant to deposition on the surface of sand grains, in the presence of 4 M Na^+ and over 100 mM Ca^{2+}.The high stability of the NPs was caused by the electrosteric stabilization provided by the triblock copolymer.

The objective of this study was to synthesize stable dispersions of sub-100 nm superparamagnetic iron oxide nanoclusters with high inorganic loadings >90%, controllable size and high salt tolerance. The diameter of the iron oxide primary particles produced by co-precipitation of iron-chloride salts in aqueous alkaline media ranged from 3-10 nm.[10] The size of nanoclusters of these primary particles was lowered by adsorbing

citrate ions to increase electrostatic repulsion. The size of the clusters was examined by DLS and TEM upon changing the salinity and pH, initially and after three weeks. In addition the zeta potential was determined. It was not necessary to utilize templating agents such as polymers to control the cluster size. Application of an external magnetic field on nanoclusters adsorbed on oil-water interfaces produces an external force resulting in mechanical displacement that can serve as a diagnostic signal. The larger volume of the clusters, relative to the primary nanoparticles is beneficial for increasing the magnetic force on the particles. The magnetization per gram of Fe for the clusters and for the primary particles was similar, indicating a lack of magnetic coupling between the primary particles as seen previously.[15, 21] The large adsorption of the citrate coating is shown to produce a large surface charge.[12] We show that the surface charge on the particles is sufficient even at high salinities up to 4 wt% (680 mM) NaCl at certain pH values to maintain stable nanoclusters. The ability to form stable superparamagnetic nanoclusters at high salinities with a large V_p is beneficial for achieving a strong magnetic force to move the nanoparticles and generate an acoustic signal of interest in magnetomotive acoustic imaging of oil reservoirs and reservoirs of interest in CO_2 sequestration. The citrate coating and the small size of the nanoclusters is shown to reduce retention during transport through negatively charged porous sandstone and limestone media including subsurface reservoirs.

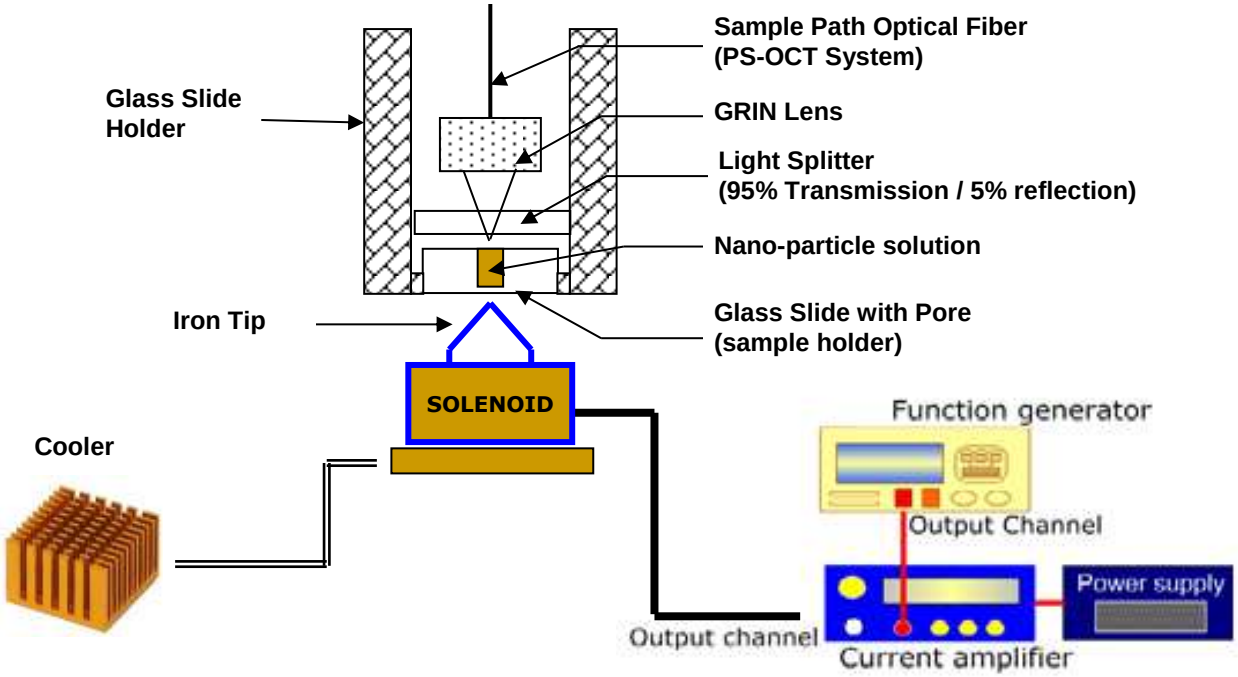

Figure 3.1 Schematic diagram of phase sensitive optical coherence tomograph (PS-OCT) setup.

3.2 Experimental Details

3.2.1 Materials

Ferrous chloride tetrahydrate ($FeCl_2 \cdot 4H_2O$; MW=198.81 g; catalog number: I90-500), ferric chloride hexahydrate ($FeCl_3 \cdot 6H_2O$; MW=270.32 g; catalog number: I88-100), citric acid monohydrate (CA; MW=210.14 g; catalog number: A 104-500) and sodium chloride (NaCl, MW=58.44 g; catalog number: S671-3) were purchased from Fisher Scientific, USA. Tetramethylammonium hydroxide pentahydrate, 99% (TMAOH; MW=181.23 g; catalog number: AC420535000) was purchased from Acros Organics, USA. Hydrochloric acid (HCl; MW=36.46 g; catalog number: UN1789) and sodium

hydroxide (NaOH; MW=40 g; catalog number: UN1823) were purchased from EM Science, Germany.

3.2.2 Nanoparticle synthesis and nanocluster formation

The Fe_3O_4 NPs were prepared by coprecipitation of Fe(II) and Fe(III) chlorides (Fe^{II}/Fe^{III} ratio of 0.5) in an alkaline solution. [10, 12c] Briefly, 10 ml 0.05 M $FeCl_2$ and 0.1 M $FeCl_3$ solution were added drop wise to 40 ml 1 M NaOH solution to hydrolyze the iron chlorides [22] while stirring vigorously for 30 minutes with a magnet. A black gel-like precipitate was collected on a magnet, washed twice with H_2O and twice with 0.1 M TMAOH solution. [13] The particles formed aggregates and settled in the solution. Then the particles were centrifuged (Eppendorf Centrifuge 5810) at 6000 rpm (~1300 g-force) for 5 minutes and were redispersed with probe sonication (Branson Sonifier® S-450A) in pH10 TMAOH solution. At this point, the particle dispersion was stable for weeks, without aggregation.

3.2.3 Addition of citrate stabilizer

The particle dispersion was mixed with 20 mg/ml CA solution such that the overall pH was 5 and stirred for 90 minutes at 90 ºC. At these pH values at least two carboxyl groups of the CA molecule were dissociated and formed a carboxylate complex with the Fe atoms of the particle surface.[12a] Then the solution was cooled to room temperature and the pH was adjusted to 7 by using 30 wt% TMAOH solutions. Here the third carboxylic group of the citrate dissociated, and provided electrostatic stabilization of

the dispersion. After probe sonication, approximately 20% of the large iron oxide aggregates were removed and discarded from the dispersion by centrifugation (6000 rpm for 5 min). The supernatant was then subjected to a second centrifugation to remove the excess citrate by using filter centrifuge tubes (Ultracel 30K, 30,000 MWCO, Millipore Co.). The resulting clusters were redispersed in 40 mL deionized (DI) water by bath sonication. Then the pH was adjusted to the desired value by using 30 wt% TMAOH solution or 0.1 M HCl. The iron content of the dispersions was ~1.0 mg Fe/mL and was determined using flame atomic absorption spectroscopy (FAAS).

3.2.4 Nanocluster characterization

Dynamic light scattering (DLS) analysis was performed on a custom-built apparatus and the data were analyzed using a digital autocorrelator (Brookhaven BI-9000AT) and a non-negative least-squares (NNLS) routine (Brookhaven 9KDLSW32) [23]. The scattering angle was set to 90º. The suspension concentration was 0.05 mg/mL which gave a measured count rate of approximately 200 kcps. Measurements were made over a period of 2 min at least three times on each sample.

Zeta potential measurements were performed in triplicate on the ZetaPlus dynamic light scattering apparatus (Brookhaven Instruments) at 90° scattering angle and temperature of 25 °C.

Transmission electron microscopy (TEM) was used to observe the morphology of nanoclusters. The experiments were performed on a FEI TECNAI G2 F20 X-TWIN TEM using a high-angle annular dark field detector. The samples were prepared using a “flash-

freezing" technique, in which a 200 mesh carbon-coated copper TEM grids were cooled using liquid nitrogen and then dipped into dilute aqueous nanocluster dispersion. 24 The sample was immediately dried using a Virtis Advantage Tray Lyophilizer (Virtis Company, Gardiner, NY) with 2 hours of primary drying at -40^{o}C followed by a 12 hour ramp to +25^{o}C and then 2 hours of secondary drying at 25^{o}C. In this manner the aggregation of NPs caused by capillary forces during evaporation of the liquid on the TEM grid could be avoided.

Thermo gravimetric analysis (TGA) was used to determine the amount of adsorbed citrate ligand mass on the iron nanoclusters. The experiments were performed using a Perkin–Elmer TGA 7 under nitrogen atmosphere at a gas flow rate of 20 mL/min. Excess, unadsorbed citrate ions were separated from the particles by filter centrifugation. After collection of the particles were dried to a powder. The powder samples were held at 100°C for 120 minutes to remove the remained water in the sample and then heated at a constant rate of 20 °C/min from 100°C to 800 °C and held at 800°C for 30 minutes. The loss in mass after heating accounted for the organic component of the particles.

Flame atomic absorption spectroscopy (FAAS) was used to determine the iron concentration in the dispersion by using a GBC 908AA flame atomic absorption spectrometer (GBC Scientific Equipment Pty Ltd). All measurements were conducted at 242.8 nm using an air-acetylene flame.

Superconducting quantum interference device or SQUID magnetometer (Quantum Design MPMS) was used to measure the normalized saturation magnetization of the particles at 300 K.

Phase sensitive optical coherence tomography (PS-OCT) was used to measure the displacement of an air-solution interface in response to an applied magnetic field. PS-OCT is an optical technique that is able to detect depth resolved picometer-scale optical path length change in samples 25. Samples were pipetted from a 0.1wt% colloidal nano-particle solution and put into the sample holder (diameter: 2 mm, depth: 0.65 mm) and PS-OCT light was focused on the center of the sample holder (Figure 3.1). The tip of the solenoid coil was located just below the sample holder and driven by a function generator with high power audio amplifier to produce a zero-offset sinusoidal current(f=2Hz) to produce an oscillating magnetic field. Immediately after application of the magnetic field, displacement of the air/water interface was measured by PS-OCT over a 4-second time period.

Core flood experiments were performed to study the transport of nanoparticles through porous media.[26] For the experiments two types of sedimentary rocks were used: Boise sandstone and Texas cream limestone. The experimental set-up for the core floods is schematically shown in Figure 3.2. It consists of a Hassler core holder which confines the core within a cylindrical sleeve, ensuring that flow occurs only through the core, an injection pump, a pressure transducer (measuring difference between inlet and outlet pressure), and a fraction collector for effluent samples. The pump injects fluid into an accumulator containing a movable piston with the nanoparticle dispersion on the other side. In this manner, the dispersion is displaced into the core without contacting the internal workings of the pump. A prescribed volume of the nanoparticle dispersion was injected into the core. The injectant bank was displaced using nanoparticle-free water

(with the same pH value and salinity as the nanoparticle dispersion). The flow rate was checked by weighing effluent samples. The cores were one-inch in diameter and three-inch in length. Prior to the experiments the cores were dried for more than ten days and weighted in air, then vacuumed for twenty-four hours and saturated with water (having the same pH with the nanoparticle dispersion) and weighted again. Porosity (Φ) was calculated by the weight difference and the core dimensions. Before injection of the nanoparticle dispersion, the constant-rate injection of water was carried out to obtain the permeability of the core (K), calculated by Darcy's law.

UV-visible Spectroscopy was employed to determine the nanoparticle concentration in the core flood effluent samples with a Varian Cary 5000 spectrophotometer for a 1 cm path length. The reference dispersions and core flood effluents were diluted using DI water, adjusted to the pH value of the nanoparticle dispersion. For each nanoparticle dispersion, the absorption relative to reference solutions were measured between 400 and 410 nm. Thereafter, the retention was calculated by a mass balance upon integrating the normalized effluent concentration curve.

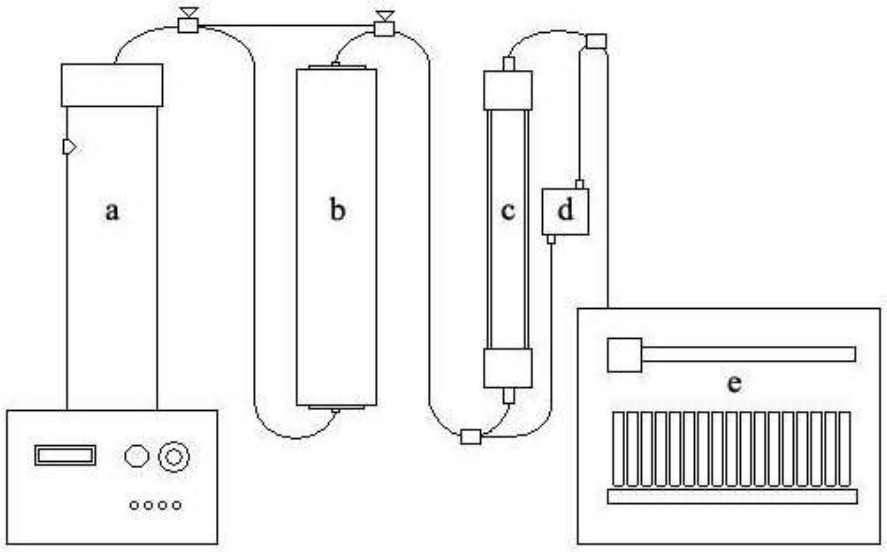

Figure 3.2 Schematic representation of coreflood set-up to determine the transport of nanoparticles through porous media. (a) syringe pump, (b) accumulator (contains nanoparticle dispersion on downstream side of internal piston), (c) coreholder, (d) transducer, and (e) sample collector.

3.3 RESULTS

3.3.1 Clustering of NPs before adding citrate

The iron oxide dispersions were studied with TEM and DLS in pH10 TMAOH solution, before adding the citrate coating. The results suggest that the particles form clusters immediately during the synthesis by co-precipitation of iron salts. On Figure 3.3 the TEM micrograph reveals nanoclusters of primary particles ranging from 3 to 10 nm, which is common in case of co-precipitation of iron-chloride salts in alkaline media.[10, 12a-c] The observed morphology is open, loosely flocculated 40 to 60 nm size clusters of the particles in pH10 TMAOH solution. During "flash-freezing" to prepare the TEM sample, it is possible that the clusters underwent changes. Thus, DLS was utilized to determine

the hydrodynamic diameter *in-situ* without potentially perturbing the morphology. The reproducibility in the volume distribution of the nanoparticles is given in the histograms shown in Figure 3.4 for NP dispersions in pH10 TMAOH solution. Each sample was prepared at identical conditions. Relatively narrow peaks can be observed between 40 and 65 nm indicating the process of cluster formation was controllable at these conditions. The sizes of the nanoclusters by TEM are in agreement with the DLS data, indicating the flash freezing technique was successful. At this pH in the TMAOH solution the dispersed clusters are stabilized by their high negative surface charge.[10] The centrifugation and probe sonication after the initial particle synthesis were important steps for producing the relatively uniform nanoclusters. At lower pH values (pH8 and 9) in TMAOH solution, the dispersions were only stable for a few hours. The point of zero charge of iron oxide is at ~ pH 7. The smaller number of negative charges on the iron oxide surface at pH8 and pH9 compared to pH 10 appeared to provide insufficient electrostatic repulsion to counteract the attraction and aggregation caused by VDW forces between the clusters.

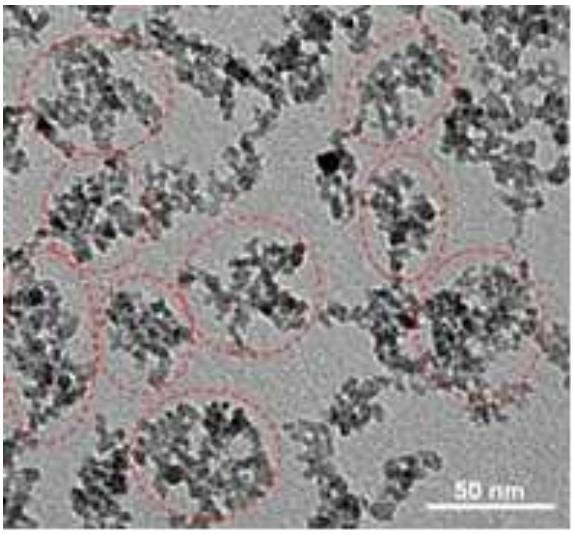

Figure 3.3 TEM image of iron oxide nanoclusters before adding citrate stabilizer to the dispersion, in TMAOH solution at pH10. The circles with dashed line are guides for the eye.

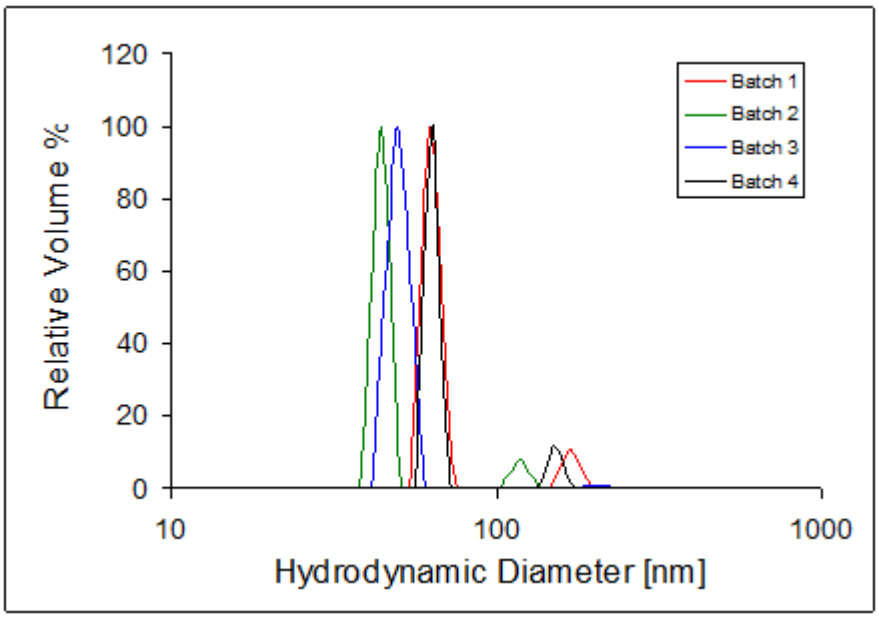

Figure 3.4 DLS measurements on clusters of 0.1 wt% iron oxide NPs before adding citrate stabilizer to the dispersion, in pH10 TMAOH solution from four different syntheses.

3.3.2 Dispersions stabilized with citrate and particle/cluster sizing

Figure 3.5 shows photos of the dispersions containing 0.1 wt% (0.017M) synthesized magnetic NPs after purification (excess citrate removed with filter centrifugation). The salinity tests were carried out in the range from 0.1 wt% (0.017M, Debye length: 2.33 nm) to 4 wt% (0.683M, debye length: 0.3.67 nm) NaCl. The particles at pH 6 (Figure 3.5a) and pH 8 (Figure 3.5b) are well dispersed in water. The dispersions were stable against settling at high salinities for at least 2 months at pH8 and for 3 months at pH6 even up to 3.5 wt% NaCl. The particles at pH10 did not tolerate salt to the extent observed at lower pH values, for example, the dispersions are stable for weeks with only 0.1 wt% NaCl (Figure 3.5c). In this case change in the intensity of the color of the dispersion or settling were negligible, which suggests minimal aggregation. With 0.5 wt% added NaCl at pH10 (Figure 3.5d) the particles sediment. Here, the solution has a light brownish color indicating that only small amount of particles remained dispersed in the water phase. A gel-like precipitate was observed on the bottom of the vial. At 1 wt% NaCl (Figure 5e), the particles completely settled after about 5 minutes, and the solution above the precipitate was transparent. The particles were not redispersable with probe sonication.

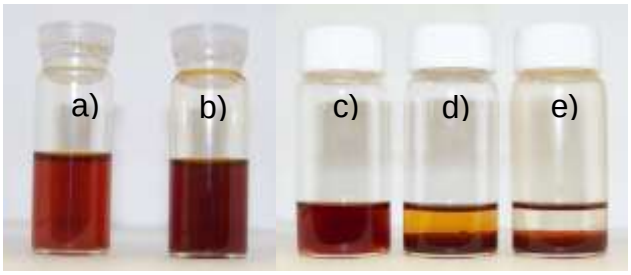

Figure 3.5 Pictures of 0.1 wt% iron oxide NP dispersions immediately after formation, stabilized with citrate at pH 6 and 3.5 wt% NaCl (a) at pH 8 and 3.5 wt% NaCl (b), at pH10 and 0.1 wt% NaCl (c), pH10 and 0.5 wt% NaCl (d) and at pH10 and 1 wt% NaCl (e). The appearance of the dispersions didn't change over 8 weeks.

The effect of salt on the particle clustering at different pH values was studied by dynamic light scattering, as shown in Figures 3.6 and 3.7 at pH 6 and 8, respectively at different salinities. Without added salt, the hydrodynamic diameter was ~ 13 nm at pH 6 and ~ 12 nm at pH 8, At pH10 the measured size of the clusters without salt was around 9 nm. These sizes are much smaller, between 9 and 13 nm, compared to the clusters without citrate coating at pH10 TMAOH solution shown in Figures 3.3 and 3.4, which were between 40 and 65 nm. The adsorption of citrate on the particle surfaces led to deaggregation of the larger clusters. Figure 3.8 summarizes average D_{50} values (50% of the clusters by volume are below this diameter) of the citrate coated iron oxide nanoclusters versus salinity at pH values of 6; 8 and 10. At pH 6 (Figures 3.6 and 3.8), the hydrodynamic diameters with added citrate changed only a small amount with added salt, demonstrating highly effective stabilization. In Figure 3.7 at pH 8, the cluster size increases with salinity, unlike the case at pH 6. A small amount of NaCl, 0.1 wt%, caused

a relatively large jump in the cluster size to 48 nm. The cluster growth continues more gradually with increasing salinity reaching 92 nm. Upon adding 0.1 wt% NaCl a pH 10 the size reached 500 nm (not shown), indicating a large loss in stability.

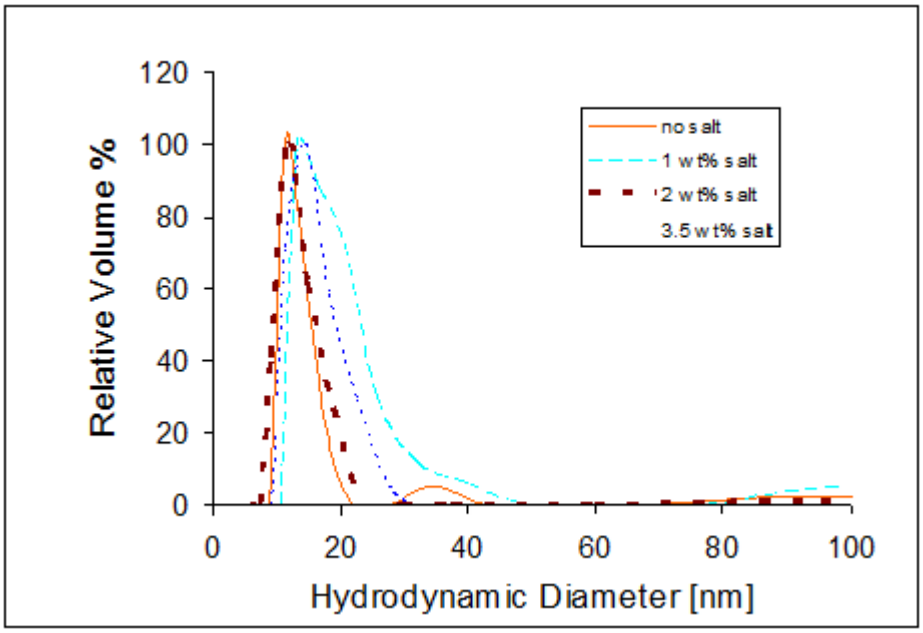

Figure 3.6 Volume fraction based distributions of citrate coated iron oxide NPs at pH6 with different salinities, measured with DLS.

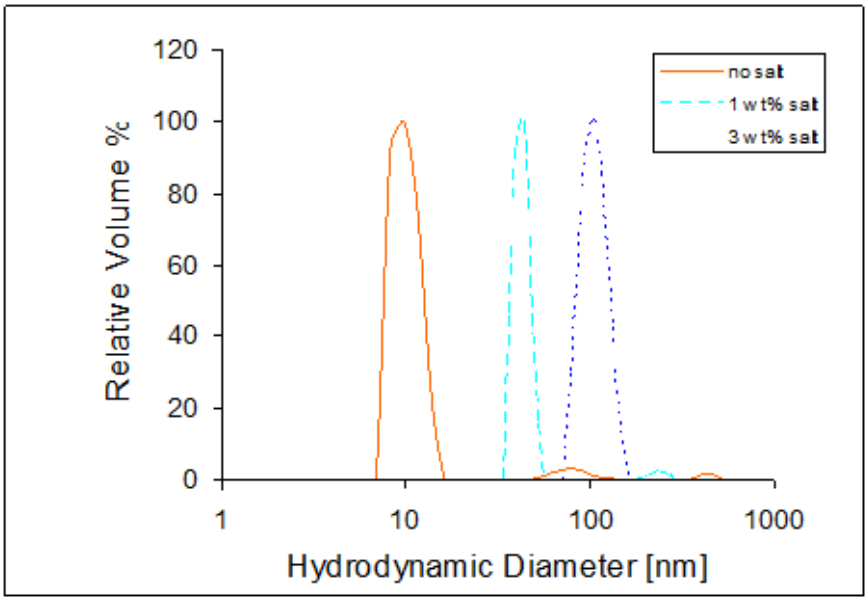

Figure 3.7 Volume fraction based distributions of citrate coated iron oxide NPs at pH8 with different salinities, measured with DLS.

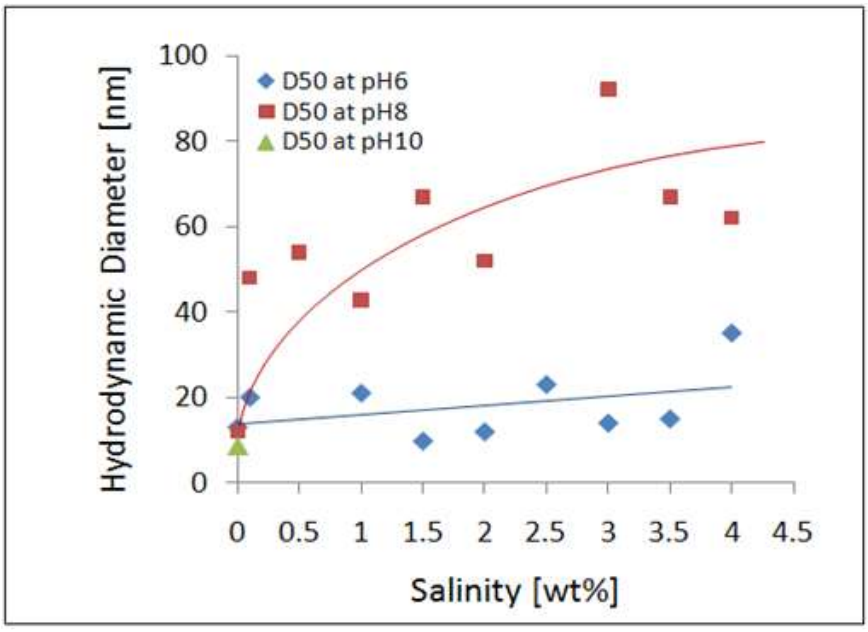

Figure 3.8 Hydrodynamic diameters (D50) of iron oxide nanoclusters stabilized with citrate determined with dynamic light scattering right after their formation, as a function of salinity at pH6 (♦), at pH8 (■) and at pH10 (▲). The lines are guides for the eye.

Figure 3.9a presents TEMs of the clusters formed in pH8 solution without salt. Many of the clusters were very small, consistent with the DLS value of 12 nm. Some of the larger aggregates may have been formed during the sample preparation. Furthermore the hydrodynamic diameter will be smaller than the geometric diameter from TEM, as the drag force for the cluster will be smaller than for a solid sphere given the somewhat open structure. In Figure 3.9b for the sample at pH8 with 1.5 wt% NaCl, the nanocluster is covered with a salt crystal, which formed on the TEM grid during drying. The size of the nanocluster is larger compared to the clusters formed at pH8, without salt, consistent with DLS (Figure 3.9a).

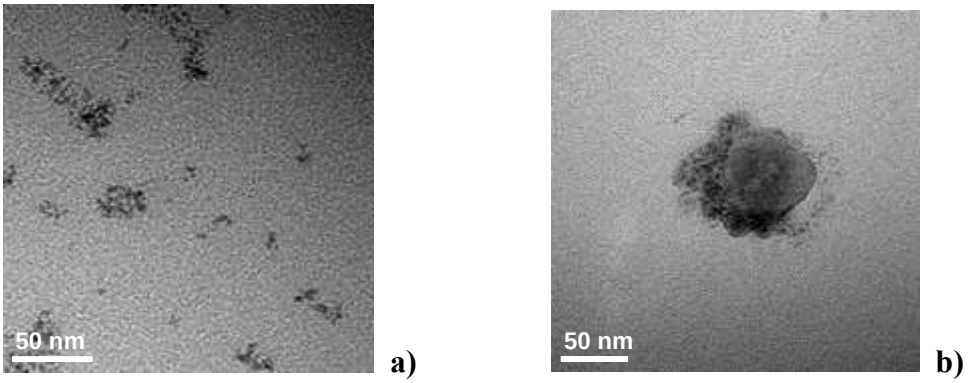

Figure 3.9 TEM images of iron oxide nanoclusters stabilized with citrate at pH 8 (**a**) and at pH8 + 1.5 wt% NaCl (**b**).

The stability of the clusters stored for three weeks in solution at 0.1 wt% NP concentration was analyzed with DLS. In Figure 3.10 the solid symbols represent the

sizes of the clusters 3 weeks after, the open symbols immediately after dispersion formation for various pH values and salinities. Without added salt, after 3 weeks the average D_{50} values were between 9 and 13 nm at all three pH values, essentially the same as for the initially formed clusters (see also Figure 3.8), indicating very effective stabilization. The changes after three weeks with added salt were very interesting in that the sizes decreased from the original values. At pH6 and 4 wt% salinity, the size decreased from 35 nm to 13 nm. With 2 wt% salt the size didn't change remarkably. In case of pH8 the size of the clusters increases with increasing salinity, as it was observed initially (Figure 3.8), but to a smaller extent. After 3 weeks the average cluster sizes measured for 2 and 4 wt% salinities were about the half as it was observed initially. The mechanism for shrinkage of the clusters with time is unclear, but may involve reorganization of counterions on the particles.

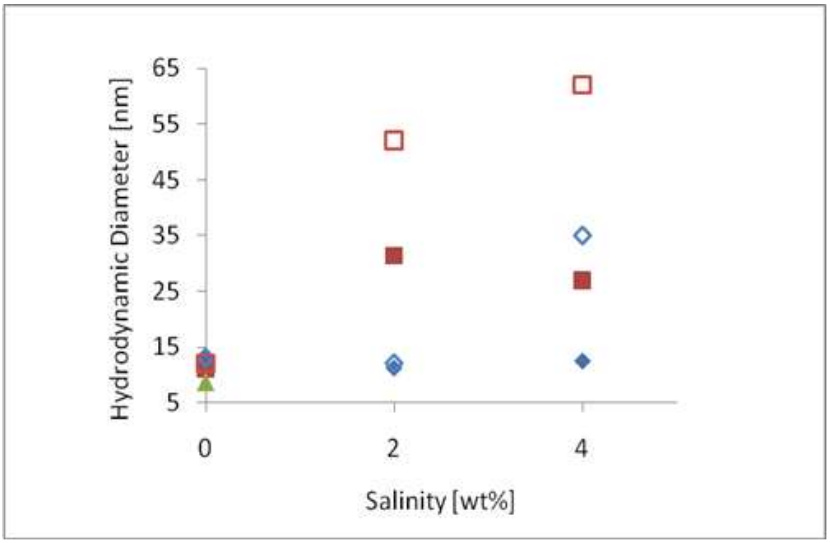

Figure 3.10 Sizes of iron oxide nanoclusters stabilized with citrate after 3 weeks of their formation, as a function of salinity at pH6 (♦), at pH8 (■) and at pH10 (▲). determined with dynamic light scattering. The open symbols represent the original values at pH6 (◊), at pH8 (□) and at pH10 (Δ)

3.3.3 Zeta Potential

The surface charge of the citrate coated iron oxide nanoclusters was characterized by zeta potential measurements as a function of pH and salinity. Figure 3.11 shows effect of pH without added salt. The adsorption of citrate on the surface causes a shift in the point of zero charge (PZC) from the neutral pH region to a much lower acidic value, to around pH2. The pK_{a1} of citric acid is ~ 3.1, pK_{a2} is ~ 4.8 and pK_{a3} is 6.4.[12a] The large negative zeta potential of the clusters coated with citrate was observed over a wide range of pH. Between pH6 and pH10, it varied between -35 and -55 mV. This amount of charge provided electrostatic repulsion that contributed to stabilization of the nanoclusters. The zeta potential becomes more negative with increasing pH with the deprotonation of the carboxylate groups of the citrate.

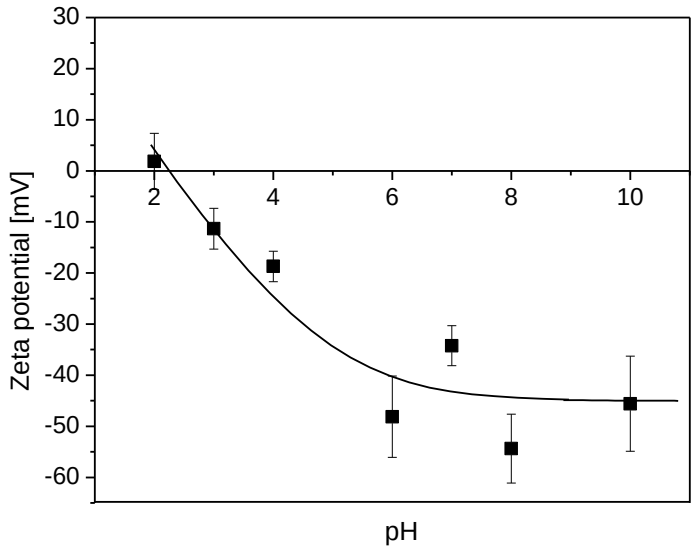

Figure 3.11 Zeta potential values of iron oxide NPs stabilized with citrate, without added salt, as a function of pH. The line is guide for the eye.

Figure 3.12 presents the effect of salt on the zeta potential of the citrate coated clusters at pH values 6 and 8. The magnitude of the zeta potential steeply decreases by adding NaCl, as the thickness of the electrical double layer decreases. The results are quite similar for these two pH values well above pK_{a2}. Even at the highest salt content a significantly negative zeta potential of around -20 mV is maintained, which provided electrostatic stabilization. At pH10 the measured zeta potential value was -45.6 mV without salt and -45.7 mV with 0.1 wt% NaCl (not shown). At higher salt content the particles settle at pH 10, and the zeta potential could not be measured.

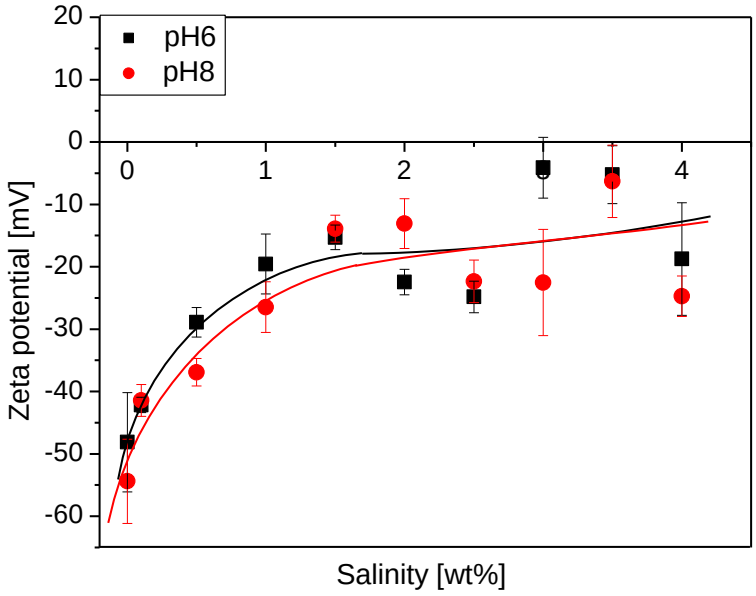

Figure 3.12 Zeta potential of Iron Oxide NPs stabilized with citrate as a function of salinity at pH 6 and pH8. The lines are guides for the eye.

The mass of the adsorbed organic components on the surface of particles was determined with TGA. The mass loss of the dried particles (dispersion at pH8, without salt) after heating was 10.3 wt% which accounts for the mass of the citrate coating. The inorganic loading of 90% for iron oxide was extremely high, relative to polymer stabilized NPs with much thicker coatings.

Figure 3.13 shows the magnetization of the iron oxide NPs in emu/g units for Fe at 300 K up to 36000 Oersted (Oe). The clusters were superparamagnetic and the magnetization reached 41 emu/g Fe. Here the magnetization did not reach saturation. Higher values of magnetization may be obtained by varying the conditions of the iron oxide hydrolysis.[12b]

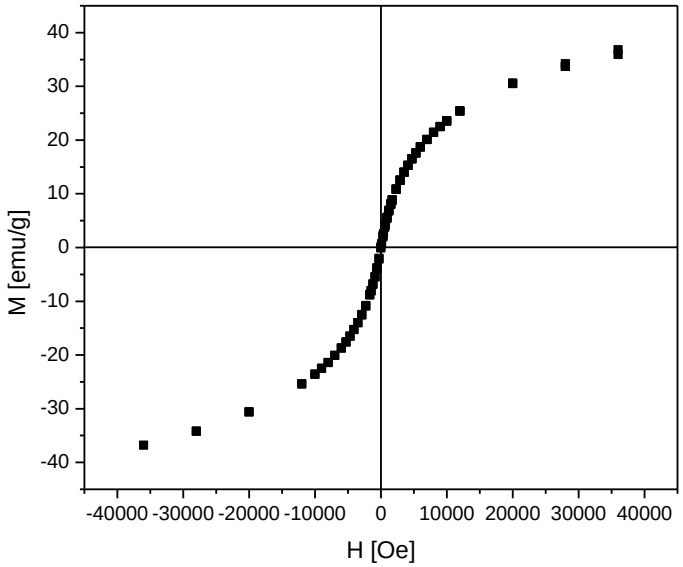

Figure 3.13 Magnetization (M) of iron oxide NPs in emu/g units for Fe vs. magnetic field (H). The measurement was taken at 300 K temperature. To measure the magnetization, citrate coated particles were used at pH8, without NaCl.

Figure 3.14 represents the recorded displacement of the air/dispersion interface of citrate-coated NPs at pH 8 without NaCl, measured by PS-OCT corresponding to three magnetic field amplitudes (915; 1728 and 2338 Gauss) at 2Hz frequency. The frequency of oscillation of the air/dispersion interface in response to the applied magnetic field (2Hz) was doubled (4Hz). Frequency doubling of the interface oscillation is expected from Eq. 1 since the magnetic force is proportional to the product of H and M both of which oscillate at 2Hz. The amplitude of the interface oscillation at 4Hz scaled with the applied magnetic field strength increasing from 30 to 110 nm.

Two core flood experiments were carried out to test the transport characteristics of nanoclusters coated with citrate in reservoir rocks. In both cases the dispersions contained 0.1 wt% iron oxide and 3 wt% NaCl and the pH value was 8. The summary of the core flood conditions is provided in Table 3.1. The first experiment was performed in a Boise sandstone core having a permeability of 576 mD. Three pore volumes (PV) thus 34 mL of nanoparticle dispersion were injected at a flow rate (q) of 3.13 mL/min. A mass balance showed that only a very small portion, 2.7 wt% of the injected nanoparticles were retained after a post-flush of four pore volumes. The second core flood was carried out in a Texas Cream limestone, this core having a low permeability of 17.5 mD. 31 mL (2.8 pore volumes) of nanocluster dispersion were injected at a flow rate of 2 mL/min. In this case the mass balance showed that 16.4 wt% of the injected nanoparticles were retained after a post-flush of four pore volumes, which is larger than for the Boise sandstone core flood. A possible explanation is that the higher negative surface charge of Boise sandstone at pH8 enabled more effective transport of the negatively charged iron oxide

nanoclusters. At pH 8, the surface charge for limestone is relatively neutral. However, the retention of the citrate-coated particles in sandstone is low, and may be expected to be lower in limestone at higher pH values, which indicates the potential ability for the particles to travel long distances.

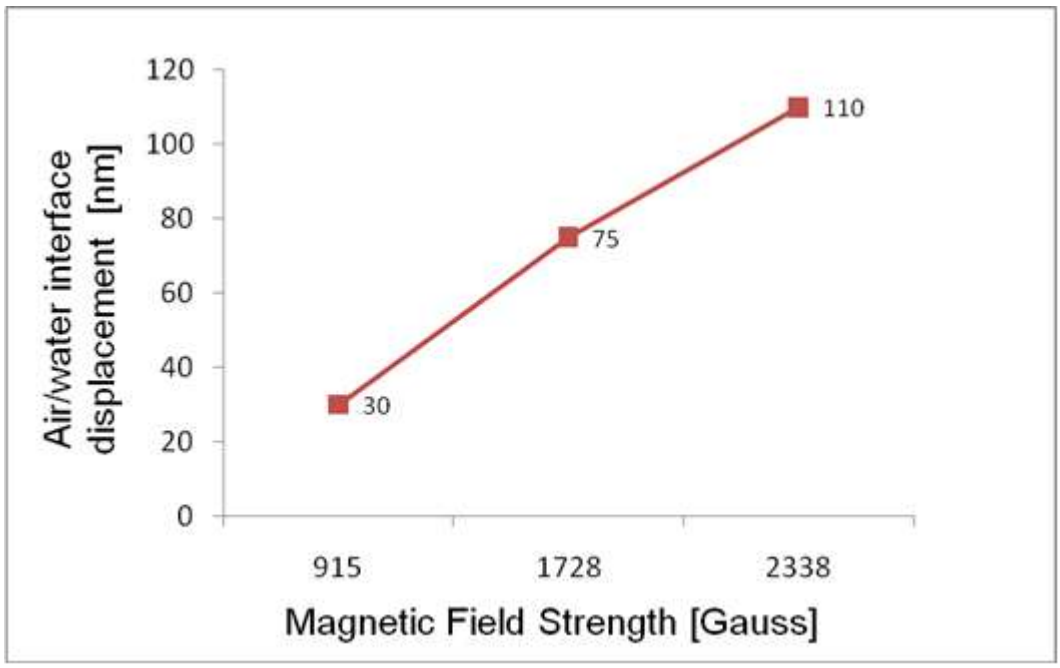

Figure 3.14 Displacement of air/dispersion interface vs. applied magnetic field strength measured with phase sensitive optical coherence tomography (PS-OCT). For the experiments 0.1 wt% citrate coated particles were used at pH8, without NaCl

Table 3.1 Summary of core flood conditions and results. In the experiments dispersions containing 0.1 wt% iron oxide and 3 wt% NaCl at pH 8 were used.

Porous Medium	K (mD)	Porosity	PV (mL)	q (mL/min)	PV injected	PV postflush	Retention (%)
Boise Sandstone	576	0.271	10.47	3.13	3.22	7	2.7
Texas Cream Limestone	17.5	0.289	11.16	2	2.8	7	16.4

3.4 DISCUSSION

3.4.1 Nanoparticle clusters - effect of citrate stabilizer (without added salt)

Cluster formation of iron oxide NPs without stabilizer, synthesized by co-precipitation of Fe(II) and Fe(III) salts in alkaline medium has been characterized by Philipse et al.[13] Addition of TMAOH resulted in a dispersion of nanoclusters without visible aggregates. Based on TEM and SAXS measurements, clusters with an average size of 26 nm were formed from individual particles smaller than 10 nm. The variation in the choice of base and Fe-salt concentrations led to larger, 40-65 nm sized clusters in our study. We used about four times lower concentration of iron chlorides and instead of ammonia, NaOH as base. After particle nucleation VDW and electrostatic interactions govern the formation of clusters. Despite the negative surface charge of the particles in the alkali medium (~ pH12), VDW attraction overcomes the electrostatic repulsion.[17] The addition of TMAOH to the solution stabilizes the clusters against further growth, as reported previously.[10] After adsorbing the citrate ions to the surface of the particles and

after probe sonication the sizes of clusters decreased to between 9 and 13 nm, depending on the pH. Therefore, from a practical point of view, the difference in sizes of the transient loosely bonded clusters prior to citrate addition for our study relatively to Philipse et al. [13] appears to be unimportant.

After citrate addition, the nanocluster size decreased markedly. However the clusters were still larger than the size of individual iron oxide crystals, but only to a relatively modest degree. Therefore, the interactions of iron oxide primary particles in denser domains of the clusters prevented deaggregation to a greater degree than in more weakly flocculated domains of the clusters. The decrease in the cluster size after adding the citrate coating indicated that repulsive forces overcame the attractive VDW forces. The measured high negative values of zeta potential of citrate-coated particles (-35 to -55 mV) characterize the contribution to stabilization from electrostatic repulsion. The potential between two particles was determined as a function distance with DLVO theory. As a consequence of the small Debye length of only 0.367 nm at 4 wt. % NaCl, the potential between two particles was attractive over a wide range of particle separation according to this theory. This theory does not include effects of the Stern layer on the potential. Thus, other non-DLVO forces including specific ion effects and hydration forces contributed to the stability. Furthermore, the effect of the attractive force on the colloidal stability (stability ratio) decreases as the volume fraction of the nanoparticles goes down.

Similar zeta potentials have been reported for other citrate-coated iron oxide particles.[12a] Two of the three carboxylate groups of the citrate, which are dissociated at ~

pH5 [12a] provide very strong binding to the iron oxide particle surface. By raising pH the third carboxylic group of citrate dissociates (at pH6.4) and provides negatively charged surface for the iron oxide. Given the small size of the citrate ion, the steric stabilization is relatively small. A contribution from the electrostatic stabilization is evident in the three week stability of the clusters.

3.4.2 Nanoparticle clusters – effect of salt

For citrate coated iron oxide particles, changes in size of the nanoclusters was observed as a function of the electrostatic and VDW interactions. In the case of bare iron oxide, the lowest repulsion between the particles occurs at ~ pH7, the point of zero charge [12a]. The PZC shifts to ~ pH2 in presence of the citrate coating. At pH 6, the shrinkage of the diffuse electric double layer around the particles [17] as the zeta potential increased to ~-20 mV appeared to have little effect on the particle size even at high salinity. Clusters because of their porosity have weaker VDW attraction than for solid particles, which favors colloidal stability. Thus the electrostatic repulsion was sufficient to provide high stability even for 3 months. At pH 8, the behavior was somewhat similar but with significant growth for the initial clusters. At pH 10 the growth was even larger. Thus a large negative zeta potential was not enough to provide stability with added salt.

We propose that this loss of stability may be attributed to complicated changes in citrate and hydroxide ion adsorption and counterion interactions with pH, as seen for other types of ions on iron oxide particles. We hypothesize that there is a competition in

adsorption onto the Fe ion surfaces between the carboxylic group of the citrate ions and hydroxide ions (OH^-). At the higher pH values the interactions of OH^- with the iron cations may displace some of the citrate ions. Furthermore, the smaller OH^- ions may not provide the degree of steric stabilization affored by the citrate ions. Finally, the interactions between surfaces will be further influences by the counterion effects. The characterization of these complex adsorption and counter ion binding effects would require additional *in situ* spectroscopic studies, for example FTIR spectroscopy, that are beyond the scope of this study.

Various studies have considered the stability of iron oxide NP dispersions stabilized with small ligands with the addition of salt. For addition of NaCl above 250 mM, NPs stabilized with an oleic acid bilayer precipitated as the result of screened electrostatic repulsion between particles.[19] In another study [20] zerovalent iron NPs coated with a triblock copolymer, with polyaspartate and with sodium dodecyl benzene sulfonate (SBDS) were investigated at different Na^+ and Ca^{2+} concentrations at pH7.7. DLS measurements indicated an average hydrodynamic diameter of 146 nm for the bare nanoiron clusters in 1 mM $NaHCO_3$ solution.[27] It was found that adsorption of polyaspartate on the NPs caused smaller cluster size, around 66 nm. In addition, the critical deposition concentration (CDC) of the particles on sand grains was around 770 mM Na^+ and 4 mM for Ca^{2+}. SDBS coating resulted in less salt tolerance while the triblock copolymer-modified particles had the highest zeta potential and salt tolerance: CDC at 4 M for Na^+ and over 100 mM for Ca^{2+}.

Random copolymers of acrylic acid, styrenesulfonic acid, and vinylsulfonic acid were used to form iron oxide clusters at different pH values and salinities by Ditsch et al. [7] The particles were nucleated by chemical co-precipitation, where one polymer was already present in the solution. A secondary polymer was added to completely coat the vacant iron oxide surface sites. By using the appropriate molecular weight, amount and type of primary polymers, the clusters were stable in 5M NaCl. In another study, covalently attached carboxymethyldextran was used to stabilize iron oxide clusters synthesized by co-precipitation of iron chloride salts in alkaline medium.[28] The stability and the size of the clusters were tuned by adding up to 140 mM NaCl to the dispersion. The size of the clusters was ~ 110 nm and appeared to be independent of pH and salinity, caused by the steric stabilization mechanism of carboxymethyldextran.

From these data reported in the literature [7, 14-15, 20, 28] one can see that carefully selected polymeric stabilizers allow the engineering of stable clusters with the desired size and high salt tolerance. As the MW of the polymeric stabilizer and thus the thickness of the coating on the surface increases, the iron oxide fraction decreases. Citrate-coated clusters have the advantage of high mass fraction, around 90 wt% of iron oxide relative to the total mass and yet very high salt tolerance. Thus electrostatic stabilization, with only minimal steric stabilization can provide stability at high salinities, to compliment previous studies that utilized polymers for a much greater steric component in electrostatic stabilization.

3.4.3 Magnetic force for nanoclusters verus smaller primary particles

Magnetic nanoparticle dispersions may be used as imaging agents in biomedical applications or in detection of phases and interfaces in oil reservoirs.[5] The motion of a magnetic particle may be utilized to generate ultrasonic [2b] or acoustic [5b] signals. Sub-15 nm crystals of iron oxide provide superparamagnetic properties with higher magnetic susceptibility compared to paramagnetic materials.[2d, 29] The relationship between magnetic force F_m and field H was given in eq. 1. The increase in V_p raises F_m and thus the motion of the clusters in a magnetic field[8] which can enhance signals in magnetomotive imaging. The requirement for superparamagnetism is alignment of spins in iron oxide crystal domains smaller than15 nm. Due to this V_p and thus F_m can be limited [30].The strategy to overcome the limitation of V_p and thus F_m is to form clusters of sub-15 nm primary particles. Even with very small spacing of the particles in the cluster, the coupling between neighboring particles is small and does not influence the magnetization per mass of iron.[15, 21] Thus, M_p remains the same for the clusters as for the individual primary particles relative to the mass of iron. However, relative to volume, there is some loss due to the porosity of the cluster. Lower magnetic force per unit volume occurs by using high MW polymeric stabilizers that result in lower overall metal loading of the cluster. The high iron oxide loading for citrate-coated magnetic clusters is advantageous for increasing M_p and F_m relative to heavier polymer coated particles with thicker coatings.

3.4.4 Magnetic clusters in oil recovery and imaging of oil reservoirs

Stability of magnetic NP dispersions at high salinities is important at pH values between 6 and 10. The sub 100 nm particle sizes will facilitate transport through limestone and sandstone formations based on similar studies with silica particles [31]. Furthermore, the negative surface charge is beneficial for repulsion from negatively charged rock surfaces. As described in 3.4.3, the large V_p of a nanocluster may be expected to increase displacement of the air/dispersion interface to a greater extent than a small primary particle (data not shown), for a given magnetization per mass of iron. The greater displacement will generate a larger acoustic signal for nanoclusters at oil/water interfaces in a reservoir rock.

3.5 CONCLUSIONS

Superparamagnetic sub-100 nm nanoclusters of iron oxide primary particles were stabilized with small amounts of citrate ion, even for salinities up to 4 wt% (680 mM). The high loading of 90% iron oxide relative particles with polymeric stabilizers is beneficial for increasing the magnetization per unit particle volume, and the magnetic force on the particles. The large volume of the still superparamagnetic nanoclusters relative to the primary particles is also beneficial for increasing the magnetic force. The strongly negative zeta potentials even at high salinity indicate the strongly adsorbed citrate ions provide electrostatic stabilization in aqueous media encountered in subsurface reservoirs. The nanoparticle dispersions were stable for at least 2 months with high salt

concentrations of 680 mM at pH6 and pH8. The cluster sizes at pH 6 were somewhat smaller than at pH 8 at high salinity, whereas salt tolerance decayed markedly at pH 10. This change with pH may indicate competition in complex formation with the iron cations on the NP surface between the carboxylate group of the citrate ions and the hydroxide ions. Transport experiments showed that the particles exhibit little retention in negatively charged sandstone and limestone due to their surface coating and small cluster size. The superparamagnetic properties and high salt tolerance are highly beneficial in various applications. In particular, nanoclusters targeted to cellular interfaces related to a pathological condition, can serve as a diagnostic source for magneto-optic tomographic imaging modalities. Similarly, nanoclusters targeted to oil-water interfaces in petroleum reservoirs can serve as a diagnostic source for magneto-acoustic tomography.

3.6 REFERENCES

1. Bee, A.; Massart, R.; Neveu, S., Synthesis of very fine maghemite particles. *Journal of Magnetism and Magnetic Materials* **1995,** *149*, 6-9.

2. (a) Gupta, A. K.; Gupta, M., Synthesis and surface engineering of iron oxide nanoparticles for biomedical applications. *Biomaterials* **2005,** *26*, 3995–4021; (b) Oh, J.; Feldman, M. D.; Kim, J.; Condit, C.; Emelianov, S.; Milner, T. E., Detection of magnetic nanoparticles in tissue using magneto-motive ultrasound. *Nanotechnology* **2006,** *17* (16), 4183-4190; (c) Safarik, I.; Safarikova, M., Magnetic nanoparticles and biosciences. *Monatsh. Chem.* **2002,** *133*, 737–759.; (d) Lu, A.-H.; Salabas, E. L.; Schueth, F., Magnetic nanoparticles: synthesis, protection, functionalization and application. *Angew. Chem. Int. Ed.* **2007,** *46*, 1222-1244; (e) Ingram, D. R.; Kotsmar, C.; Yoon, K. Y.; Shao, S.; Huh, C.; Bryant, S. L.; Milner, T.; Johnston, k. P., Superparamagnetic nanoclusters

coated with oleic acid bilayers for stabilization of emulsions of water and oil at low loncentration. *J. Colloid Interface Sci.* **2010,** *351*, 225-232; (f) Massart, R.; Dubois, E.; Cabuil, V.; Hasmonay, E., Preparation and Properties of Monodisperse Magnetic Fluids. *Journal of Magnetizm and Magnetic Materials* **1995,** *149*, 1-5.

3. Ju, B.; Fan, T.; Ma, M., Enhanced oil recovery by flooding with hydrophilic nanoparticles. *China Particuology* **2006,** *4*, 41-46.

4. (a) Dickson, J. L.; Binks, B. P.; Johnston, K. P., Stabilization of carbon dioxide-in-water emulsions with silica nanoparticles. *Langmuir* **2004,** *20* (19), 7976-7983; (b) Golomb, D.; Pennell, S.; Ryan, D.; Barry, E.; Swett, P., Ocean sequestration of carbon dioxide: modeling of the deep ocean release of a dense emulsion of liquid CO_2-in-water stabilized by pulverised limestone particles. *Environ. Sci. Technol.* **2007,** *41*, 4698-4704; (c) Adkins, S. S.; Gohil, D.; Dickson, J. L.; Webber, S. E.; Johnston, K. P., Water-in-carbon dioxyde emulsions stabilized with hydrophobic silica particles. *Phys. Chem. Chem. Phys.* **2007,** *9*, 6333-6343.

5. (a) Prodanovic, M.; Ryoo, S.; Rahmani, A. R.; Kuranov, R.; Kotsmar, C.; Milner, T. E.; Johnston, K. P.; Bryant, S. L.; Huh, C., Effects of magnetic field on the motion of multiphase fluids containing paramagnetic particles in porous media. *17th SPE Improved Oil Recovery Symposium Tulsa, OK* **2010,** *SPE 129850*; (b) Ryoo, S.; Rahmani, A. R.; Yoon, K. Y.; Prodanovic, M.; Kotsmar, C.; Milner, T. E.; Johnston, K. P.; Bryant, S. L.; Huh, C., Theoretical and experimental investigation of the motion of multiphase fluids containing paramagnetic nanoparticles in porous media. *SPE Annual Meeting, Florence, Italy* **2010,** *SPE 134879*.

6. Gerber, R.; Birss, R. R., *High Gradient Magnetic Separation*. Research Studies Press: London, 1983.

7. Ditsch, A.; Laibinis, P. E.; Wang, D. I. C.; Hatton, T. A., Controlled Clustering and Enhanced Stability of Polymer-Coated Magnetic Nanoparticles. *Langmuir* **2005,** *21* (13), 6006-6018.

8. Moeser, G. D.; Roach, K. A.; Green, W. H.; Laibinis, P. E.; Hatton, T. A., High-gradient magnetic separation of coated magnetic nanoparticles. *AIChE Journal* **2004,** *50*, 2835-2848.

9. (a) Moeser, G. D.; Roach, K. A.; Green, W. H.; Laibinis, P. E.; Hatton, T. A., Water-based magnetic fluids as extractants for synthetic organic compounds. *Ind. Eng. Chem. Res.* **2002,** *41*, 4739-4749.; (b) Bucak, S.; Jones, D. A.; Laibinis, P. E.; Hatton, T. A., Protein separations using colloidal magnetic nanoparticles. *Biotechnol. nProg.* **2003,** *19*, 477-484.

10. Massart, R., Preparation of aqueous magnetic liquids in alkaline and acidic media. *IEEE Trans. Magn.* **1981,** *17*, 1247-1248.

11. Lan, Q.; Liu, C.; Yang, F.; Liu, S.; Xu, J.; Sun, D., Synthesis of bilayer oleic acid-coated Fe3O4 nanoparticles and their application in pH-responsive Pickering emulsions. *J. Colloid Interface Sci.* **2007,** *310*, 260-269.

12. (a) Campelj, S.; Makovec, D.; Drofenik, M., Preparation and properties of water-based magnetic fluids. *J. Phys.: Condens. Matter* **2008,** *20*, 204101-204105.; (b) Sahoo, Y.; Goodarzi, A.; Swihart, M. T.; Ohulchanskyy, T. Y.; Kaur, N.; Furlani, E. P.; Prasad, P. N., Aqueous ferrofluid of magnetite nanoparticles: fluorescence labeling and magnetophoretic control. *J. Phys. Chem. B* **2005,** *109*, 3879–3885; (c) Lyon, J. L.; Fleming, D. A.; Stone, M. B.; Schiffer, P.; Williams, M. E., Synthesis of Fe oxide core/Au shell nanoparticles by iterative hydroxylamine seeding. *Nano Letters* **2004,** *4*, 719-723.; (d) Hui, C.; Shen, C.; Yang, T.; Bao, L.; Tian, J.; Ding, H.; Li, C.; Gao, H.-J., Large-scale Fe3O4 nanoparticles soluble in water synthesized by a facile method. *J. Phys. Chem. C* **2008,** *112*, 11336–11339.

13. Philipse, A. P.; van Bruggen, M. P. B.; Pathmamanoharan, C., Magnetic silica dispersions: preparation and stability of surface-modified silica particles with a magnetic core. *Langmuir* **1994,** *10*, 92-99.

14. Berret, J.-F.; Schonbeck, N.; Gazeau, F.; El Kharrat, D.; Sandre, O.; Vacher, A.; Airiau, M., Controlled clustering of superparamagnetic nanoparticles using block copolymers: design of new contrast agents for magnetic resonance imaging. *J. Am. Chem. Soc.* **2006,** *128*, 1755-1761.

15. Ma, L. L.; Feldman, M. D.; Tam, J. M.; Paranjape, A. S.; Cheruku, K. K.; Larson, T. A.; Tam, J. O.; Ingram, D. R.; Paramita, V.; Villard, J. W.; Clarke, G. D.; Jenkins, J. T.; Asmis, R.; Sokolov, K.; Chandrasekar, B.; Milner, T. E.; Johnston, K. P., Small multifunctional nanoclusters (Nanoroses) for targeted cellular imaging and therapy. *ACS Nano* **2009,** *3*, 2686-2696.

16. Matteucci, M. E.; Paguio, J. C.; Miller, M. A.; Williams, R. O., III; Johnston, K. P., Flocculated amorphous nanoparticles for highly supersaturated solutions. *Pharmaceutical Research* **2008,** *25* (11), 2477-2487.

17. Hiemenz, P. C.; Rajagopalan, R.; Editors, *Principles of Colloid and Surface Chemistry, Third Edition, Revised and Expanded*. Marcel Dekker Inc.: New York, 1997; p 688 pp.

18. Yu, W., W.; Chang, E.; Falkner, J. C.; Zhang, J.; Al-Somali, A. M.; Sayes, C. M.; Johns, J.; Drezek, R.; Colvin, V. L., Forming Biocompatible and Nonaggregated Nanocrystals in Water Using Amphiphilic Polymers. *Journal of American Chemical Society* **2007,** *129*, 2871-2879.

19. Prakash, A.; Zhu, H.; Jones, C. J.; Benoit, D. N.; Ellsworth, A. Z.; Bryant, E. L.; Colvin, V. L., Bylayers as Phase Transfer Agents for Nanocrystals Prepared in Nonpolar Solvents. *ACS Nano* **2009,** *3*, 2139-2146.

20. Saleh, N.; Kim, H.-J.; Phenrat, T.; Matyjaszewski, K.; Tilton, R. D.; Lowry, G. V., Ionic strength and composition affect the mobility of surface-modified Fe^0 nanoparticles in water-saturated sand columns. *Environ. Sci. Technol.* **2008,** *42*, 3349-3355.

21. Ditsch, A. P.; Lindemann, S.; Laibnis, P. E.; Wang, D. I. C.; Hatton, T. A., High-gradient magnetic separation of magnetic nanoclusters. *Ind. Eng. Chem. Res.* **2005,** *44*, 6824-6836.

22. (a) Kang, Y. S.; Risbud, S.; Rabolt, J. F.; Stroeve, P., Synthesis and characterization of nanometer-size Fe3O4 and gamma-Fe2O3 particles. *Chem. Mater.* **1996,** *8*, 2209-2211.; (b) Pham, T. T. H.; Cao, C.; Sim, S. J., Application of citrate-stabilized gold-coated ferric oxide composite nanoparticles for biological separations. *J. Magn. Magn. Mat.* **2008,** *320*, 2049–2055.

23. Ryoo, W.; Webber, S. E.; Johnston, K. P., Water-in-Carbon Dioxide Microemulsions with Methylated Branched Hydrocarbon Surfactants. *Ind. Eng. Chem. Res.* **2003,** *42*, 6348-6358.

24. Tam, J. M.; Murthy, A. K.; Ingram, D. R.; Nguyen, R.; Sokolov, K. V.; P., J. K., Kinetic assembly of near-IR active gold nanoclusters using weakly adsorbing polymers to control size. *Langmuir* **2010,** *26*, 8988-8999.

25. Kuranov, R.; McElroy, A.; Kemp, N.; Baranov, S.; Taber, J.; Milner, T. E., Gas-cell referenced swept source phase sensitive optical coherence tomography. *submitted to Optical Technology Letters*.

26. Yu, H.; Kotsmar, C.; Yoon, K. Y.; Ingram, D. R.; Johnston, K. P.; Bryant, S. L.; Huh, C., Transport and retention of aqueous dispersions of paramagnetic nanoparticles in reservoir rocks. *17th SPE Improved Oil Recovery Symposium Tulsa, OK* **2010,** *SPE 129887*.

27. Saleh, N.; Phenrat, T.; Sirk, K.; Dufour, B.; Ok, J.; Sarbu, T.; Matyjaszewski, K.; Tilton, R. D.; Lowry, G. V., Adsorbed Triblock Copolymers Deliver Reactive Iron Nanoparticles to the Oil/Water Interface. *Nano Letters* **2005,** *5* (12), 2489-2494.

28. Herrera, A. P.; Barrera, C.; Rinaldi, C., Synthesis and functionalization of magnetite nanoparticles with aminopropylsilane and carboxymethyldextran. *J. Mater. Chem.* **2008,** *18*, 3650-3654.

29. Wu, W.; He, Q.; Jiang, C., Magnetic iron oxide nanoparticles: synthesis and surface functionalization strategies. *Nanoscale Research Letters* **2008,** *3*, 397-415.

30. Yavuz, C. T.; Mayo, J. T.; Yu, W. W.; Prakash, A.; Falkner, J. C.; Yean, S.; Cong, L.; Shipley, H. J.; Kan, A.; Tomson, M.; Natelson, D.; Colvin, V. L., Low-field magnetic separation of monodisperse Fe3O4 nanocrystals. *Science* **2006,** *314*, 964-967.

31. Rodriguez, E.; Roberts, M. R.; Yu, H.; Huh, C.; Bryant, S. L., Enhanced migration of surface-treated nanoparticles in sedimentary rocks. *SPE Annual Technical Conference and Exhibition, New Orleans, LA, USA* **2009,** *SPE 124418*.

Chapter 4: Effect of adsorbed amphiphilic copolymers on the interfacial activity of superparamagnetic nanoclusters and emulsification of oil in water

A series of sub-100 nm superparamagnetic iron oxide nanoparticles with amphiphilic poly(acrylic acid-*b*-butylacrylate); PAA-*b*-PBA) copolymer shells were synthesized and characterized by NMR spectroscopy, dynamic light scattering (DLS), transmission electron microscopy (TEM), thermogravimetric analysis (TGA), and a superconducting quantum interference device (SQUID) to investigate the effect of the polymer structure on the interfacial tension for nanoparticles adsorbed at the dodecane-water interface. Large reductions in interfacial tension of up to 27.6 mN/m were measured at nanoparticle concentrations of 0.27 wt%, indicating significant nanoparticle adsorption and interaction between the oil and water molecules at the interface. The adsorption energy of the polymer-coated nanoparticles at the dodecane/water interface was determined from the interfacial tension and nanoparticle radius, and analyzed in terms of the structure of the polymer stabilizer. Furthermore, the equilibrium adsorption of amphiphilic copolymer-functionalized iron oxide nanoclusters at the oil-water interface was determined by material balance from the concentration in the excess water phase and the known overall oil/water interfacial area. The formation and stabilization of oil droplets were on the order of 10 μm in water with unusually low nanoparticle concentrations was explained in terms of the high interfacial activity of the particles.

4.1 INTRODUCTION

Nanoparticles may be used to stabilize Pickering emulsions and foams via adsorption at the interfaces between two liquids.[1] While conventional surfactants or polymers are typically used to lower oil/water interfacial tension (γ), Pickering emulsions with micron size droplets are often formed with a relatively small reduction of interfacial tension[2]. There have been a number of interesting studies using nanoparticles as well as mixtures of particles and surfactants to effect interfacial surface tension reduction.[1e, 3] Adsorbed nanoparticles with surfactant or homopolymer coatings at oil/water interfaces can lower interfacial tension because the surfactant or polymer segments block contact between the oil and water phases.[2b, 4] Despite their importance in many industrial applications including food, cosmetics, pharmaceuticals, and oil recovery, there is limited understanding of how polymer-stabilized nanoparticles adsorb at interfaces and lower γ.[2b, 4-5] Furthermore, while amphiphilic copolymers have been investigated as stabilizers on various inorganic nanoparticle cores, the resulting reduction in γ and subsequent increase in surface pressure ($\Pi = \gamma_o - \gamma$) has not been reported to the best of our knowledge.[5] The use of amphiphilic copolymers on the nanoparticle surfaces may have the potential to raise the interfacial adsorption of the particles and also reduce γ more effectively than homopolymer coatings.

While aqueous dispersions of nanoparticles with polymer coatings have been widely studied,[6] relatively few studies have examined their adsorption at oil/water interfaces,[5, 7] and particularly, how they reduce γ.[4] The adsorption may be controlled by

tuning the concentration and hydrophilicity/hydrophobicity of a low molecular weight or polymeric stabilizer on the nanoparticle surface.[1d, 5, 8] For example, Zhou et al. formed ~ 80 μm oil droplets using 1 wt% unmodified iron oxide nanoparticles, but did not report changes in the interfacial tension.[7] Silica particles stabilized with grafted polymer coatings such as poly(styrenesulfonate) (PSS)[2b] and poly(2-(dimethylamino)ethyl methacrylate) (PDMAEMA)[4] produced stable oil/water emulsions. Specifically, silica nanoparticles stabilized with grafted PSS[2b] reduced γ by ~5 and 15 mN/m at concentrations of 0.04 and 1 wt%, respectively. Silica particles stabilized with grafted PDMAEMA[4] reduced γ by 38 mN/m at a relatively high nanoparticle concentration of 2 wt%. Iron nanoparticles functionalized with a poly(methacrylic acid)-*b*-(methyl methacrylate)-*b*-(styrenesulfonate) triblock copolymer stabilized oil/water emulsions however the reduction in γ was not reported.[5] Thus, it remains a significant challenge to design sub-100 nm nanoparticles with polymer stabilizers to achieve large reduction of interfacial tension at oil/water interface. Such particles are expected to enhance formation and stabilization of small droplets (~ 10 μm) of oil in water at low nanoparticle concentrations (< 0.3 wt%).

Recently, magnetic iron oxide particles have found utility in biomedical applications[6d, 9] including imaging, therapy, drug delivery, *in vitro* cell separation, as well as in the oil industry for imaging of subsurface reservoirs.[10,9e, 11] Moreover, magnetic nanoparticles have been adsorbed at an oil/water interface and oscillated with an electromagnetic field to generate acoustic waves[12] which may then be analyzed to determine the oil saturation of a reservoir. By judiciously designing the interfacial

properties of stabilizers on the nanoparticle surface, magnetic nanoparticles can be effective for stabilizing Pickering emulsions of oil and water.[7, 8b, 13] Additionally, we have shown that nanoclusters composed of 5-10 nm primary particles offer advantages over solid nanospheres for stabilization of emulsions.[14] Because nanoclusters are porous, they occupy a larger area at the oil/water interface than do nanospheres, and therefore a smaller mass of nanoclusters is required to stabilize an emulsion.

A wide variety of stabilizers may be used during synthesis of nanoclusters to control the size and colloidal stability based on the approach of Massart et al.[15] Magnetic nanoparticles have been stabilized with adsorbed polymeric ligands or surfactants,[16] including polyelectrolytes,[17] block copolymers,[18] poly(acrylic acid)[19] and poly(acrylic acid)-based co-polymers[6a, 20], biopolymers,[9e] or small polar molecules such as citric acid (CA).[5, 17b] Polyelectrolyte molecules simultaneously provide steric stabilization in addition to electrostatic repulsion, resulting in so-called electrosteric stabilization.[17b] For example, Ditsch et al. used random copolymers of acrylic acid, styrenesulfonic acid, and vinylsulfonic acid to stabilize iron oxide nanoclusters of controlled size over a wide range of different pH values and salinities. The attachment of the polymer to the nanoparticle surface must not interfere with the inorganic crystal structure and surface properties or it may degrade the saturation magnetization. It is therefore desirable for the polymer coating to provide control over the crystallinity during the nanoparticle synthesis.

Herein we report the surface pressure (reduction in interfacial tension) at the dodecane/water interface for a rationally designed series of copolymer-coated superparamagnetic iron oxide nanoclusters as a function of the polymer structure. Both

block and random copolymers of poly(acrylic acid) (PAA) and poly(butyl acrylate) (PBA) were synthesized with varying lengths of hydrophilic and hydrophobic blocks and used to stabilize iron oxide nanoclusters. The objective was to demonstrate that nanoparticles with non-covalently adsorbed amphiphilic copolymer stabilizers produce very large reductions in interfacial tension (surface pressures of 27.6 mN/m) at low nanoparticle concentrations of only 0.27 wt%. To our knowledge, significant surface pressures have not been reported at such low concentrations with homopolymer stabilizers.[2b, 4]. Sub-100 nm iron oxide nanoclusters with shells composed of poly(acrylic acid-*b*-butyl acrylate) (PAA-*b*-PBA) stabilized 10-57 μm oil droplets in water at low nanoparticle concentrations (0.27 wt%) and over a broad range of pH conditions. The high surface pressures resulting from efficient nanoparticle adsorption at the oil/water interface and the interactions of the polymer shells with the oil and water phases were found to favor the formation and stabilization of oil/water emulsions with small droplets. Furthermore, the polymers enabled controlled nanoparticle synthesis to produce Fe_3O_4 nanoclusters with sizes below 100 nm (determined by DLS) and with less than 20% organic content adsorbed on the particle surface (determined by TGA) in order to maintain high saturation magnetization.

4.2 EXPERIMENTAL SECTION

4.2.1 Materials

All solvents were purchased from Fisher Scientific and used without further purification unless otherwise noted. *n*-Butyl acrylate (BA) and *t*-butyl acrylate (*t*BA)

were filtered through a short plug of basic alumina to remove the 4-methoxyphenol (MEHQ) stabilizer. All other chemicals were used without further purification. Ferrous chloride cetrahydrate ($FeCl_2 \cdot 4H_2O$; MW=198.81 g; catalog number: I90-500), ferric chloride hexahydrate ($FeCl_3 \cdot 6H_2O$; MW=270.32 g; catalog number: I88-100), ammonium hydroxide (NH_4OH, 28% catalog number: A669-212), poly(acrylic acid, sodium salt) (PAA, MW=5100, catalog number: 447013-100G) and sodium chloride (NaCl, MW=58.44 g; catalog number: S671-3) were purchased from Fisher Scientific, USA. Hydrochloric Acid (HCl; MW=36.46 g; catalog number: UN1789) and sodium hydroxide (NaOH; MW=40 g; catalog number: UN1823) were purchased from EM Science, Germany. Dialysis tubing (Spectra/Por® 6; 50,000 MWCO; lot number 3246779) was purchased from Spectrum Laboratories, Inc., USA.

4.2.2 General Procedure for Synthesis of Polymer Coatings

The polymer coatings were prepared by atom transfer radical polymerization (ATRP) of *n*-butyl acrylate and *tert*-butyl acrylate followed by acidolysis to afford poly(acrylic acid-*co*-butyl acrylate). P*t*BA-*b*-PBA block copolymers were prepared by ATRP from P*t*BA macroinitiators. Generally, to an oven-dried 100 mL Schlenk flask with a magnetic stir bar was added copper(I) bromide, monomer (*n*-butyl acrylate and/or *tert*-butyl acrylate) and initiator (ethyl 2-bromoisobutyrate or macroinitiator P*t*BA) under an atmosphere of nitrogen. After one freeze-pump-thaw cycle, *N,N,N',N',N*-pentamethyldiethylenetriamine was added via a gas-tight syringe that had been purged with nitrogen. After three freeze-pump-thaw cycles, the reaction mixture was allowed to

return to ambient temperature, and the reaction flask was backfilled with nitrogen, sealed and placed in an oil bath at 65 °C. The reaction mixture was allowed to stir for 2-4 h prior to quenching by immersion in liquid nitrogen. The reaction mixture was then taken up into THF and passed through a plug of neutral alumina to remove the Cu/ligand catalyst system. The polymer mixture was concentrated and precipitated three times into cold methanol/water mixture (1/1, v/v). After characterization by NMR spectroscopy and gel permeation chromatography, the isolated poly(*t*-butyl acrylate-*co*-*n*-butyl acrylate) was dissolved in dichloromethane in a round-bottom flask with a magnetic stir bar and excess trifluoroacetic acid was added. The reaction mixture was stirred at room temperature for 18 h, and the dichloromethane and trifluoroacetic acid were removed under reduced pressure. The residue was dissolved in DI water and dialyzed for 3 days against DI water.

P*t*BA$_{114}$: GPC: M_n = 14,650, M_w/M_n = 1.32. MW = 14,500 Da from ^{1}H NMR spectroscopy. Yield 16.6 g, 80%. ^{1}H NMR ($CDCl_3$, ppm): δ 4.05 (m, br), 2.30-2.10 (s, br), 1.88-1.68 (s, br), 1.65-1.30 (m, br).

P*t*BA$_{114}$-*b*-PBA$_{26}$: M_n = 18,830 Da from GPC, M_w/M_n = 1.38. MW = 18,000 Da from ^{1}H NMR spectroscopy. Yield 1.98 g, 88%. ^{1}H NMR ($CDCl_3$, ppm): δ 3.95 (m, br), 2.30-2.10 (m, br), 1.88-1.20 ((m, br), 0.80 (t, br).

P*t*BA$_{114}$-*b*-PBA$_{38}$: M_n = 21,490 Da from GPC, M_w/M_n = 1.39. MW = 19,500 Da from ^{1}H NMR spectroscopy. Yield 4.93 g, 75%. ^{1}H NMR ($CDCl_3$, ppm): δ 3.95 (m, br), 2.30-2.10 (m, br), 1.88-1.20 (m, br), 0.80 (t, br).

P*t*BA$_{114}$-*b*-PBA$_{67}$: M_n = 27,900 Da from GPC, M_w/M_n = 1.45. MW = 23200 Da from ^{1}H NMR spectroscopy. Yield 3.83 g, 82%. ^{1}H NMR ($CDCl_3$, ppm): δ 3.95 (m, br), 2.30-2.10 (m, br), 1.88-1.20 (m, br), 0.80 (t, br).

P*t*BA$_{133}$-*co*-PBA$_{44}$: M_n = 22,910 Da from GPC, M_w/M_n = 1.34. MW = 22,600 Da from ^{1}H NMR spectroscopy. Yield 13.8 g, 69%. ^{1}H NMR ($CDCl_3$, ppm): δ 4.12-3.95 (m, br), 2.42-2.08 (m, br), 1.92-1.70 (m, br), 1.65-1.20 (m, br), 0.80 (t, br).

4.2.3 Nanoparticle synthesis and nanocluster formation

The nanoclusters were formed by hydrolysis of iron chlorides under aqueous alkaline conditions by modifying well established synthetic approaches.[21-22] Briefly, in a three-necked flask $FeCl_2$ and $FeCl_3$ (1:2 molar ratio) and polymer (PAA, PAA-*b*-PBA, or PAA-*co*-PBA) were dissolved in 30 mL DI water and the solution was stirred vigorously with a magnetic stirrer for 30 minutes under an atmosphere of nitrogen. The weight ratio of polymer to total iron chloride was 1:4. The mixture was heated to 90 ^oC while stirring and 10 ml of 28 wt % NH_4OH solution was added to the reaction mixture to nucleate and grow iron oxide nanoparticles. The reaction was further stirred and heated for 2 hours, then cooled to room temperature. The stable dispersion was centrifuged at 9000 rpm for 10 minutes and the sediment was redispersed in 40 ml DI water by probe sonication. The final dispersion contained ~0.5 wt% Fe as determined by flame atomic absorption spectroscopy (FAAS), and the pH value was measured to be 9.4. After probe sonication (Branson Sonifier® S-450A) the largest iron oxide aggregates above ~400 nm were removed from the

dispersion by centrifugation (6000 rpm for 5 min) and discarded. The clusters were redispersed in deionized (DI) water by probe sonication.

4.2.4 Characterization

Nuclear magnetic resonance (NMR) analysis was performed using a Varian Gemini (300 MHz or 400 MHz) spectrometer. Chemical shifts (δ) are expressed in parts per million (ppm) downfield from tetramethylsilane using the residual protic solvent as an internal standard ($CDCl_3$, 7.24 ppm). Gel permeation chromatography (GPC) was performed on a Viscotek system equipped with a VE 1122 pump, a VE 7510 degasser, two fluorinated polystyrene columns (IMBHW-3078 and I-MBLMW-3078) thermostated to 30 °C (using a ELDEX CH 150 column heater) and arranged in series, using refractive index (RI) detection. Molecular weight and polydispersity data are reported relative to polystyrene standards in tetrahydrofuran (THF).

Dynamic light scattering (DLS) analysis was performed at 90^o on a custom-built apparatus and the data were analyzed using a digital autocorrelator (Brookhaven BI-9000AT) and a non-negative least-squares (NNLS) routine (Brookhaven 9KDLSW32).[32] The suspension concentration was 0.05 mg/mL which gave a measured count rate of approximately 100-200 kcps. Measurements were made over a period of 2 min at least three times on each sample. Zeta potential measurements were performed in triplicate on the ZetaPlus dynamic light scattering apparatus (Brookhaven Instruments) at 90° scattering angle and temperature of 25 °C. The zeta potential was determined from the

electrophoretic mobility by assuming κa « 1. The zeta potential in only an effective value because the polyelectrolyte on the particle surface is permeable.[33]

Transmission electron microscopy (TEM) was used to observe the morphology of nanoclusters. The experiments were performed on a FEI TECNAI G2 F20 X-TWIN TEM using a high-angle annular dark field detector. The samples were prepared using a "flash-freezing" technique, in which a 200 mesh carbon-coated copper TEM grids were cooled using liquid nitrogen and then dipped into dilute aqueous nanocluster dispersion.[34] The sample was dried using a Virtis Advantage Tray Lyophilizer (Virtis Company, Gardiner, NY) with 2 hours of primary drying at -40^{o}C followed by a 12 hour ramp to 25^{o}C and then 2 hours of secondary drying at 25^{o}C. In this manner the aggregation of NPs caused by capillary forces during drying of the liquid on the TEM grid could be minimized. Scanning electron microscopy (SEM) was used to observe iron oxide nanoparticles at the interface. The experiments were performed using Zeiss Supra 40 VP field-emission SEM was operated at an accelerating voltage of 5 kV. SEM samples were prepared using a "flash-freezing" technique, which was dropping oil/water emulsion of iron oxide nanoclusters onto 200 mesh carbon-coated copper TEM grids cooled using liquid nitrogen. The sample was dried into Virtis Advantage Tray Lyophilizer (Virtis Company, Gardiner, NY) with 2 hours of primary drying at -40 ^{o}C followed by a 12 hour ramp to 25 ^{o}C and then 2 hours of secondary drying at 25 ^{o}C. Thermogravimetric analysis (TGA) was used to determine the mass of adsorbed polymer on the iron nanoclusters. The experiments were performed using a Perkin–Elmer TGA 7 under nitrogen atmosphere at a gas flow rate of 20 mL/min. The powder samples were held at 100 °C for 120 minutes

to remove the remaining water and then heated at a constant rate of 20 °C/min from 100 °C to 800 °C and held at 800°C for 30 minutes. Flame atomic absorption spectroscopy (FAAS) was used to determine the iron concentration in the dispersion by using a GBC 908AA flame atomic absorption spectrometer (GBC Scientific Equipment Pty Ltd). All measurements were conducted at 242.8 nm using an air-acetylene flame. Superconducting quantum interference device (SQUID) magnetometer (Quantum Design MPMS) was used to measure the normalized saturation magnetization of the particles at 300 K.

The interfacial tension interference device analysis (software package CAM200 (KSV Ltd., Finland) with a pendant water droplet containing a known concentration of nanparticles in equilibrium with an excess oil phase, as described previously.[35] The average was taken of at least 10 measurements that were acquired every 10 s. The pendant drop was illuminated with a monochromatic light source and the digital images were recorded. The coordinates of the profiles were then analyzed through a computer program imbedded in a software package CAM200 (KSV Ltd., Finland) according to the Laplace equation.[35] For the emulsions, the images were analyzed to determine the droplet size using NIH Image J.

4.3 RESULTS AND DISCUSSION

4.3.1 Nanoparticle dispersions in aqueous media

The size of nanoclusters may be controlled by synthesis in one step in the presence of the final stabilizer[19, 21] or multiple steps.[6a] The single step method was used to

form iron oxide nanoclusters consisting of primary nanoparticles, which were nucleated and grown by co-precipitation of Fe(II) and Fe(III) chlorides under alkaline conditions[21-22] in the presence of PAA-*b*-PBA or PAA-*co*-PBA copolymers. Upon nucleation, the carboxylate groups of the PAA coordinated with the iron, facilitating polymer adsorption and consequently electrosteric stabilization of both the primary particles and the nanoclusters.[19b] The presence of the polymer coating on the iron oxide surface was confirmed by thermogravimetric analysis (TGA), which revealed a loss of 13.0 – 28.2 wt % of organic material (Table 4.1). As the length of the PBA hydrophobic block increased, the adsorption of polymer on the iron oxide increased as the greater hydrophobicity enhanced the tendency of the polymer to leave water. Given the hydrophobicity of the PBA group, it is likely that block copolymers formed hemi-micelles on the nanoparticle surface, as seen in a previous study, which resulted in adsorption of a larger amount of organic material (28.2 wt %) on the nanoparticles.[23]

Table 4.1 Percentage weight loss obtained from TGA and zeta potential measurement of polymer stabilized iron oxide NPs at pH = 8.

Type of polymer stabilizer	DLS with D50 value[nm] ± std. dev.	TGA [weight % loss]	Electrophoretic Mobility [(μ/s)/(V/cm)] ± std. dev.	Zeta Potential [mV] ± std. dev.
PAA coated NPs	61 ± 6	14.0 %	-3.03 ± 0.11	-39.7 ± 1.50
PAA_{114}-*b*-PBA_{26} coated NPs	81 ± 2	13.0 %	-4.11 ± 0.25	-55.61 ± 3.33
PAA_{114}-*b*-PBA_{38} coated NPs	82 ± 3	19.5 %	-3.41 ± 0.05	-46.17 ± 0.71
PAA_{114}-*b*-PBA_{67} coated NPs	71 ± 3	28.2 %	-2.99 ± 0.13	-40.55 ± 1.82
PAA_{133}-*co*-PBA_{44} coated NPs	151 ± 3	14.4 %	-3.33 ± 0.11	-45.07 ± 1.54

The morphologies of PAA-*b*-PBA and PAA-*co*-PBA copolymer coated iron oxide particles were characterized by transmission electron microscopy (TEM), which revealed that small primary particles had aggregated to form nanoclusters (Figure 4.1). The nanoclusters with 60-140 nm diameters were composed of the primary crystals with sizes of 3–10 nm, which occurs commonly with co-precipitation of iron-chloride salts in alkaline media.[21-22, 24] Similar morphologies and aggregation behavior were previously reported for PAA-coated iron oxide nanoclusters.[19a,19b] The use of the "flash-freezing"

technique to prepare the TEM samples minimized aggregation between multiple nanoclusters; however, it is possible that the procedure modestly perturbed the morphology of the original dispersion.

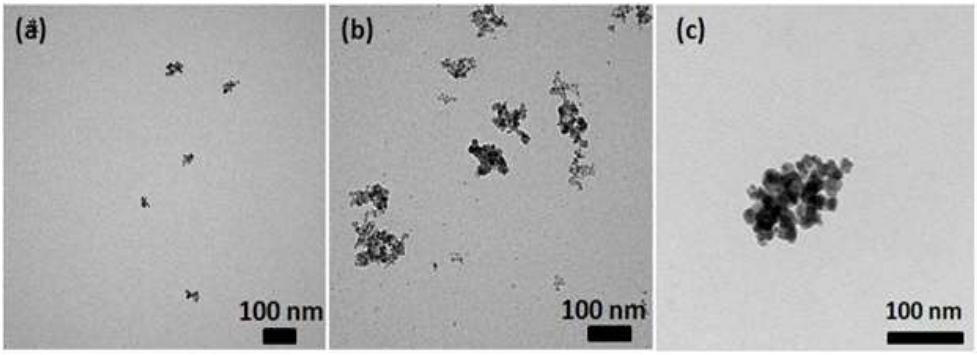

Figure 4.1 TEM images of (a) PAA coated NPs (b) PAA_{114}-*b*-PBA_{26} coated NPs (c) PAA_{133}-*r*-PBA_{64} coated NPs

The hydrodynamic diameters of the nanoclusters dispersed in water at pH = 8 were investigated by dynamic light scattering (DLS) (Figure 4.2). Average D_{50} values (50% of the clusters by volume are below this diameter) of 70-85 nm were observed for the PAA-*b*-PBA stabilized nanoclusters (Table 4.1). The cluster diameter was modestly smaller (D_{50} = 61 nm) for clusters stabilized with PAA homopolymer. Among the three block copolymers, the cluster size was smallest for the one with the largest hydrophobic block. Relatively narrow size distributions were observed for the nanoclusters stabilized by the block copolymers, exemplifying the controlled process of cluster formation under these conditions. Much larger diameters, 120-160 nm, were observed for the PAA-*co*-PBA coated particles (Figure 4.2) indicating somewhat weaker passivation during growth.

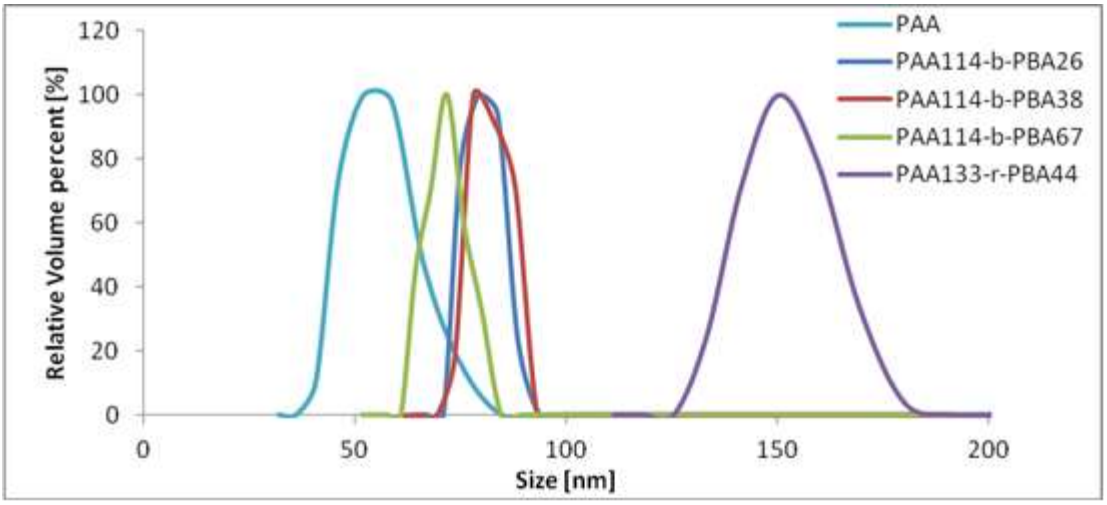

Figure 4.2 Volume fraction based distributions by DLS of PAA_{114}-*b*-PBA_n, PAA-*co*-PBA, and PAA coated iron oxide nanoclusters at pH = 8

The magnetization curves for the iron oxide nanoclusters with PAA-*b*-PBA or PAA-*co*-PBA copolymer stabilizers revealed superparamagnetic behavior without hysteresis (Figure 4.3). The saturation magnetization values were between 60-86 emu/g Fe, compared to a theoretical magnetization value for magnetite of 92–100 emu/g.[20] The modest decrease in magnetization was influenced by the polymer coordination with the iron cations which attenuates the net charge on the particle surface.[25] The saturation magnetization was highest for pure PAA, and lower for the block copolymers, however it did not decrease as a monotonic function of the amount of PBA. The observed reduction in saturated magnetization is likely a result of the increase in contact areas between iron oxide and polymer with longer PBA blocks, which leads to a larger number of inactive spins on the surface. However, in nanoclusters the polymer coats primarily the outer surface of the cluster and not all of the surface area of the primary particles, which prevents the polymer shell from significantly lowering the magnetization.[20]

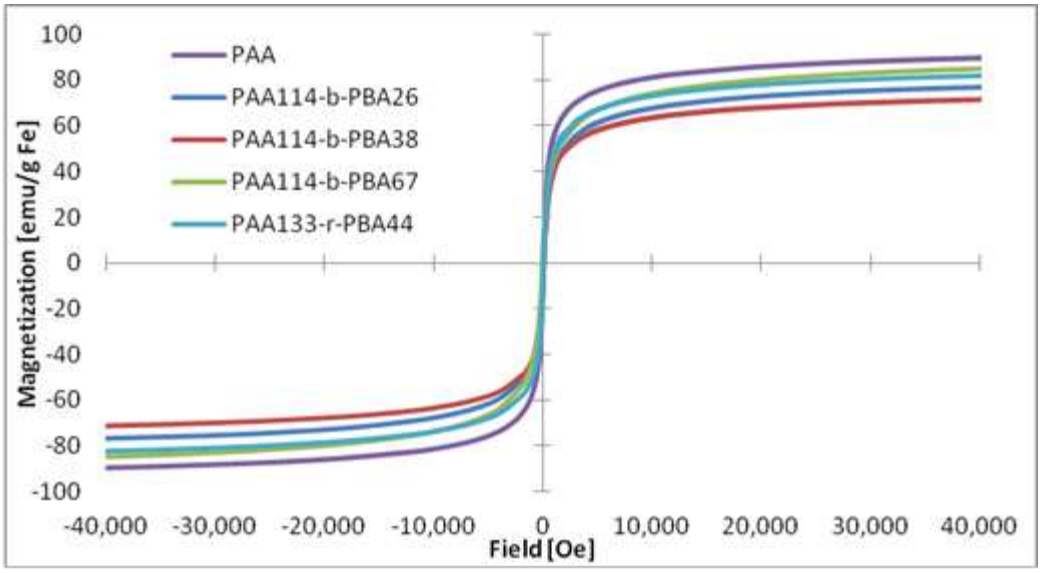

Figure 4.3 SQUID measurement of PAA_{114}-*b*-PBA_n,, PAA, and PAA-*co*-PBA coated iron oxide nanoclusters at pH = 8.

4.3.2 Oil-water interfacial tension and nanoparticle adsorption energy

The interfacial activity of iron oxide nanoclusters with various coatings was studied by measuring the equilibrium interfacial tension γ of a pendant water droplet at the dodecane interface as shown in Table 4.2.

Table 4.2 Nanoparticle size, interfacial tension and adsorption energy of a single particle to the dodecane/water interface.

Type of nanoparticles[a]	***γ* [mN/m]** [b]	***a* [nm]**	***ΔE* [kT]**[c]
Citrate coated NP's	no change (highly hydrophilic)	50	N/A
PAA coated NPs	no change (highly hydrophilic)	31	N/A
PAA_{114}-*b*-PBA_{26} coated NPs	25.2	41	$-3.9.E\times10^{4}$
PAA_{114}-*b*-PBA_{38} coated NPs	28.0	41	$-3.5.E\times10^{4}$
PAA_{114}-*b*-PBA_{67} coated NPs	30.3	36	$-2.4.E\times10^{4}$
PAA_{133}-*co*-PBA_{44} coated NPs	28.2	76	$-1.2.E\times10^{5}$

[a] Measured at pH = 8. [b] Determined from equation 1.

The interfacial tension of the bare dodecane/water interface without any stabilizer was measured to be γ_o = 52.8 mN/m. In the case of PAA_{114}-*b*-PBA_{67} polymer, the interfacial tension was 27.85 mN/m at 0.125 wt% and 26.71 mN/m at 0.25 wt%. However, for the polymer coated nanoparticles, the total PAA_{114}-*b*-PBA_{67} concentration was 0.076 wt%. Therefore, it appears that the polymer has a significant effect on the reduction in interfacial tension when associated with the nanoparticles, although some of the polymer may have desorbed from the surface. Particles coated with a conventional ligand such as citrate, or a hydrophilic polymer such as PAA, showed no change in γ, indicating that the particles were too hydrophilic to be interfacially active between oil and

water. However when the aqueous phase contained a low concentration (0.27 wt%) of PAA-*b*-PBA or PAA-*co*-PBA stabilized nanoparticles γ was reduced by nearly one-half. The particles stabilized with the block copolymer with 26 PBA units produced the lowest γ. Upon adding additional PBA segments, γ increased monotonically. The large decrease in γ indicates that the amphiphilic polymer stabilizers caused the iron oxide nanoclusters to adsorb strongly at the oil/water interface, unlike the particles coated with the hydrophilic PAA homopolymer coating. The observed increase in surface pressure $\gamma_o - \gamma$ as a function of the nanoparticle concentrations was far more pronounced than in previous studies. The surface pressure was calculated to be 25.2-30.3 mN/m for the PAA-*b*-PBA or PAA-*co*-PBA stabilized nanoparticles, whereas previous studies using poly(styrenesulfonate) (PSS)-grafted silica particles[2b] reported much lower surface pressures ($\gamma_o - \gamma$ =15.5 mN/m)[2b] with 1 wt% or required larger nanoparticle concentration (2 wt%) to achieve similar surface pressure ($\gamma_o - \gamma$ = 38 mN/m).[4] The significant decrease in γ observed with such low concentrations of PAA-*b*-PBA or PAA-*co*-PBA stabilized nanoparticles reflects the ability of the amphiphilic polymer segments to efficiently interact with the oil and water on each side of the interface.[2b, 4]

While the block copolymer-coated particles lowered γ over a range of pH values from pH = 6 to 10, the behavior of the nanoparticles with random copolymer shells at the dodecane/water interface was less robust. At lowered pH (pH = 6) these polymers were not completely soluble at a concentration of 0.27 wt% and were unable to stabilize emulsions. Similarly at elevated pH (pH = 10) the random copolymers exhibited

decreased solubility and were ineffective at stabilizing emulsions, likely because the ionic strength of the basic solution was too high for solvation of the hydrophobic PBA groups. However, at pH = 8, the polymer was fully soluble and at a concentration of 0.27 wt.% the γ measured for PAA_{133}-*co*-PBA_{44} nanoparticles ($\gamma = 28.2$ mN/m) was similar to the value for the block copolymer with the closest homopolymer ratio, PAA_{114}-*b*-PBA_{38} ($\gamma = 28.0$ mN/m) (Table 4.2).

Having measured the interfacial tension of the series of nanoclusters, efforts were directed towards calculating the adsorption energy ΔE of one nanocluster at the dodecane-water interface to gain a better understanding of the interaction between the particles and the interface. The adsorption energy was determined from the measured decrease in interfacial tension upon addition of nanoparticles, $\gamma - \gamma_o$ for a contact angle of 90^o (Table 4.2) using Equation 1,

$$\Delta E = \frac{-(\gamma - \gamma_0)\pi a^2}{\eta} \qquad \text{Eq. 1}$$

where a is the particle radius and η is the 2-dimensional packing fraction. Given that the contact angle of the nanoparticle was unknown, we assumed a value of 90^o based upon the approach of a previous study.[26] In this model, the adsorption energy is a function of the total interfacial area blocked by the nanoparticles. For simplicity, we assumed a close-packed interface where η = 0.91. The resulting ΔE values may be corrected based on the approximated packing fraction, however the corrections are relatively modest.

Given the similar values of $\gamma - \gamma_o$ observed in the various copolymer-stabilized iron oxide systems, we expected that differences in ΔE would result more significantly from the variation in particle radius, a. In all cases, the calculated ΔE values were large, indicating that the nanoparticles adsorbed strongly to the interface and that their adsorption may be expected to be relatively irreversible. For the PAA_{114}-*b*-PBA_{26} stabilized nanoclusters, a value of $\Delta E = -3.9\times10^4\ k_BT$ for a = 41 nm was calculated, which was consistent with values reported previously for small nanoparticles.[26] For larger nanoclusters stabilized with PAA_{133}-*co*-PBA_{44} where a = 76 nm, ΔE increased as expected to reach $\Delta E = -1.2\times10^5\ k_BT$ (Table 4.2). In comparison, Du et al. reported ΔE = -5.1 k_BT for a Au nanoparticle with an extremely small radius (a = 2.5 nm), and ΔE = -9 $\times10^5\ k_BT$ for a large polystyrene sphere with a = 1.05 μm.[26] The experiments were performed with a constant concentration in the aqueous phase. However, this concentration is maintained only if only a small fraction of the nanoparticles partitioned to the oil phase.

As the PBA length increased, it is possible that nanoparticles may have been lost to the oil phase with the increase in lipophilicity. Future studies would be required to attempt to understand the detailed conformation of the various polymers on the nanoparticle surfaces and at the oil-water interface. Finally the results may be complicated by any desorption of polymer from the nanoparticle surface to the oil-water interface. One way to ensure that any desorption is prevented in the future would be to cross-link the polymer shells on the nanoparticles surfaces, and studies of such cross-linked polymer shells are currently underway.[6c] However, since no particle aggregation

was observed, as would be expected if the polymer desorbed from the surface, we believe it is unlikely that significant polymer desorption occurred. Furthermore, since the total surface area between the nanoparticles and water within one pendant drop was 6800 times larger than surface area between water and oil in the pendant drop, any desorbed polymer would likely diffuse into the water phase rather than to the oil-water interface, and would not result in any additional interfacial tension lowering.

4.3.3 Properties of the emulsions

In order to determine the partition coefficient of the polymer-coated iron oxide nanoparticles between the water and dodecane phases, experiments were performed with equal volumes of 0.27 wt% aqueous solutions of iron oxide particles and dodecane by gentle agitation, to avoid emulsification. For all polymer coatings in this study, the nanoparticles favored the lower aqueous phase, to form a transparent colored dispersion, and the organic phase was colorless. When probe sonication was used, emulsions of dodecane and water (1:1 volume ratio) were formed with nanoparticle concentrations of only 0.27% Fe_3O_4 (w/v) in water for PAA-*b*-PBA or PAA-*co*-PBA-coated nanoclusters at pH = 8. Photographs of the colors and textures of the biphasic samples taken 24 hrs after probe sonication (Figure 4.4) indicated that the amphiphilic copolymer-coated particles formed a stable emulsion above an excess water phase. The aqueous phases below the emulsion phase were always colored by the presence of nanoparticles indicating that an oil/water emulsion phase was present above the excess aqueous phase, which grew as the oil droplets creamed. According to the Bancroft rule, the continuous phase of the

emulsions will be the phase favored by the nanoparticles between bulk oil and water phases at equilibrium, without any shear or droplet formation. Thus, the presence of oil-in-water emulsions was consistent with the Bancroft rule.[27]

In contrast, when mixtures of dodecane and aqueous dispersions of PAA-coated nanoclusters were subjected to probe sonication, emulsification of the entire volume of the oil and water phases occurred, but the emulsion separated completely into oil and water phases after several hours and the nanoparticles remained in the lower aqueous phase (Figure 4.4a). The lack of emulsion stability was in good agreement with the fact that γ was not lowered for these hydrophilic particles (Table 4.2), as they partitioned too strongly to the aqueous phase.

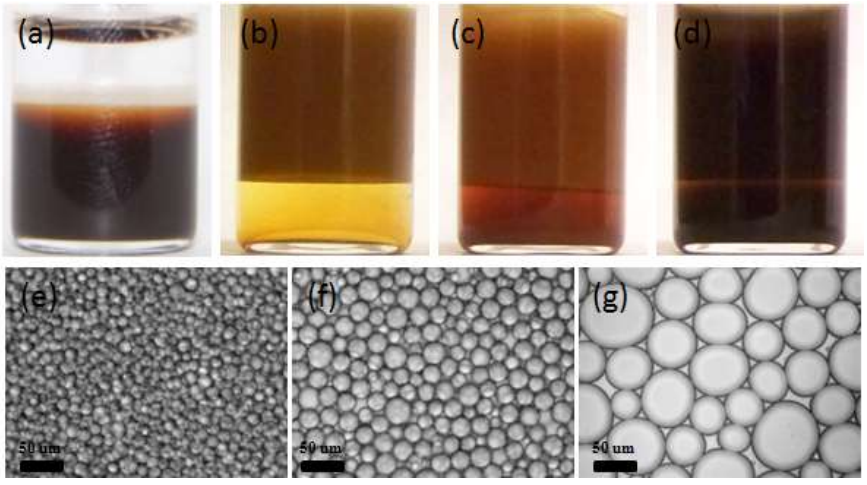

Figure 4.4 Photographs and microscopy images of oil-in-water emulsions formed between dodecane and aqueous dispersions of (a) PAA coated NPs, (b) (e) PAA_{114}-b-PBA_{26} coated NPs, (c) (f) PAA_{114}-b-PBA_{38} coated NPs, and (d) (g) PAA_{114}-b-PBA_{67} coated NPs. Images were acquired after 1 day at pH = 8 with equal volumes of oil and water phases.

Table 4.3 Average emulsion droplet size by image analysis.

	Average emulsion droplet sizes [µm]		
	pH 6	**pH 8**	**pH 10**
PAA_{114}-*b*-PBA_{26} coated NPs	12.1	14.7	12.9
PAA_{114}-*b*-PBA_{38} coated NPs	19.7	22.7	16.6
PAA_{114}-*b*-PBA_{67} coated NPs	37.7	62.8	41.3
PAA_{133}-*co*-PBA_{44} coated NPs	n/a	12.9	n/a

Analysis of microscopy images revealed that the emulsions stabilized by PAA-*b*-PBA-coated nanoclusters consisted of oil droplets ranging from 12.9 to 62.8 µm in diameter (Figure 4.4, Table 4.3). These emulsions only partially phase separated after 1 day leaving an excess water phase. For the three block copolymer shells, the intensity of the color of the excess aqueous phase increased with increasing PBA block length, suggesting that more particles remained in the aqueous layer with increasing PBA content. The concentration of nanoparticles in the excess water phase and the fraction of the total nanoparticles in the upper emulsion phase (excluding the bottom excess water phase) are given in Table 4.4. The smallest oil droplets (14.7 µm) were formed with PAA_{114}-*b*-PBA_{26} stabilized nanoclusters above a light brown excess water phase, with 91% of the nanoparticles in the emulsion phase. As the PBA block length increased, the droplet size increased and reached 22.7 µm for PAA_{114}-*b*-PBA_{38} with 76% of the nanoparticles in the emulsion phase. The somewhat larger droplet size is consistent with the greater water resolution and lower nanoparticle concentration in the emulsion phase. In the emulsions stabilized by PAA_{114}-*b*-PBA_{67}-coated nanoclusters (Figure 4.4g) the excess aqueous

phase was very dark and the droplet size reached 62.8 μm. The changes in the droplet size as a function of PBA length follow the same trends observed in γ and adsorption energy. The smaller droplet sizes observed with shorter PBA lengths are reflected by the lower γ and stronger adsorption of particles to oil/water interfaces.[27]

Table 4.4 Nanoparticle concentration in the oil and water phases.

	Concentration of Excess Water Phase[wt% of Fe]			**Amount of NPs in oil phase [%][a]**		
	pH 6	**pH 8**	**pH 10**	**pH 6**	**pH 8**	**pH 10**
PAA_{114}-*b*-PBA_{26} coated NPs	0.006	0.019	0.103	97.0	90.5	48.5
PAA_{114}-*b*-PBA_{38} coated NPs	0.023	0.048	0.108	88.5	76.0	46.0
PAA_{133}-*co*-PBA_{44} coated NP	n/a	0 wt%	n/a	n/a	100	n/a

[a] Calculated by material balance given known concentration in the excess lower aqueous phase.

When dodecane/water emulsions were formed with nanoparticles coated with the random copolymers at pH = 8, the lower aqueous phase was nearly clear and the nanoparticle concentration in the excess water phase was immeasurably low, indicating that most of the nanoparticles had left the water phase and partitioned into the upper oil phase (Table 4.4). Additionally, the observed droplet sizes were smaller than those observed for the block copolymer-stabilized particles. However, at pH = 6 and pH = 10, the nanoclusters with random copolymer shells were incapable of stabilizing the emulsions, as may be expected given their low water solubility.

A method to determine the packing fraction of nanoparticles on the oil/water interface is given in the Appendix 1. In summary, the interfacial surface area per nanoparticle, *A*, may be estimated from the nanoparticle radius, *a*, and the 2-dimensional packing fraction on an oil droplet, η, with the expression

$$A = \frac{\pi a^2}{\eta} \qquad \text{Eq. 2}$$

The total mass of particles in the emulsion phase, *M*, is used to estimate η with the expression

$$\eta = \frac{MR}{4V_{EP}\phi_c a \rho_p} \qquad \text{Eq. 3}$$

where *R* is the oil droplet radius, *V* is the volume of the emulsion phase, ϕ_c is the oil droplet volume fraction in the emulsion phase (assumed to be 0.74 for close packed spheres), and ρ_p is the nanocluster density (assumed to be half of the bulk iron oxide density of 5.24 g/mL).[1e, 28] For example, when 1 mL of an aqueous dispersion (0.27% w/v) of iron oxide particles coated with PAA_{114}-*b*-PBA_{26} (a = 41 nm) was emulsified with 1 mL of dodecane to form 14 μm oil droplets in water, the resulting interfacial area per nanoparticle was calculated to be $A = 1.2 \times 10^5$ nm^2 (Table 4.5) at pH = 8. When the pH was varied, the changes in *A* were relatively small. The nanoparticle adsorption was on the order of 6-10 % of a monolayer. As the PBA block was increased to 38 units, *A* decreased significantly, and the adsorption reached 22% of a monolayer at pH = 8. Given the significant amount of nanoparticles in the lower aqueous phase, it appeared that the nanoparticle partitioning between phases reached a "quasi" equilibrium value. We use the term quasi as emulsions droplets are not in a state of thermodynamic equilibrium, but

over time will phase separate. For the case of PAA_{133}-*co*-PBA_{44}, the interface was not saturated with nanoparticles as the aqueous excess phase was clear (Figure 4.5). Here the interfacial area was much larger given the smaller droplets, such that the nanoparticles only covered 4% of the interface (Figure 4.6, Table 4.5). Upon doubling the Fe_3O_4 concentration to 0.54% (w/v) the entire volume was emulsified and excess phase was not present even after 2 weeks.

Table 4.5 Estimate of percentage of full monolayer at oil/water interface.[a]

	Monolayer calculation [%]			**Interfacial area/Nanocluster [nm^2]**		
	pH 6	pH 8	pH 10	pH 6	pH 8	pH 10
PAA_{114}-*b*-PBA_{26} coated NPs	7.04	10.02	6.09	$1.4*10^5$	$1.2*10^5$	$1.8*10^5$
PAA_{114}-*b*-PBA_{38} coated NPs	17.87	22.15	10.09	$9.2*10^4$	$8.5*10^4$	$1.4*10^5$
PAA_{133}-*co*-PBA_{44} coated NPs	n/a	4.12	n/a	n/a	$5.1*10^5$	n/a

[a]Determined from material balance in Table 4.4.

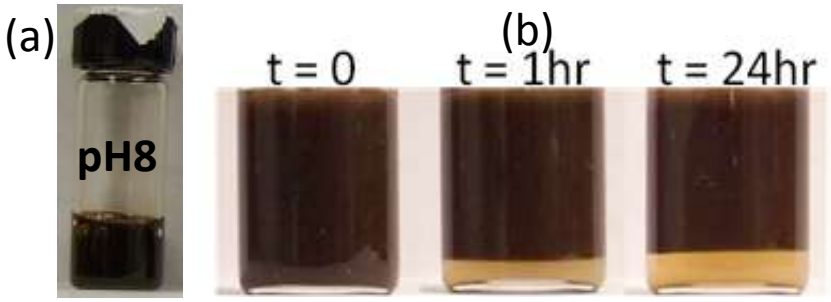

Figure 4.5 (a) Photographs of PAA_{133}-*co*-PBA_{44}-coated iron oxide nanoparticle dispersions after 1 day at pH = 8. (b) Photographs of emulsions formed with equal volume fractions of dodecane and aqueous dispersion of 0.27 wt% PAA_{133}-*co*-PBA_{44}-coated iron oxide particles at pH 8.

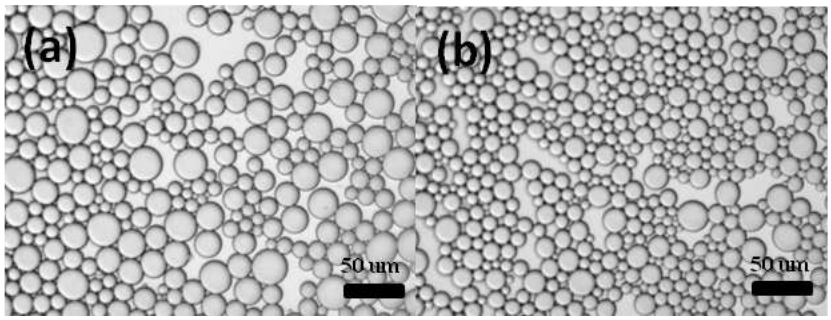

Figure 4.6 Optical micrographs of emulsions formed at pH = 8 at conditions in Figure 7. (a) PAA_{133}-*co*-PBA_{44}, 0 wt% NaCl; (b) PAA_{133}-*co*-PBA_{44}, 3 wt% NaCl. The optical micrographs were taken 24 h after emulsion formation.

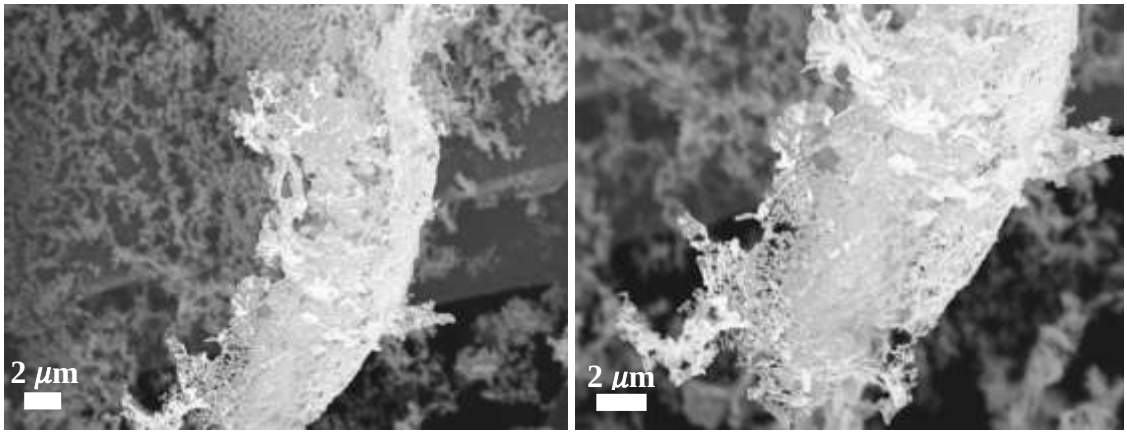

Figure 4.7 SEM images formed by freezing a droplet of the emulsion on a TEM grid pre-cooled in liquid nitrogen. The images (at two different magnifications) show the same single droplet of oil-in water-coated by much less than a monolayer of PAA_{114}-*b*-PBA_{26} coated NPs.

The SEM images in Figure 4.7 are consistent with Table 4.5 in that they show partial monolayers of the nanoparticles on a 30~40 micron diameter oil droplet. These images provide direct evidence that the nanoparticles adsorbed at the oil-water interface. The size of the oil droplet is comparable to that from optical microscopy. On the left hand side of the image, corresponding to the back of the spherical droplet, distinct large open spaces may be seen between the nanoparticles. The surface coverage from SEM is only semi-quantitative given the various angles in the image and the fact that some rearrangement may have taken place during sample preparation. Clearly a tightly packed near full monolayer is not present as was the case in Binks et al.[29], as may be expected for the much lower nanoparticle concentration in the current study.

The mechanism for stabilization of emulsions with only fractional monolayer coverage is not fully understood. Vignati et al. reported that nanoparticles adsorbed on the oil/water interface with approximately 5% of a monolayer of the droplet surfaces

provided emulsion stabilization.[2c] A bilayer of nanoparticles formed a "bridge" between two oil droplets, which prevented coalescence. It is reasonable to assume the same mechanism was operative in our emulsions. The oil droplets were stabilized by a bilayer of nanoparticles at the contact point of the droplets.[30] The high negative surface charge on the nanoparticles, as measured by the zeta potential (Table 4.1) aided the repulsion between two oil droplets.[3b] The observed increase in emulsion droplet size with increasing PBA length in the block copolymers may be explained by their increased hydrophobicity, which prevented sufficient repulsion between oil droplets in the bilayers.[30]

At first it may seem surprising that only a partial monolayer is formed despite the large adsorption energy of 10^4 kT per particle, as has also been seen in previous studies.[2c, 3b, 28] Several factors may contribute to the observation that a full monolayer was not formed. Repulsive interactions between the charged nanoparticles on the surface, as a result of finite ion size effects will decrease the driving force for forming a monolayer[31]. The adsorption of nanoparticles onto the surface may be kinetically limited at the interface and for diffusion through the aqueous channels between the oil droplets. The adsorption may have reached a steady state for the kinetically defined interfacial area. The model does not include interactions between the nanoparticles at the interface, or the effect of a polymer shell on the nanoparticle surfaces. Finally, the low concentration of the nanoparticles in the aqueous phase lowers their chemical potential which will lower the adsorption.

The random copolymers were insufficiently solvated by water (too hydrophobic) to form a stable bilayer in the water channels of two approaching droplets at pH = 6, most likely due to the fact that at pH = 6 the acrylic acid groups were not sufficiently charged given their proximity to PBA groups. At pH = 8, the zeta potentials were similar for the nanoclusters coated by random and block copolymers. The random copolymer chains that extend into water are more hydrophobic than those for the block copolymers, due to the distribution of the PBA groups throughout the polymer chain. Thus the nanoparticles are less hydrophilic and essentially all the iron oxide particles left the water phase and partitioned into the emulsion phase. Furthermore, these highly interfacially active nanoparticles, based on the reduction in γ, stabilized the smallest droplets of any of the NPs tested. However at pH = 6 and pH = 10, where the random copolymer was not soluble and did not lower γ, emulsions could not be formed.

4.4 CONCLUSIONS

A series of sub-100 nm superparamagnetic iron oxide nanoclusters stabilized by amphiphilic PAA-*b*-PBA and PAA-*co*-PBA copolymers were synthesized and shown to induce large reductions in the interfacial tension (high surface pressures) at the dodecane-water interface. During the nanoparticle synthesis, small amounts of copolymer coatings (< 20 % (w/w) by TGA) were adsorbed on the Fe_3O_4 particle surface and mediated the nucleation and growth of nanoclusters to control the nanocluster size, as evidenced by TEM and DLS measurements. The thin copolymer shells on iron oxide played a key role

in enabling high surface pressures at the oil-water interface as a function of the monomer ratio, although some of the effect may have been from desorbed polymer at the interface. Notably, large surface pressures were achieved at much lower nanoparticle concentrations than previously reported for homopolymer-coated nanoparticles.[2b] Sufficient adsorption of the nanoparticles at the oil-water interface stabilized oil droplets as small as 12.1 μm in water at 24 hours, despite the low nanoparticle concentrations (0.27 wt %), indicating high emulsification efficiency. Furthermore, the emulsion droplet formation was facilitated by the low interfacial tensions, which were also shown to be dependent upon the polymer composition. The block copolymer coatings effectively stabilized emulsions over a broad range of pH values (pH = 6-10), while the random copolymer coatings were effective at pH = 8.

The adsorption of the nanoclusters at the oil-water interface was estimated from the concentration of nanoclusters in the excess phase and the interfacial surface area calculated using microscopy images. The most interfacially active was the block copolymer with 26 PBA units, which stabilized the emulsions with a lower fraction of monolayer coverage than with 38 PBA units. Given that the surface coverage was well below that of a monolayer, upon collision of two droplets, the oil droplets were most likely stabilized by a bilayer patch of nanoparticles at the contact point of the droplets, based on an earlier study[30b]. Collectively these results demonstrate that amphiphilic block copolymer shells on iron oxide nanoparticles promote high interfacial activity (large surface pressures), resulting in high emulsification efficiency and unusually small oil droplet sizes at low nanocluster concentrations. The ability to achieve significant

adsorption at the oil/water interface and high surface pressures for nanoparticles, including superparamagnetic nanoclusters with amphiphilic copolymer shells is expected to find utility in a wide variety of practical applications including magnetic imaging in biomedical and subsurface engineering and in enhanced oil recovery. Future studies of the conformation of the copolymers on the iron oxide surface may be used to provide insight into the mechanism of the reduction of interfacial tension.

4.5 REFERENCES

1. (a) Binks, B. P., Particles as surfactants similarities and differences. *Current Opinion in Colloid and Interface Science* **2002,** *7*, 21-41; (b) Hunter, T. N.; Pugh, R. J.; Franks, G. V.; Jameson, G. J., The role of particles in stabilising foams and emulsions. *Advances in Colloid and Interface Science* **2008,** *137*, 57-81; (c) Binks, B. P., Silica Particle-Stabilized Emulsions of Silicone Oil and Water: Aspects of Emulsification. *Langmuir* **2004,** *20*, 1130-1137; (d) Melle, S.; Lask, M.; Fuller, G. G., Pickering emulsions with controllable stability. *Langmuir* **2005,** *21*, 2158-2162; (e) Tcholakova, S.; Denkov, N. D.; Lips, A., Comparison of solid particles, globular proteins and surfactants as emulsifiers. *Phys. Chem. Chem. Phys.* **2008,** *10*, 1608–1627; (f) Aveyard, R.; Clint, J. H.; Horozov, T. S., Aspects of the stabilisation of emulsions by solid particles: Effects of line tension and monolayer curvature energy. *Phys. Chem. Chem. Phys.* **2003,** *5*, 2398–2409; (g) Schwartz, H.; Harel, Y.; and Efrima, S., Surface Behavior and Buckling of Silver Interfacial Colloid Films. *Langmuir* **2001,** *17*, 3884-3892; (h) Lin, Y.; Skaff, H.; Emrick, T.; Dinsmore, A. D.; and Russell, T. P., Nanoparticle Assembly and Transport at Liquid-Liquid Interfaces. *Science* **2003,** *299*, 226-229.

2. (a) Wang, W.; Zhou, Z.; Nandakumar, K.; Xu, Z.; H., a. M. J., Effect of charged colloidal particles on adsorption of surfactants at oil–water interface. *J. Colloid Interface Sci.* **2003,** *274*, 625–630; (b) Saleh, N.; Sarbu, T.; Sirk, K.; Lowry, G. V.; Matyjaszewski, K.; Tilton, R. D., Oil-in-Water Emulsions Stabilized by Highly Charged Polyelectrolyte-Grafted Silica Nanoparticles. *Langmuir* **2005,** *21*, 9873-9878; (c) Vignati, E.; and Piazza, R., Pickering Emulsions: Interfacial Tension, Colloidal Layer Morphology, and Trapped-Particle Motion. *Langmuir* **2003,** *19*, 6650-6656.

3. (a) Ma, H.; Luo, M.; Dai, L. L., Influences of surfactant and nanoparticle assembly on effective interfacial tensions. *Physical Chemistry Chemical Physics* **2008,** *10*, 2207-2213; (b) Binks, B. P.; Rodrigues, J. A., Enhanced stabilization of emulsions due to surfactant-induced nanoparticle flocculation. *Langmuir* **2007,** *23*, 7436-7439; (c) Stocco, A.; Drenckhan, W.; Rio, E.; Langevin, D.; Binks, B. P., Particle-stabilised foams: an interfacial study. *Soft Matter* **2009,** *5*, 2215–2222.

4. Saigal, T.; Dong, H. C.; Matyjaszewski, K.; Tilton, R. D., Pickering Emulsions Stabilized by Nanoparticles with Thermally Responsive Grafted Polymer Brushes. *Langmuir* **2010,** *26* (19), 15200-15209.

5. Saleh, N.; Phenrat, T.; Sirk, K.; Dufour, B.; Ok, J.; Sarbu, T.; Matyjaszewski, K.; Tilton, R. D.; Lowry, G. V., Adsorbed Triblock Copolymers Deliver Reactive Iron Nanoparticles to the Oil/Water Interface. *Nano Letters* **2005,** *5* (12), 2489-2494.

6. (a) Ditsch, A.; Laibinis, P. E.; Wang, D. I. C.; Hatton, T. A., Controlled Clustering and Enhanced Stability of Polymer-Coated Magnetic Nanoparticles. *Langmuir* **2005,** *21* (13), 6006-6018; (b) Kotsmar, C.; Yoon, K. Y.; Ingram, D. R.; Ryoo, S. Y.; Barth, J.; Shao, S.; Prodanovic´, M.; Milner, T.; Bryant, S. L.; Huh, C.; Johnston, k. P., Stable Citrate-Coated Iron Oxide Superparamagnetic Nanoclusters at High Salinity. *Ind. Eng. Chem. Res.* **2010,** *49*, 12435–12443; (c) Yoon, K. Y.; Kotsmar, C.; Ingram, D. R.; Huh, C.; Bryant, S. L.; Milner, T. E.; Johnston, K. P., Stabilization of Superparamagnetic Iron Oxide Nanoclusters in Concentrated Brine with Cross-Linked Polymer Shells.

Langmuir **2011,** *27*, 10962-10969; (d) Esser-Kahn, A. P.; Odom, S. A.; Sottos, N. R.; White, S. R.; Moore, J. S., Triggered Release from Polymer Capsules. *Macromolecules* **2011,** *44*, 5539–5553.

7. Zhou, J.; Qiao, X.; Binks, B. P.; Sun, K.; Bai, M.; Li, Y.; Liu, Y., Magnetic Pickering Emulsions Stabilized by Fe3O4 Nanoparticles. *Langmuir* **2011,** *27*, 3308–3316.

8. (a) Binks, B. P.; Kirkland, M., Interfacial structure of solid-stabilised emulsions studied by scanning electron microscopy. *Phys. Chem. Chem. Phys.* **2002,** *4*, 3727-3733; (b) Lan, Q.; Liu, C.; Yang, F.; Liu, S.; Sun, D., Synthesis of bilayer oleic acid-coated Fe3O4 nanoparticles and their application in pH-responsive Pickering emulsions. *Journal of Colloid and Interface Science* **2007,** *310*, 260-269.

9. (a) Gupta, A. K.; Gupta, M., Synthesis and surface engineering of iron oxide nanoparticles for biomedical applications. *Biomaterials* **2005,** *26*, 3995–4021; (b) Oh, J.; Feldman, M. D.; Kim, J.; Condit, C.; Emelianov, S.; Milner, T. E., Detection of magnetic nanoparticles in tissue using magneto-motive ultrasound. *Nanotechnology* **2006,** *17* (16), 4183-4190; (c) Lattuada, M.; Hatton, T. A., Preparation and Controlled Self-Assembly of Janus Magnetic Nanoparticles. *Journal of the American Chemical Society* **2007,** *129* (42), 12878-12889; (d) Lu, A.-H.; Salabas, E. L.; Schueth, F., Magnetic nanoparticles: synthesis, protection, functionalization and application. *Angew. Chem. Int. Ed.* **2007,** *46*, 1222-1244; (e) Ma, L. L.; Feldman, M. D.; Tam, J. M.; Paranjape, A. S.; Cheruku, K. K.; Larson, T. A.; Tam, J. O.; Ingram, D. R.; Paramita, V.; Villard, J. W.; Clarke, G. D.; Jenkins, J. T.; Asmis, R.; Sokolov, K.; Chandrasekar, B.; Milner, T. E.; Johnston, K. P., Small multifunctional nanoclusters (Nanoroses) for targeted cellular imaging and therapy. *ACS Nano* **2009,** *3*, 2686-2696; (f) Sun, B.; Sun, M.-J.; Gu, Z.; Shen, Q.-D.; Jiang, S.-J.; Xu, Y.; Wang, Y., Conjugated Polymer Fluorescence Probe for Intracellular Imaging of Magnetic Nanoparticles. *Macromolecules* **2010,** *43*, 10348–10354.

10. Adkins, S. S.; Gohil, D.; Dickson, J. L.; Webber, S. E.; Johnston, K. P., Water-in-carbon dioxide emulsions stabilized with hydrophobic silica particles. *Physical Chemistry Chemical Physics* **2007,** *9* (48), 6333-6343.

11. (a) Yu, H.; Kotsmar, C.; Yoon, K. Y.; Ingram, D. R.; Johnston, K. P.; Bryant, S. L.; Huh, C., Transport and retention of aqueous dispersions of paramagnetic nanoparticles in reservoir rocks. *17th SPE Improved Oil Recovery Symposium Tulsa, OK* **2010,** *SPE 129887*; (b) Prodanovic, M.; Ryoo, S.; Rahmani, A. R.; Kuranov, R.; Kotsmar, C.; Milner, T. E.; Johnston, K. P.; Bryant, S. L.; Huh, C., Effects of magnetic field on the motion of multiphase fluids containing paramagnetic particles in porous media. *17th SPE Improved Oil Recovery Symposium Tulsa, OK* **2010,** *SPE 129850*; (c) Prakash, A.; Zhu, H.; Jones, C. J.; Benoit, D. N.; Ellsworth, A. Z.; Bryant, E. L.; Colvin, V. L., Bylayers as Phase Transfer Agents for Nanocrystals Prepared in Nonpolar Solvents. *ACS Nano* **2009,** *3*, 2139-2146; (d) Adkins, S. S.; Gohil, D.; Dickson, J. L.; Webber, S. E.; Johnston, K. P., Water-in-carbon dioxyde emulsions stabilized with hydrophobic silica particles. *Phys. Chem. Chem. Phys.* **2007,** *9*, 6333-6343.

12. Ryoo, S.; Rahmani, A. R.; Yoon, K. Y.; Prodanovic, M.; Kotsmar, C.; Milner, T. E.; Johnston, K. P.; Bryant, S. L.; Huh, C., Theoretical and experimental investigation of the motion of multiphase fluids containing paramagnetic nanoparticles in porous media. *SPE Annual Meeting, Florence, Italy* **2010,** *SPE 134879*.

13. Melle, S.; Lask, M.; Fuller, G. G., Pickering emulsions with controllable stability. *Langmuir* **2005,** *21*, 2158-2162.

14. Ingram, D. R.; Kotsmar, C.; Yoon, K. Y.; Shao, S.; Huh, C.; Bryant, S. L.; Milner, T.; Johnston, k. P., Superparamagnetic nanoclusters coated with oleic acid bilayers for stabilization of emulsions of water and oil at low loncentration. *J. Colloid Interface Sci.* **2010,** *351*, 225-232.

15. Massart, R.; Dubois, E.; Cabuil, V.; Hasmonay, E., Preparation and properties of monodisperse magnetic fluids. *Journal of Magnetism and Magnetic Materials* **1995,** *149*, 1-5.

16. Bacri, J.; Perzynski, R.; Salin, D.; Cabuil, V.; Massart, R., *J. Magn. Magn. Mater.* **1990,** *85*, 27.

17. (a) Kim, H. J.; Phenrat, T.; Tilton, R. D.; Lowry, G. V., *Environ. Sci. Technol.* **2008,** *43*, 3824-3830; (b) Saleh, N.; Kim, H.-J.; Phenrat, T.; Matyjaszewski, K.; Tilton, R. D.; Lowry, G. V., Ionic strength and composition affect the mobility of surface-modified Fe^0 nanoparticles in water-saturated sand columns. *Environ. Sci. Technol.* **2008,** *42*, 3349-3355.

18. (a) Berret, J.-F., Stoichiometry of Electrostatic Complexes Determined by Light Scattering. *Macromolecules* **2007,** *40*, 4260-4266; (b) Berret, J.-F.; Schonbeck, N.; Gazeau, F.; El Kharrat, D.; Sandre, O.; Vacher, A.; Airiau, M., Controlled clustering of superparamagnetic nanoparticles using block copolymers: design of new contrast agents for magnetic resonance imaging. *J. Am. Chem. Soc.* **2006,** *128*, 1755-1761.

19. (a) Lin, C.-L.; Lee, C.-F.; Chiu, W.-Y., Preparation and properties of poly(acrylic acid) oligomer stabilized superparamagnetic ferrofluid. *J. Colloid Interf. Sci.* **2005,** *291*, 411-420; (b) Ge, J.; Hu, Y.; Biasini, M.; Beyermann, W. P.; Yin, Y., Superparamagnetic magnetite colloidal nanocrystal clusters. *Angew. Chem. Int. Ed.* **2007,** *46*, 4342-4345.

20. Sondjaja, R.; Hatton, A. T.; Tam, M. K. C., Clustering of magnetic nanoparticles using a double hydrophilic block copolymer, poly(ethylene oxide)-b-poly(acrylic acid). *J. Magn. Magn. Mat.* **2009,** *321*, 2393-2397.

21. Sahoo, Y.; Goodarzi, A.; Swihart, M. T.; Ohulchanskyy, T. Y.; Kaur, N.; Furlani, E. P.; Prasad, P. N., Aqueous ferrofluid of magnetite nanoparticles: fluorescence labeling and magnetophoretic control. *J. Phys. Chem. B* **2005,** *109*, 3879–3885.

22. (a) Massart, R., Preparation of aqueous magnetic liquids in alkaline and acidic media. *IEEE Trans. Magn.* **1981,** *17*, 1247-1248; (b) Lyon, J. L.; Fleming, D. A.; Stone, M. B.; Schiffer, P.; Williams, M. E., Synthesis of Fe oxide core/Au shell nanoparticles by iterative hydroxylamine seeding. *Nano Letters* **2004,** *4*, 719-723.

23. Jacquin, M.; Muller, P.; R., T.-P.; H., C.; J.F., B.; T., F., Chemical analysis and aqueous solution properties of charged amphiphilic block copolymers PBA-b-PAA synthesized by MADIX®. *J. Colloid Interface Sci.* **2007,** *316*, 897–911.

24. Campelj, S.; Makovec, D.; Drofenik, M., Preparation and properties of water-based magnetic fluids. *J. Phys.: Condens. Matter* **2008,** *20*, 204101-204105.

25. Berkowitz, A. E.; Lahut, J. A.; Sacobs, I. S.; Levinson, L. M.; forester, D. W., Spin Pinning at Ferrite-Organic Interfaces. *Phys.Rev.Lett.* **1975,** *34* (10), 594–597.

26. Du, K.; Glogowski, E.; Emrick, T.; Russell, T. P.; Dinsmore, A. D., Adsorption Energy of Nano- and Microparticles at Liquid-Liquid Interfaces. *Langmuir* **2010,** *26* (15), 12518-12522.

27. Binks, B. P., Particles as surfactantssimilarities and differences. *Current Opinion in Colloid and Interface Science* **2002,** *7*, 21-41.

28. Golemanov, K.; Tcholakova, S.; Kralchevsky, P. A.; Ananthapadmanabhan, K. P.; and Lips, A., Latex-Particle-Stabilized Emulsions of Anti-Bancroft Type. *Langmuir* **2006,** *22*, 4968-4977.

29. Binks, B. P.; Kirkland, M.; Rodrigues, J. A., Origin of stabilisation of aqueous foams in nanoparticle–surfactant mixtures. *Soft Matter* **2008,** *4*, 2373–2382.

30. (a) Horozov, T. S., Foams and foam films stabilised by solid particles. *Current Opinion in Colloid & Interface Science* **2008,** *13*, 134-140; (b) Horozov, T. S.; Binks, B.

P., Particle-Stabilized Emulsions: A Bilayer or a Bridging Monolayer? *Angew. Chem. Int. Ed.* **2006,** *45*, 773-776.

31. Masschaele, K.; Park, B. J.; Furst, E. M.; Fransaer, J.; and Vermant, J., Finite Ion-Size Effects Dominate the Interaction between Charged Colloidal Particles at an Oil-Water Interface. *Physical Review Letters* **2010,** *105*, 048303.

32. Ryoo, W.; Webber, S. E.; Johnston, K. P., Water-in-Carbon Dioxide Microemulsions with Methylated Branched Hydrocarbon Surfactants. *Ind. Eng. Chem. Res.* **2003,** *42*, 6348-6358.

33. (a) Ohshima, H., Electrophoretic mobility of soft particles. *Colloids Surfaces A: Physicochem. Eng. Aspects* **1995,** *103*, 249-255; (b) Ohshima, H.; and Makino, K., Electrophoretic mobility of a particle covered with a partially Electrophoretic mobility of a particle covered with a partially. *Colloids Surfaces A: Physicochem. Eng. Aspects* **1996,** *109*, 71-75.

34. Tam, J. M.; Murthy, A. K.; Ingram, D. R.; Nguyen, R.; Sokolov, K. V.; P., J. K., Kinetic assembly of near-IR active gold nanoclusters using weakly adsorbing polymers to control size. *Langmuir* **2010,** *26*, 8988-8999.

35. Chen, X.; Adkins, S. S.; Nguyen, Q. P.; Sanders, A. W.; Johnston, K. P., Interfacial tension and the behavior of microemulsions and macroemulsions of water and carbon dioxide with a branched hydrocarbon nonionic surfactant. *J. of Supercritical Fluids* **2010,** *55*, 712–723.

Chapter 5: Graphene Oxide Nanoplatelet Dispersions in Concentrated NaCl and Stabilization of Oil/Water Emulsions

Stable dispersions of graphene oxide nanoplatelets were formed in water at pH 2 to 10 even with 5 wt% NaCl. For these conditions, oil-in-water emulsions stabilized with graphene oxide nanoplatelets remained partially stable for one year. The droplet sizes were as small as ~1 μm with a low nanoplatelet concentration of 0.2 wt%. Stable emulsions could also be formed even for nanoplatelet concentrations down to 0.001 wt%. The stabilities of the emulsions even at high salinity may be attributed to the high anion density at the platelet edges which protrude into the water phase. Furthermore, the plates are shown to adsorb on the surfaces of the oil droplets. The conceptual picture of nanoplatelets adsorbed to a greater extent on the water side of the oil/water interface, along with the high density of anions on the platelet edges, cause the oil/water interface to curve about the oil phase, resulting in oil-in-water emulsion droplets. The robust dispersion stability with a very small amount of, graphite-based stabilizer, offers an intriguing opportunity for applications including CO_2 sequestration in deep subsurface formations, which generally contain high-salinity brines; and also enhanced oil recovery from deep reservoirs.

5.1 INTRODUCTION

Nanoplatelets of graphene or graphene oxide are drawing considerable interest for potential applications, because of their extremely large surface area per mass and their

unique properties including very high electrical and thermal conductivities and high elasticity. Research activities are extensive for graphene oxide, *e.g.*, in developing polymer composites with durable high elasticity,[1] as nano-scale sensors that can be deployed in highly confined spaces,[2] or as catalytic supports in facilitating oxidation and hydration reactions. As a pathway to distribute nanoplatelets uniformly in polymer phases, stable aqueous dispersions have been successfully designed.[3] Graphene oxide nanoplatelets (GON) have also been shown to stabilize oil-in-water emulsions.[4]

As GON can easily disperse in water due to the highly negative carboxylate groups on the edge of GON, they may be considered as a hydrophilic. GON dispersed in high salinity brines are shown here to be highly stable against aggregation or settling. However, as GON have an edge-to-center distribution of hydrophilic and hydrophobic properties, they are amphiphilic and can adsorb to oil/water interfaces and lower the interfacial energy.[5] Therefore, GON are interesting candidates for formation and stabilization of even CO_2/water emulsion or foams, so that CO_2 could be securely stored in deep subsurface formations. Solid-stabilized foams and emulsions generally exhibit more robust dispersion stability than surfactant-stabilized foams/emulsions, and the use of various solid particles for CO_2 foam stabilization has been studied.[6] Generally, plate-like particles have been shown to produce highly stable foams and emulsions due to the steric hindrance provided by the adsorbed particles at the interface.[7] Similarly, since GON can cover an extremely large interfacial area for a given mass, ~600 m^2/g,[2] they may be expected to be highly efficient stabilizers at low concentrations. Not only do the GON stabilize emulsions, but they offer multifunctionality in upstream oil industry. They

may be used for electrical sensing, to increase the effective viscosity of the oil-displacing fluids, and/or to deliver certain chemicals at downhole locations or even into reservoir formations. Similar use of nanoparticles for potential oilfield applications is an active research area, *e.g.*, for silica nanosphere-stabilized oil/water emulsions[8] and CO_2 foams[9] for improved oil displacement, and for delivery of superparamagnetic nanoparticles deep into reservoirs for improved oil detection.[10]

The objectives of this study are three fold; (1) dispersion of graphene oxide nanoplatelets in water over a wide range of pH and salinity up to 5 wt.% NaCl, (2) stabilization of oil-in-water emulsions with graphene oxide nanoplatelets (GON) at various concentrations as low as 0.001 wt% loading, and (3) stabilization of emulsions in high salinity brines, even up to 5 wt% NaCl. The GON-stabilized Pickering emulsions remained partially stable for one year. The emulsion stability at high salinity is believed to be due to the high anion density at the GON edges, which are most likely in the water phase and provide electrostatic stabilization, and to the steric separation of the oil droplets. A key consideration for subsurface applications is that aqueous dispersions of GON are stable and that GON stabilize emulsions at high salinity conditions that generally prevail in deep aquifers and in oil reservoirs.

5.2 EXPERIMENTAL DETAILS

5.2.1 Preparation of Graphene Oxide Nanoplatelets (GON)

Graphite oxide was synthesized by the modified Hummer's method.[11] One gram of natural graphite (Bay Carbon, SP-1) was first mixed with 50 ml concentrated H_2SO_4 in a flask, which was then cooled to 0 ^oC in an ice bath, followed by the addition of 5 g of $KMnO_4$ over a 30- minute duration. The mixture was then heated and stirred at 35 ^oC for 2 hours. An ice bath was subsequently used to cool down the solution to 3-4 ^oC; and 23 ml of de-ionized water was slowly added into the flask while stirring to minimize heating. The temperature in the ice bath was monitored and controlled to be no higher than 7 ^oC, by adding water, and ice if needed. Once the temperature was stabilized, more DI water (270 ml) was added to dilute the suspension, by stirring at 300 rpm. H_2O_2 (30 wt% in water) was added in drops to remove excessive $KMnO_4$. The final suspension was filtered and washed by HCl (10% in water) five times, which was suction-dried for 12 hours in the glass filter. Further drying was done in vacuum at room temperature for one day.

A uniform and stable suspension of 0.2 wt% graphene oxide nanoplatelets in water was obtained by sonication (VWR B2500A-MT) for 2 hours at room temperature.

5.2.2 Pickering emulsion preparation

The GON aqueous dispersion (0.2 wt%) was used for the emulsion preparation. 1ml of the dodecane was added to 1 ml of the GON dispersion in a glass flask. The system was emulsified using a probe sonicator for 1 min., to irradiate with ultrasound in the pulse mode. To study the effects of salinity on emulsification, brines of 1, 3, or 5wt% of NaCl where used. The dodecane–water emulsions were kept for a month to study the

stability against phase separation, by measuring the changes in emulsion volume with time.

5.2.3 Characterization

Zeta potential was measured with a Brookhaven ZetaPALS instrument at 25 °C. Measurements were conducted in 10 mM KCl (Debye length κ^{-1} = 3 nm) and zeta potential was determined with Smoulchwoski model ($\kappa a >> 1$). Transmission electron microscopy (TEM) was used to observe the surface of oil-in-water emulsion. The experiments were performed on a FEI TECNAI G2 F20 X-TWIN TEM using a high-angle annular dark field detector. The samples were prepared using a "flash-freezing" technique, in which a 200 mesh carbon-coated copper TEM grids were cooled using liquid nitrogen and then dipped into dilute aqueous graphene oxide nanoplatelet dispersion.[12]

Scanning electron microscopy (SEM) was used to observe the morphology of Graphene Oxide nanoplatelets (GON). The experiments were performed using Zeiss Supra 40 VP field-emission SEM was operated at an accelerating voltage of 5 kV.

The interfacial tension (γ) was measured from axisymmetric drop shape analysis of a pendant water droplet containing a known concentration of nanoplatelets in equilibrium with an excess oil phase, as described previously.[13] The average was taken of at least 5 measurements that were acquired every 10 s. The pendant drop was illuminated with a monochromatic light source and the digital images were recorded. The coordinates of the profiles were then analyzed through a computer program imbedded in a software

package CAM200 (KSV Ltd., Finland) according to the Laplace equation.[13] For the emulsions, the images were analyzed to determine the droplet size using NIH Image J.

5.3 RESULTS AND DISCUSSION

5.3.1 Aqueous dispersion of GON

Figure 5.1 shows an SEM image of GON. While each GON is only a monolayer-thick, its areal dimension is fairly large with a wide size distribution, because it was generated by simple mechanical crushing, after the exfoliation of the graphene oxide sheets. The particle length varied from less than 1 μm to a few μm. Figure 5.2 shows the aqueous dispersions of GON for different NaCl salinity and pH. The uniform dark appearance of the samples indicates that the dispersions are stable and homogeneous. The areal dimension of the GON was in the range of several microns. The interior surfaces are sparsely charged but the edges are known to be highly charged.[4a, 5] The aqueous stability of the resulting GON dispersion, due to dense negative charges at their edges and the small inter-platelet attraction.[14]

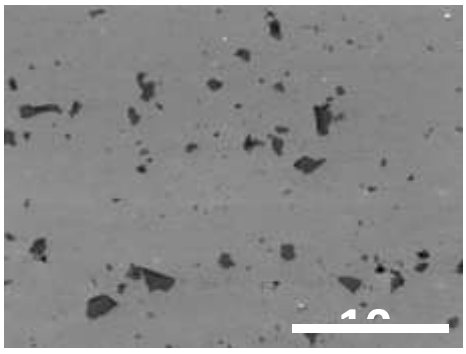

Figure 5.1 Scanning electron microscopy (SEM) image of the graphene oxide nanoplatelets (GON).

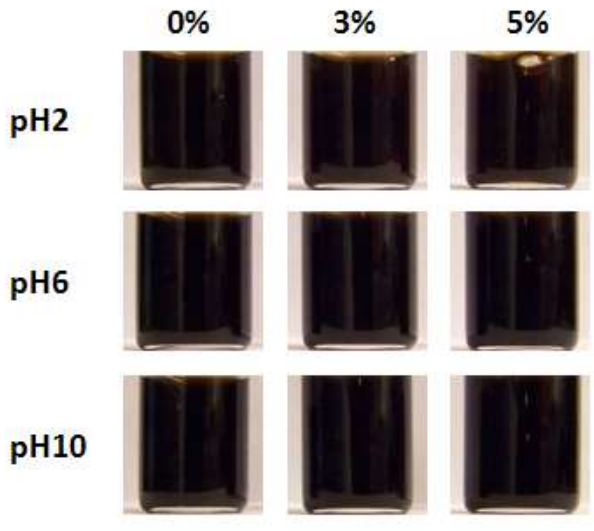

Figure 5.2 Photographs of GON aqueous dispersions (0.2 wt% concentration) after 1day at pH 2, 6, and 10 and with 0, 3, and 5 wt% NaCl salinity. The uniformly dark color means that the aqueous dispersion is stable.

The zeta potential for the GON dispersion were -41.8, -53.1, and -52.8 mV with no salt at pH 2, 6, and 10, respectively(Figure 5.3). In addition, even after adding up to 5 wt% NaCl, the zeta potential of GON dispersion was about -15 mV at pH 2, 6, and 10. The maintenance of a moderate zeta potential without salt reflects the high charge density at the nanoplatelet edges.[14-15]

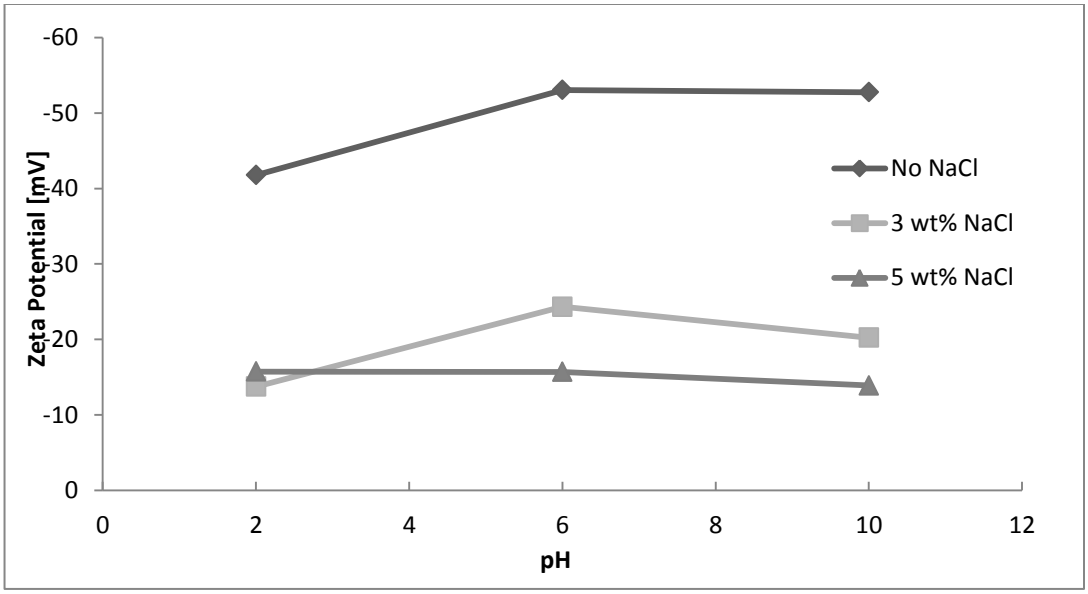

Figure 5.3 Zeta potential measurement of GON with different level of NaCl concentration at pH 2, 6, and 10.

The stabilization mechanism for GON dispersion is known to be the electrostatic repulsion by the surface anions.Thus, the stabilization is quite different than in the case of a polymeric stabilizer, which provides steric stabilization as a function of the length of extended chains.[2, 5] This robust stability for wide ranges of salinity up to 5% and pH is quite unusual. For other charge-stabilized colloidal dispersions at 5% salinity, the thin double layers often lead to loss of electrostatic stabilization. This stabilization may be due to the fact that GON (*i*) have a high charge density at the edges favoring electrostatic repulsion; and (*ii*) are extremely thin thus weakening the van der Waals attraction between the platelets, which lowers the probability of platelet aggregation.[4a]

5.3.2 Properties of the emulsions

For GON to serve as an emulsion stabilizer, it must adsorb at the oil/water interface, occupying a substantial interfacial area to prevent droplet coalescence. While the interfacial adsorption of colloidal particles may require energy to first form an oil/water interface, once they are adsorbed at the oil/water interface, they may provide emulsion stability.[16] The formation of the oil/water interface is provided by the high shear rate to overcome the Laplace pressure, which was produced by sonication. For nanoparticles with a high adsorption energy and surface coverage at the oil/water interface, emulsion droplets may be stabilized for long time periods. [4a]

The emulsification of oil/water using GON adsorbed at the interface has been achieved with simple shaking to form large oil droplets.[4a, 16d, 17] Sharif and coworkers also reported the formation of GON stabilized oil/water emulsions using high power sonication to form droplets less than 5 μm with 1-5 wt% GON.[4b] As with the conventional Pickering emulsions, energy input is required for droplet formation whereby the GON then must overcome the adsorption energy barrier and attach GON at the oil/water interface.

Qualitative analysis of the interfacial activity of GON was attempted by carrying out phase partitioning experiments, by mixing the GON-containing water and dodecane gently. Even at low pH, GONs are too hydrophilic to disperse in dodecane and simply remain stable in the water phase. It is visibly evident that GON has a high charge density at its edges (electrical conductivities of 0.2 wt% GON dispersion: 725 μS/cm, 395 μS/cm, and 298 μS/cm at pH 2, 6, and 10). Therefore, the van der Waals attraction between the

platelets is very small, which lowers the probability of GON aggregation and precipitation.

In order to determine the partition coefficient of the GON between water and dodecane, experiments were performed by forming emulsions with equal volumes of a 0.2 wt% of GON dispersion without added salt and dodecane by gentle hand shaking (low shear). The GON favored the lower aqueous phase and the dodecane phase was clear. Therefore, in the experiments below at high shear, it was expected that the GON would favor the water side of the interface and stabilize oil/water emulsions at high shear by the Bancroft rule. [16a]

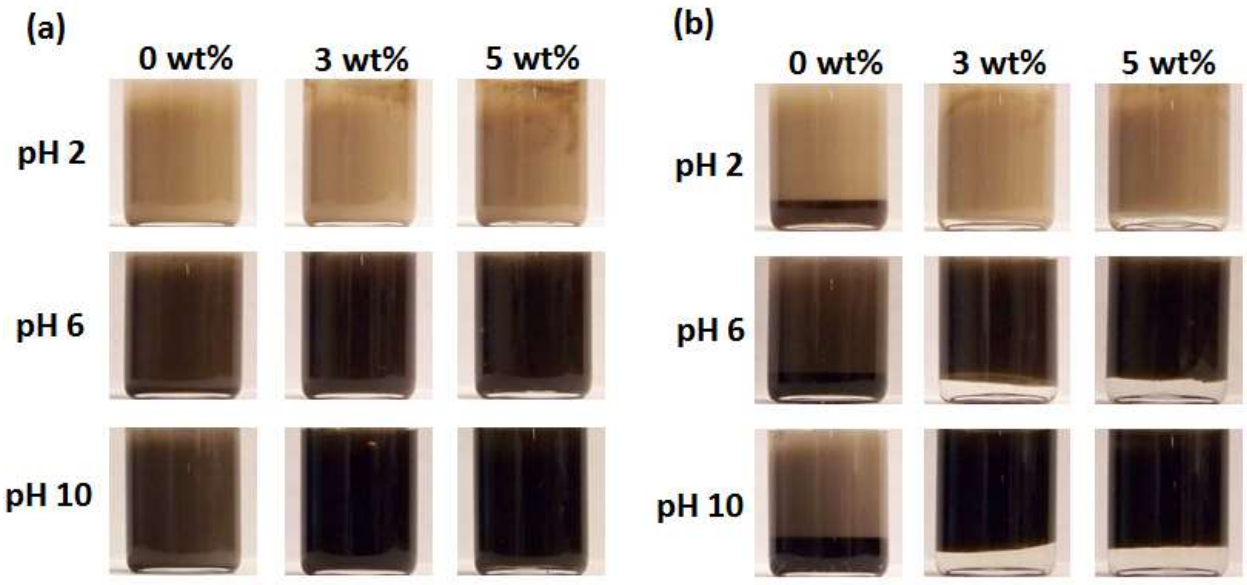

Figure 5.4 Emulsions formed with equal volume fractions of dodecane and an aqueous dispersion of 0.2 wt% GON at pH 2, 6, and 10 with 0, 3, and 5 wt% NaCl salinity. The photos were taken (a) immediately (b) 24 hours after emulsion formation. Initially after emulsion formation, all vials appeared as a full emulsion.

Figure 5.4 shows dodecane-in-brine emulsions, stabilized with GON at 0.2 wt% concentration, at different NaCl salinities and pH values. Photographs of the colors and textures of the phases of the samples are shown immediately (Figure 5.4a) after sonication and 24 hours later (Figure 5.4b). For these emulsions, aqueous dispersions with GON concentration of 0.2 wt% were mixed with an equal volume of dodecane and sonicated. The ultrasound sonication produced emulsions with a droplet size range of 1–60 μm, as further described below (Figure 5.5 and Figure 5.6). In all cases the emulsion filled the entire volume of the vessel after sonication (Figure 5.4a). A darker color was observed at pH 6 and 10 versus pH 2. In the case of GON, without salt, the oil-in-water emulsion filled the entire volume initially (Figure 5.4a) but phase separated to a slightly smaller emulsion volume (Figure 5.4b) within 24 hours. A drop of the emulsion phase was added to water to confirm that it was indeed a dodecane-in-water (O/W) emulsion. The high electrical conductivities of (151.3 μS/cm, 161.5 μS/cm, and 178.5 μS/cm with no salt at pH 2, 6, and 10 indicate that water was the continuous phase for the O/W emulsion. These large conductivities indicate the aqueous phase was the continuous phase. This curvature about oil was expected for hydrophilic GON with high negative surface charge, as they favored the water side over the oil side of the interface.

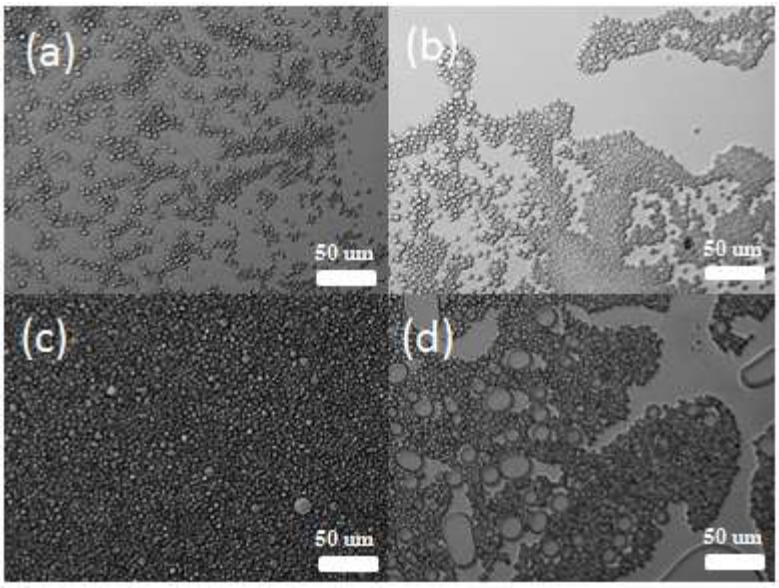

Figure 5.5 Optical micrographs of emulsions without added salt at pH 6: (a) immediately after emulsion formation with 0.2 wt% GON (b) 24 hrs later (c) immediately after emulsion formation with 0.01 wt% GON (d) 24 hrs later.

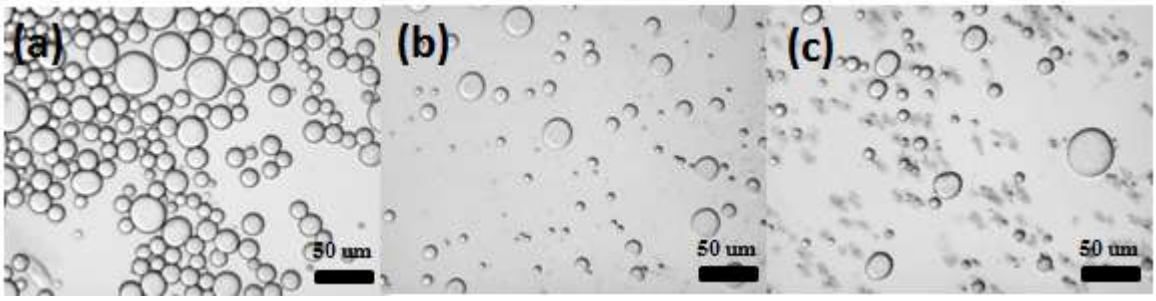

Figure 5.6 Microscopy images of emulsions immediately after formation with 0.2 wt % GON with varying concentrations of NaCl from (a)1% ,(b) 3% , and (c) 5% at pH 2.

For the GON stabilized emulsion with 0-5 wt% NaCl at pH 2 (Figure 5.4), the emulsions were light brown, indicating scattering by the oil droplets and interfaces. Without added salt at each pH, the lower phase was brown as it contained GON. With

added salt, an extremely thin colorless lower aqueous phase was present after 24 hours. At pH 6 and 10 after 24 hours, approximately 80% of the total volume was still the top emulsion phase, and the aqueous phase was colorless. Here the salt drove the GON out of water to the interface. The emulsion stability is enhanced by the irreversible adsorption of particles to oil/water interfaces.[16a]

Micrographs taken immediately after emulsion formation are presented in Figure 5.5a, Figure 5.5c, and Figure 5.6. Analysis of microscopy images revealed that the emulsions stabilized by GON consisted of oil droplets ranging from 1 to 60 μm in diameter. In the case of no added salt, the majority of the emulsion droplets were smaller than 10 μm, even 1 day later after emulsion formation (Figure 5.5b and Figure 5.5d). Emulsion droplet sizes were relatively insensitive to changes in concentration of NaCl, even though they were polydisperse with diameters ranging between 1 and 60 μm (Figure 5.6). At all pH values, after the excess aqueous phase was resolved after 1 day (Figure 5.4b), a stable emulsion with large oil and water volume fractions still remained after 1 year (Figure 5.7).

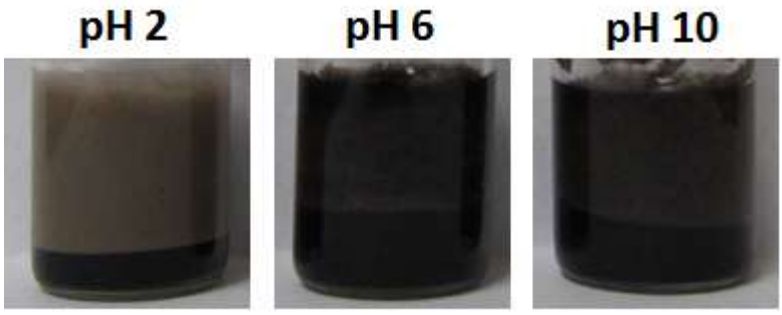

Figure 5.7 Emulsions formed with equal volume fractions of dodecane and an aqueous dispersion of 0.2 wt% GON at pH 2, 6, and 10 without added salt. The photos were taken 1 year after emulsion formation.

Figure 5.8 shows two oil droplets in O/W emulsions stabilized with GON at 0.2 wt% by transmission electron microscopy (TEM). The TEM images show graphene oxide layers at the oil/water interface that stabilize the oil droplets against coalescence. Long platelets may be observed extending deeply into the aqueous phase at various angles in multilayers, particularly in the image on the right. Furthermore, individual GON and aggregated GON are observable on the oil droplets **(**Figure 5.8). In the case of rods, entanglement of the rods has been shown to increase emulsion stability.[7a] The emulsion stability may also be attributed to the electrostatic repulsion between the oil droplets coated with the highly charged GON's. Furthermore, when the size of GON was larger than the emulsion droplets, highly wrinkled sheets were observed by Sharif and coworker[4b]. In Figure 5.8, some of the GONs may have spanned adjoining oil droplets, while keeping them separate.

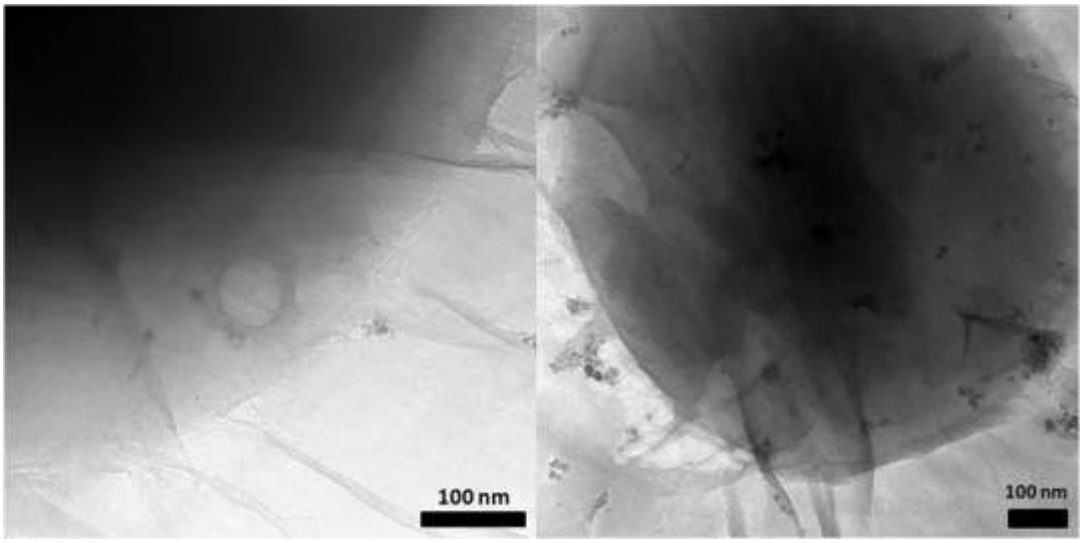

Figure 5.8 TEM image of the graphene oxide nanoplatelets at the interface of oil/water emulsion at pH 6 without added salt.

For extremely low GON concentrations, down to 0.001 wt%, emulsions of dodecane and water (1:1 volume ratio could still be formed at pH 6 by probe sonication. Photographs of the emulsions taken 24 hours after their formation (Figure 5.9 and Figure 5.10) revealed the colors and phases of the emulsions. The ability to form and stabilize emulsions with a very small amount of GON may offer opportunities for applications including CO_2 sequestration in deep subsurface formations and enhanced oil recovery from reservoirs, which generally contains high-salinity brines.

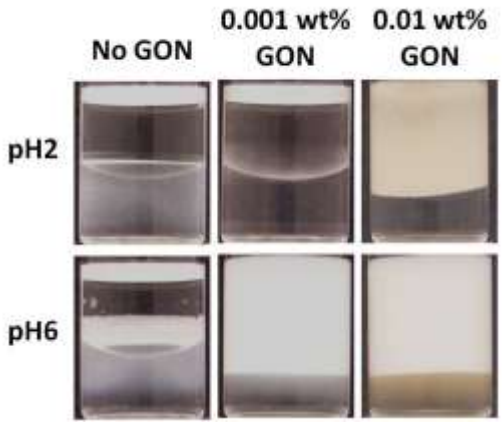

Figure 5.9 Emulsions formed with equal volume fractions of dodecane and an aqueous dispersion (without added salt) without any GON, or with 0.01 wt%, and 0.001 wt% of GONs at pH 2 and 6 without salt. The photos were taken 24 hrs after emulsion formation.

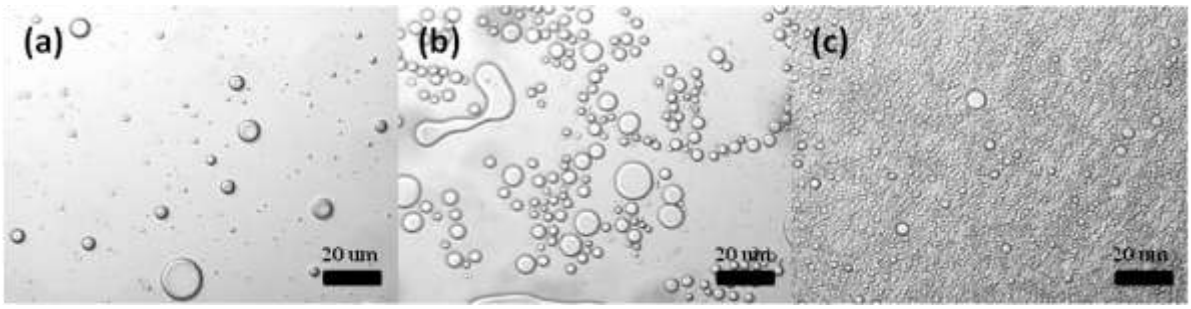

Figure 5.10 Microscopy images of emulsions immediately after formation with 0.001wt% GON at (a) pH2 (b)pH 6 and (c) pH10 without added salt.

5.3.3 Interfacial tension measurement of GON dispersion

GON may be expected to be amphiphilic from structural considerations as it has an edge-to-center variation of hydrophilicity. The edge carboxylate groups are hydrophilic, whereas the sp^2 carbon on the center surfaces is hydrophobic. GON has been shown to lower the interfacial tension between water and oil.[4a, 5] Consequently, adsorbed GON at an oil/water interface has the potential to stabilize an emulsion droplet, as was shown in Figures 5.5 and 5.6. Therefore, the compact GONs at the interface in oil-in-water emulsions interact with each other by van der Waals attractions, electrostatic interactions, and hydrogen bonding.[18] The earlier studies [1, 4a, 15, 16d, 18] indicate that the edge of GON is still hydrophilic with high concentration of carboxylates while the basal plane is hydrophobic. Just as with the robust stability of the aqueous GON dispersions above, the long-term stability of the oil-in-water emulsions for wide ranges of salinity and pH is remarkable, in view of the fact that at high salinities, the electrostatic repulsion will diminish significantly. One possible mechanism is that the oil interacts more strongly with the hydrophobic center of the basal GON, while the hydrophilic edge from

carboxylate group still residing in the water phase[18] and providing sufficient electrostatic repulsion with highly negative charge density. In view of its monolayer thinness and its high elasticity, a slight bending of the platelet, concave to water, will allow a majority of anionic charges from the carboxylate group still remain in the water side of the oil/water interface of the emulsion droplets.

The pH-dependent equilibrium interfacial tension at the dodecane/water interface, for 0.2 wt% GON dispersed in water, was investigated with a pendant water droplet as shown in Figure 5.11. The interfacial tension increases with pH, and decreases with salinity. The interfacial tension of the bare dodecane/water interface was 52.8 mN/m.19 The interfacial tension at the dedecane/water interface decreased from 47.8 mN/m at pH 10 to 44.4 mN/m pH 2 without added NaCl salt. After adding 5 wt% NaCl salt to the GON dispersion, the dodecane/water interfacial tension was reduced by about 3 mN/m at each pH. As expected, the salt drove the highly hydrophilic GON from the aqueous phase towards the interface. This reduction in interfacial tension with GON by about 10 mN/m was large compared to the case of spherical silica nanoparticles, which have relatively uniform surface hydrophilicities8b. Thus, the variation in hydrophilicity from the center to the edges in GON is beneficial for adding amphilicity, as reflected in the lowering of the interfacial tension. Once the large GON adsorbed onto the interfaces, they formed relatively rigid shells that provided steric hindrance and electrostatic repulsion, which provided long-term stability of the emulsion.[7a]

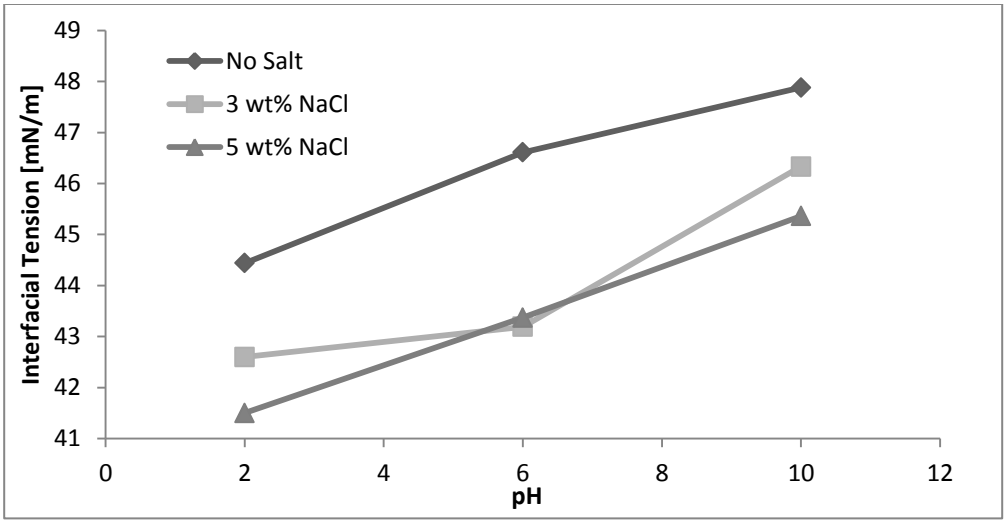

Figure 5.11 Interfacial tension measurement of 0.2 wt% GON at the dodecane-water interface with and without salt at pH 2, 6, and 10.

5.4 CONCLUSIONS

Graphene oxide nanoplatelets (GON) dispersions are stable in pure water and up to 5 wt% NaCl over a wide range in pH from 2 to 10. The stability is favored by electrostatic repulsion of the charged edges, even at high salnity, as shown by the relatively pH insenstive zeta potentials, and by the weak van der Waals attraction due to very thin dimension of the plates. Oil-in-water Pickering emulsions with droplet sizes down to ~1 μm were formed using aqueous dispersions of GON with concentrations as low as 0.001 wt%, given the extremely large surface area/mass. The adsorption of GON at the oil/water interfaces, as shown by TEM and reductions in the interfacial tension, stabilized oil droplets in water over a wide range in pH from 2 to 10 and high salinities up to 5 wt% NaCl. The stability of the emulsions even at high salinity up to 5 wt% is favored by the high anion charge density from carboxylate groups at the GON edges

which extend into the water phase, with slight bending of the highly elastic plates, about the oil droplets. The emulsions were partially stable for one year. By analogy to surfactant molecules adsorbed at the oil/water interface, the inter-platelet repulsion at the water hydrophilic side should be stronger than that at the oil (lipophilic) side, such that the oil/water interface prefers to curve toward the oil phase and forms oil-in-water emulsion droplets. Furthermore, the GON orients more on the water phase over the oil phase, given their high hydrophilicity, which also favors bending about oil. The ability to stabilize emulsions with low nanoparticle concentrations, for example thin amphiphilic platelets, would be of interest in practical subsurface applications.

5.5 REFERENCES

1. Li, D.; and Kaner, R. B., Graphene-based Materials. *Science* **2008,** *320*, 1170-1171.

2. Dreyer, D. R.; Park, S.; Bielawski, C. W.; and Ruoff, R. S., The Chemistry of Graphene Oxide. *Chem. Soc. Rev.* **2010,** *39*, 228-240.

3. (a) Stankovich, S.; Piner, R. D.; Chen, X.; Wu, N.; Nguyen, S.; and Ruoff, R. S., Stable aqueous dispersions of graphitic nanoplatelets via the reduction of exfoliated graphite oxide in the presence of poly(sodium 4-styrenesulfonate). *J. Mater. Chem.* **2006,** *16*, 155-158; (b) Stankovich, S.; Piner, R. D.; Nguyen, S.; and Ruoff, R. S., Synthesis and exfoliation of isocyanate-treated graphene oxide nanoplatelets. *carbon* **2006,** *44*, 3342-3347; (c) Park, S.; An, J.; Piner, R. D.; Jung, I.; Yang, D.; Velamakanni, A.; Nguyen, S. T.; and Ruoff, R. S., Aqueous Suspension and Characterization of Chemically Modified Graphene Sheets. *Chem. Mater.* **2008,** *20* (21), 6592-6594.

4. (a) Kim, J.; Cote, L. J.; Kim, F.; Yuan, W.; Shull, K. R.; and Huang, J., Graphene Oxide Sheets at Interfaces. *J. Am. Chem. Soc.* **2010,** *132*, 8180-8186 ; (b) Gudarzi, M. M.; Sharif, F., Self assembly of graphene oxide at the liquid–liquid interface: A new route to the fabrication of graphene based composites. *Soft Matter* **2011,** *7*, 3432-3440.

5. Cote, L. J.; kim, J.; Tung, V. C.; Luo, J.; Kim, F.; H., J., Graphene oxide as surfactant sheets. *Pure Appl. Chem.* **2011,** *83* (1), 95-110.

6. (a) Golomb, D.; Pennell, S.; Ryan, D.; Barry, E.; Swett, P., Ocean sequestration of carbon dioxide: modeling of the deep ocean release of a dense emulsion of liquid CO_2-in-water stabilized by pulverised limestone particles. *Environ. Sci. Technol.* **2007,** *41*, 4698-4704; (b) Dickson, J. L.; Binks, B. P.; Johnston, K. P., Stabilization of carbon dioxide-in-water emulsions with silica nanoparticles. *Langmuir* **2004,** *20*(19), 7976-7983; (c) Adkins, S. S.; Gohil, D.; Dickson, J. L.; Webber, S. E.; Johnston, K. P., Water-in-carbon dioxyde emulsions stabilized with hydrophobic silica particles. *Phys. Chem. Chem. Phys.* **2007,** *9*, 6333-6343.

7. (a) Wege, H. A.; Kim, S.; Paunov, V. N.; Zhong, Q.; and Velev, O. D., Long-Term Stabilization of Foams and Emulsions with In-Situ Formed Microparticles from Hydrophobic Cellulose. *Langmuir* **2008,** *24*, 9245-9253; (b) Alargova, R. G.; Warhadpande, D. S.; Paunov, V. N.; and Velev, O. D., Foam Superstabilization by Polymer Microrods. *Langmuir* **2004,** *20*, 10371.

8. (a) Zhang, T.; Davidson, D.; Bryant, S. L.; and Huh, C., Nanoparticle-Stabilized Emulsions for Applications in Enhanced Oil Recovery. *Proceeding of SPE 129885, presented at SPE/DOE Symp. Improved Oil Recovery, Tulsa, OK., Apr. 26-28, 2010.* **2010**; (b) Worthen, A. J.; Bagaria, H. G.; Chen, Y.; Bryant, S. L.; Huh, C.; And Johnston, K. P., Nanoparticle-Stabilized Carbon Dioxide-in-Water Foams with Fine Texture. *J. Colloid Interface Sci.* **2012,** *391*, 142-151.

9. Espinosa, D. A.; Caldelas, F. M.; Johnston, K. P.; Bryant, S. L.; and Huh, C., Nanoparticle-Stabilized Supercritical CO_2 Foams for Potential Mobility Control Applications. *Proceeding of SPE129925, presented at SPE/DOE Symp. Improved Oil Recovery, Tulsa, OK., Apr. 26-28, 2010.* **2010**.

10. Ryoo, S.; Rahmani, A. R.; Yoon, K. Y.; Prodanovic, M.; Kotsmar, C.; Milner, T. E.; Johnston, K. P.; Bryant, S. L.; Huh, C., Theoretical and experimental investigation of the motion of multiphase fluids containing paramagnetic nanoparticles in porous media. *SPE Annual Meeting, Florence, Italy* **2010,** *SPE 134879*.

11. Hummers Jr, W. S.; Offeman, R. E., *J. Am. Chem. Soc.* **1958,** *80*, 1339.

12. Tam, J. M.; Murthy, A. K.; Ingram, D. R.; Nguyen, R.; Sokolov, K. V.; P., J. K., Kinetic assembly of near-IR active gold nanoclusters using weakly adsorbing polymers to control size. *Langmuir* **2010,** *26*, 8988-8999.

13. Chen, X.; Adkins, S. S.; Nguyen, Q. P.; Sanders, A. W.; Johnston, K. P., Interfacial tension and the behavior of microemulsions and macroemulsions of water and carbon dioxide with a branched hydrocarbon nonionic surfactant. *J. of Supercritical Fluids* **2010,** *55*, 712–723.

14. Cote, L. J.; Kim, F.; , a. H., J., Langmuir-Blodgett Assembly of Graphite Oxide Single Layers. *J. AM. CHEM. SOC.* **2009,** *131*, 1043-1049.

15. Li, D.; Mu¨ller, M. B.; Gilje, S.; Kaner, R. B.; and Wallace, G. G., Processable aqueous dispersions of graphene nanosheets. *Nature Nanotech.* **2008,** *3*, 101-105.

16. (a) Binks, B. P., Particles as surfactantssimilarities and differences. *Current Opinion in Colloid and Interface Science* **2002,** *7*, 21-41; (b) Horozov, T. S.; Binks, B. P., Particle-Stabilized Emulsions: A Bilayer or a Bridging Monolayer? *Angew. Chem. Int. Ed.* **2006,** *45*, 773-776; (c) Binks, B. P.; Kirkland, M., Interfacial structure of solid-stabilised emulsions studied by scanning electron microscopy. *Phys. Chem. Chem. Phys.*

2002, *4*, 3727-3733; (d) kim, F.; Cote, L. J.; And Huang, J., Graphene Oxide: Surface Activity and Two-Dimensional Assembly. *adv. Mater.* **2010,** *22*, 1954-1958.

17. Imperiali, L.; Liao, K.; Clasen, C.; Fransaer, J.; Macosko, C. W.; And Vermant, J., Interfacial Rheology and Structure of Tiled Graphene Oxide Sheets. *Langmuir* **2012,** *28*, 7990-8000.

18. Guo, P.; Song, H.; and Chen, X., Hollow graphene oxide spheres self-assembled by W/O emulsion. *J. Mater. Chem.* **2010,** *20*, 4867-4874.

19. Yoon, K. Y.; Li, Z.; Neilson, B. M.; Lee, W.; Huh, C.; Bielawski, C. W.; And Johnston, K. P., Effect of Adsorbed Amphiphilic Copolymers on the Interfacial Activity of Superparamagnetic Nanoclusters and the Emulsification of Oil in Water. *Macromolecules* **2012,** *45*, 5157-5166.

Chapter 6: Control of Primary Nanoparticles in Water Dispersible Iron Oxide Nanoclusters and Their Applications in Pulsed Magneto-motive Ultrasound (MMUS) Imaging

We report here a facile synthetic approach for preparing water-soluble Fe_3O_4 nanoparticle clusters with tunable size distribution and magnetic properties. We have investigated the size control of clusters as well as individual nanoparticles via the Dynamic light scattering (DLS) analysis and Transmission electron microscopy (TEM). Superconducting quantum interference device (SQUID) was used to measure the magnetic properties of Fe_3O_4 nanoparticle at room temperature, to the effects of primary particle and cluster size distributions. Such well-defined nanoparticle clusters that are stable in brine can be utilized for various biomedical applications. In this study, we demonstrate the contrast enhancement in a newly-developed, ultrasound-based cellular and molecular imaging modality, pulsed magneto-motive ultrasound (pMMUS) imaging. Our results indicate that use of these nanoparticle clusters with superior magnetic properties can significantly enhance the pMMUS signal, which is essential key need for further development of *in vivo* pMMUS imaging.

6.1 INTRODUCTION

Magnetic iron oxide nanoparticles (NPs) have been extensively studied for their biological applications, such as medical imaging, drug delivery, and biomolecular separation, because of their unique electrical, magnetic, and chemical properties.[1] Different synthetic methods, such as coprecipitation, microemulsion, and laser pyrolysis

techniques, have been developed for making magnetic nanoparticles.[2] The size and the shape of the iron oxide NPs directly affect their magnetic properties that are critical for their biomedical applications. Also, the surface modification of NPs is crucial for clinical uses. *In vivo* use of NPs with chemically-unstable surface can lead to poor colloidal stability and low biocompatibility. In the last two decades, there has been great progress in organic solution-based synthetic methods with good size and shape control on produced NPs. While received much less attention, the aqueous-phase NP synthesis has some obvious advantages over the organic-phase synthesis. Traditional coprecipitation method that uses metal salts dissolved in water is extremely simple and environmentally friendly. Unlike organic solution synthesis, NPs synthesized in water do not need phase-transfer process for water-dispersibility and can be directly modified with biomolecules. [3]

Amongst the wide range of biomedical applications of magnetic nanoparticles, they have been recently utilized in a newly-born imaging modality, pulsed magneto-motive (pMMUS) imaging.[4] pMMUS imaging is an enhancement to the ultrasound-based imaging technique using magnetic NPs as contrast agents, and thus is capable of imaging events at small scale (such as cellular and molecular level), which was not feasible with the conventional ultrasound imaging. In pMMUS imaging, a short magnetic excitation pulse is applied to the cells or tissue which is labeled with magnetic nanoparticles. The rapid motion of the nanoparticles and the tissue associated with them is monitored by an ultrasound scanner, which shows the distribution of the magnetic nanoparticles.[3f, 5] The signal-to-noise ratio (SNR) in pMMUS imaging depends on the size and magnetic properties of the magnetic nanoparticles. To achieve better SNR, magnetic nanoparticles

with higher magnetization are desired as contrast agents for pMMUS imaging. When the particle is of nano scale so that its internal magnetic structure is "single-domain", magnetization is proportional to the particle volume.[1f] However, as the volume of the particle increases, its magnetization capacity generally decreases. In addition, its colloidal stability is decreased and there are other factors that limit the size of the magnetic contrast agents. In our previous studies[4], two different sizes of iron oxide nanoclusters were used as the magnetic agent. Primary iron oxide NPs with the sizes of 2-3 nm were synthesized first and then they were induced to form clusters in the size range from 15 nm to 55 nm. By clustering primary NPs, the net magnetic force induced on the magnetic contrast agent can be greatly amplified compared to that on the individual primary NPs.

NPs can be assembled into clusters through various noncovalent interactions including hydrogen bonding, van der Waals (VDW) forces, and electrostatic forces.[6] For superparamagnetic iron oxide NPs under external field, there are also magnetic dipole interactions between particles. To stabilize the magnetic nanoparticles in the dispersing medium, various surfactants, such as poly(acrylic acid), and citric acid (CA), have been used.[2c, 3b, 7] Ditsch and co-worker[7a] reported Iron oxide nanoparticles synthesized with random copolymers of acrylic acid, styrenesulfonic acid, and vinylsulfonic acid, used as coating/clustering agent, can control the size of the resulting nanoclusters. By using two different polymers, they formed stable 74nm-size nanoclusters.[7a, 8] In another study, Berret and coworkers[2d, 9] developed size-controllable clusters of maghemite (γ-Fe_2O_3) by using poly(trimethylammonium ethylacrylate methyl sulfate)-b-poly-(acrylamide) with different molecular weights. The cluster sizes observed with dynamic light scattering

(DLS) and transmission electron microscopy (TEM) were between 20 and 200 nm. Also, Rotello and coworkers[10] produced gold nanoparticles with polymer coating into spherical aggregates, via self-assembly with hydrogen-bonding interactions. In this method, the polymeric surfactants play a role in holding the priamry nanoparticles together to form spherical aggregates. Kinetically controlled, near-IR active, gold-coated iron oxide nanoclusters were synthesized from a dispersion of iron oxide nanoparticles, which were then utilized for biomedical applications.[1d, e] Overall, magnetic nanoclusters, consisting of primary magnetic nanoaprticles that are clustered together by various noncovalent interactions, provide high magnetization and good colloidal stability. We have previously shown that the large clusters of primary magnetic nanoparticles exhibit larger pMMUS signal than smaller clusters at the same concentration.[4] In this study, we further demonstrate improved clustering of magnetic nanoparticles with larger magnetization and better colloidal stability. We also assembled nanoclusters consisting of somewhat larger primary nanoparticles, thus larger magnetization with the consequent pMMUS signal enhancement.

In this work, we report the synthesis of highly water-dispersible iron oxide nanoclusters with uniform sizes of ~40 nm, which had been self-assembled into roughly spherical aggregates by clustering the primary particles of prescribed size under controlled conditions. Accordingly, the magnetic properties of the synthesized nanoclusters can be varied. In order to successfully produce the nanoclusters in water, citrate ligand was selected as a surfactant because of the strong binding of carboxylate groups to iron cations on the nanoparticle surface. The extra carboxylate groups that are

not boned to the nanoparticle surfaces provide a high degree of dispersion stability. The magnetic properties of synthesized nanoclusters consisting of primary superparamagnetic nanoparticles, investigated using a superconducting quantum interference device (SQUID) technique, are shown to be superparamagnetic. We also studied the size control of clusters in the solution, by examining the morphology of clustering via the Dynamic light scattering (DLS) and Transmission electron microscopy (TEM). The magnetic nanoclusters consisting of primary nanoparticles with larger sizes were also synthesized, and were utilized in a set of pMMUS experiments on tissue to demonstrate their superior contrast signal enhancement. Our results suggest that pMMUS signal enhancement by utilizing these magnetic nanoclusters can play a crucial role in potentially expanding the scope of pMMUS imaging to *in vivo* applications where larger SNR is an essential need.

6.2 EXPERIMENTAL DETAILS

6.2.1 Materials

Ferrous chloride tetrahydrate ($FeCl_2 \cdot 4H_2O$; MW=198.81), ferric chloride hexahydrate ($FeCl_3 \cdot 6H_2O$; MW=270.32), citric acid monohydrate (CA; MW=210.14), and ammonium hydroxide (NH_4OH, MW= 35.05; 28 wt%) were purchased from Fisher Scientific, USA. Hydrochloric acid (HCl, MW=36.46) and sodium hydroxide (NaOH, MW=) were purchased from EM Science, Germany. Dialysis tubing (Spectra/Por® 6; 50,000 MWCO; lot number 3246779) was purchased from Spectrum Laboratories, Inc., USA.

6.2.2 Nanoparticle synthesis and nanocluster formation

The iron oxide nanoparticles were synthesized by coprecipitation method of Fe(II) and Fe(III) chlorides (Fe^{II}/Fe^{III} ratio of 0.5) in base solution phase. In a typical synthesis for 8 nm primary nanoparticles generation, 0.86 g of Fe(II) chloride, 2.35 g of Fe(III) chloride, and 0.05g of citric acid were dissolved in D.I. water (40 mL). This solution was heated at 95 °C under nitrogen for 30 min with vigorous stirring. Making it transparent, then 10 mL of ammonium hydroxide (28 wt%) was injected rapidly into the hot mixture. The reaction solution then turned black after about few seconds and became slightly turbid. The resulting solution was stirred for one hour to form magnetite nanoparticles. The primary particles thus formed aggregates and settled in the solution. Afterwards, nanoparticle solution was cooled down to room temperature, and the iron oxide nanoparticles were centrifuged at 6000 rpm for 5 minutes. These particles were redispersed in 20 ml of citric acid solution (0.02g/ml, pH 5.2) with probe sonication (Branson Sonifier® S-450A). After probe sonication, the large iron oxide aggregates were removed from the dispersion by centrifugation (6000 rpm for 5 min) and the excess citrate was removed by using dialysis tube (25,000 MWCO, Millipore Co.). The final dispersion contained ~1 wt% Fe by FAAS, and the pH value was around 6. Complete stabilization of the iron oxide clusters in the aqueous solution were possible by the centrifugation-dispersion process.

6.2.3 Characterization of magnetic nanoclusters

Dynamic light scattering (DLS) measurement was performed on a custom-built apparatus, and the data were analyzed using a digital autocorrelator (Brookhaven BI-9000AT) and a non-negative least-squares (NNLS) routine (Brookhaven 9KDLSW32) [11]. The scattering angle was 90º. The dispersion concentration for the measurements was around 0.05 mg/mL iron oxide which gave a measured count rate of approximately 100-200 kcps. Measurements were made over a period of 2 minutes, at least three times on each sample.

Zeta potential measurements were performed in triplicate on a ZetaPlus dynamic light scattering apparatus (Brookhaven Instruments) at 90° scattering angle and temperature of 25 °C.

Transmission electron microscopy (TEM) was used to see the morphology of nanoclusters. The experiments were performed on a FEI TECNAI G2 F20 X-TWIN TEM using a high-angle annular dark field detector. The samples were prepared using a "flash-freezing" technique, in which a 200 mesh carbon-coated copper TEM grids were cooled using liquid nitrogen and then dipped into dilute aqueous nanocluster dispersion [12]. The sample was immediately dried using a Virtis Advantage Tray Lyophilizer (Virtis Company, Gardiner, NY) with 2 hours of primary drying at -40^{o}C followed by a 12 hour ramp to +25^{o}C, and then 2 hours of secondary drying at 25^{o}C. Drying in this manner avoided the aggregation of NPs, caused by capillary forces during the drying process of the liquid on the TEM grid.

Thermo gravimetric analysis (TGA) was used to determine the mass of coating on the iron oxide nanoclusters. The experiments were performed using a Mettler Toledo TGA/DSC 1 STAR system equipped with a gas controller (GC 200) and a temperature set at 25°C (Julabo). The powder samples were held at 100°C for 120 minutes to remove the remaining water in the sample and then heated at a constant rate of 20 °C/min from 100°C to 800 °C and held at 800°C for 30 minutes. The loss in mass after heating indicated the organic component of the particles.

Flame atomic absorption spectroscopy (FAAS) was used to determine the iron concentration in the dispersion by using a GBC 908AA flame atomic absorption spectrometer (GBC Scientific Equipment Pty Ltd). All measurements were conducted at 242.8 nm using an air-acetylene flame.

Superconducting quantum interference device or SQUID magnetometer (Quantum Design MPMS) was used to measure the normalized saturation magnetization of the particles at 300 K.

6.2.4 Gelatin-based phantom samples

To compare the contrast in pMMUS imaging with and without the synthesized magnetic nanoclusters, a set of measurements was performed on tissue-mimicking phantoms. The tissue mimicking phantoms was chosen because, withsuch use, the experimental parameters including the magnetic flux density, location, distribution and the concentration of magnetic nanoclusters of different typecould be controlled as desired, which is necessary for a fair comparison between their functionality. Gelatin-based

phantoms made of 6% w/w porcine (Sigma Aldrich, USA), that are mixed with precisely measured concentration of magnetic nanoclusters, were embedded into a 4% w/w gelatin background. By embedding magnetic nanoparticles into a gelatin background simulates the viscoelastic properties of the soft tissue surrounding cells (with tissue magnetically labeled in real *in vivo* situation) can be probed. Each magnetic inclusion contains identical concentration of "iron" but is made of different type of nanoclusters. 30-μm Silica beads were also added to both magnetic inclusions and the background to generate enough scatters for ultrasound imaging and speckle tracking.

6.2.5 Pulsed magneto-motive ultrasound imaging system

To perform pMMUS imaging using synthesized magnetic nanoclusters, a custom-built imaging system was utilized. The details of experimental setup are explained elsewhere.[4-5] Figure 6.1 shows the experimental setup for comparing the performance of synthesized magnetic nanoclusters in pMMUS imaging. Briefly, an electro-magnet derived by a voltage controlled current amplifier was used to generate magnetic excitation pulses with duration of 30 ms and magnetic flux density of 0.8 T, measured at the tip of a cone shaped core embedded inside the solenoid. A focused single-element ultrasound transducer operating at 25 MHz (focal depth = 50.8 mm, f_{number}=4) equipped with a manually controlled ultrasound pulser/receiver (5073PR, Olympus Co., USA) was used to acquire ultrasound RF data before, during, and after the magnetic excitation. Acquired data were stored in a computer and a post-processing procedure based upon a block-matching motion-tracking algorithm[4,13] was then utilized to calculate the

magnetically induced displacements.[14] The electro-magnet and ultrasound transducer were kept fixed while the samples were mechanically scanned using a motorized linear axis with the step size of 500 µm. Magnetic excitation pulses were also measured for each excitation pulse and where used to normalize the measured displacement to avoid the measurement error, potentially arising from the magnetic pulse variations.[4-5, 13]

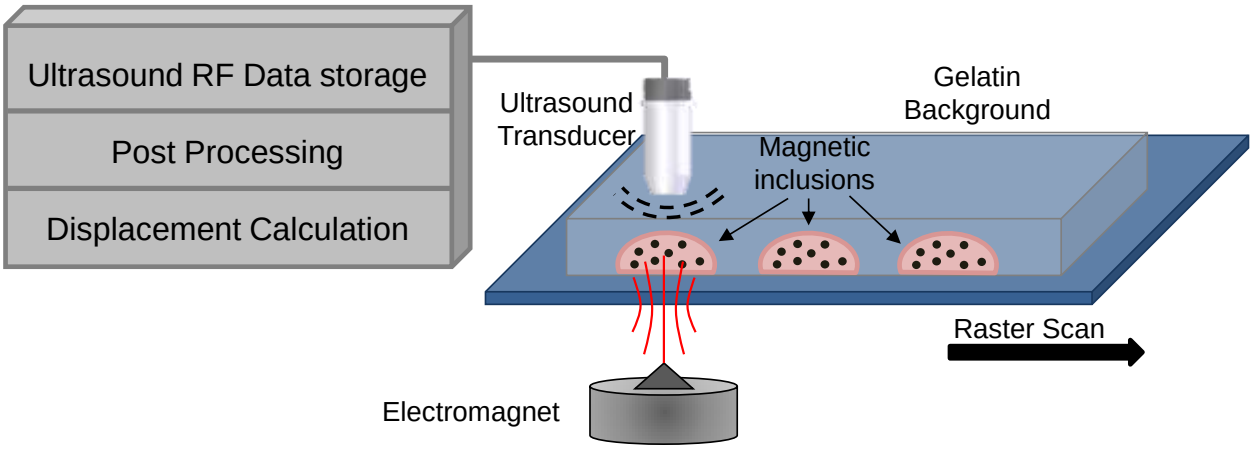

Figure 6.1 Experimental setup for comparing the functionality of synthesized magnetic nanoclusters for pMMUS imaging. Magnetic inclusions made out of different synthesized magnetic nanoclusters, embedded into a gelatin background and the magnetically induced displacement was measured while the electro-magnet and ultrasound transducer were fixed and the samples were mechanically scanned.

6.3 RESULTS AND DISCUSSION

6.3.1 Magnetic nanoclusters

To synthesize the iron oxidenanoclusters, citrate was used as a coating agent because of the strong binding between the carboxyl group and the iron cation on the nanoparticle surface. After nucleation reaction was initiated, van der Waals (VDW) force

and electrostatic interactions govern the formation of clusters. Despite the negative surface charge of the particles in the alkali medium (~ pH 12), VDW attraction overcomes the electrostatic repulsion.[15] In our study, since the nanoparticles were initially nucleated in the presence of citrate stabilizer, the amount of citrate influences the stabilization of the particles. As there is strong complexation between $Fe^{3+}$and Fe^{2+} ions and the carboxyl groups which are anchored on the particle surface during the reaction, the citrate stabilizer concentration plays an important influence on the charge density on the particle surface.[3b] After adsorbing the citrate ions to the surface of the particles and probe sonication, the size of clusters was between 30 and 50 nm. As shown in the TEM images in Figure 6.2**,** the 30-50 nm clusters are composed of small primary crystals with sizes of 3–10 nm.

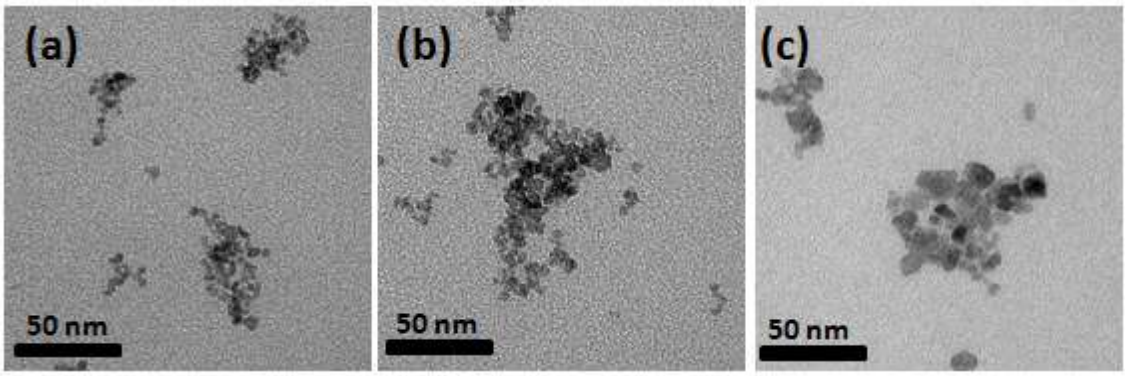

Figure 6.2 TEM images of citrate-coated iron oxide nanoclusters. (a) Cluster #1 (3.57 mg/ml of citrate); (b) Cluster #2 (2.38 mg/ml of citrate); and (c) Cluster #3 (1.19 mg/ml of citrate) prepared in pH 8 water.

DLS measurement was also carried out to measure the hydrodynamic diameter of the clusters. The volume distribution of the NPs is given in the histograms shown in

Figure 6.3 for the nanocluster dispersions. Narrow peaks can be observed between 30 and 50 nm, indicating that the process of cluster formation was controlled at these conditions. Therefore, the interactions between iron oxide primary nanoparticles of the clusters prevented deaggregation or further aggregation. The average diameter of the clusters is between 30 and 50 nm (see Figure 6.3, Table 6.1). The sizes of the nanoclusters by TEM are in agreement with the DLS values. The dispersed nanoclusters are stabilized electrosterically by the negative surface charge of the citrate ligand. As citrate is a small molecule, the steric stabilization is relatively weak. In addition, the high negative value of zeta potential of the citrate-stabilized nanoclusters consisting 8-nm primary particles -52 mV provides further evidence for the strong electrostatic repulsion. Similar zeta potentials were reported in our previous results for citrate-coated IO particles. [6b] The clusters remained stable for several months.

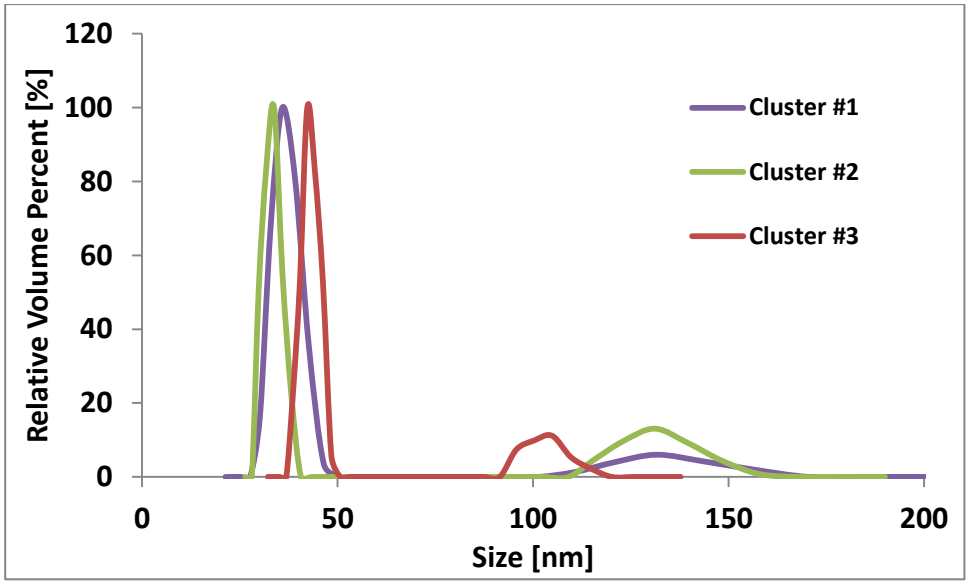

Figure 6.3 Volume fraction based distributions of citrate-coated iron oxide nanoclusters at pH8, after dialysis.

Table 6.1 Summary table for iron oxide nanoclusters with different amount of citrate stabilizer.

name	Amount of citric acid (mg/mL)	Amount of ammonia (mL)	Size of cluster (nm)	Primary Size (nm)	Magnetization (emu/g Fe)
Cluster #1	3.57	10	35	4.98±0.96	53.2
Cluster #2	2.38	10	32	6.38±1.02	67.7
Cluster #3	1.19	10	42	7.52±1.14	79.0

The presence of the citrate coating on the iron oxide surface was confirmed by thermogravimetric analysis (TGA), which revealed a loss of 8-38 wt % of organic material (Figure 6.3). The results from the TGA conducted on the particle dispersion before and after dialysis are also shown in Figure 6.4. The total dry mass loss of the undialyzed sample is 38%. Here, the binding of the carboxyl ions to the Fe cations was not strong enough to balance the favorable hydration of the stabilizer in the bulk water, as well as unbounded citrate molecules in the dispersing medium. The TGA results after dialysis of iron oxide dispersion showed a loss of 8-11 % of organic contents, which indicate strong adsorption of citrate stabilizer on the iron oxide surface, thereby providing strong electrostatic stabilization.

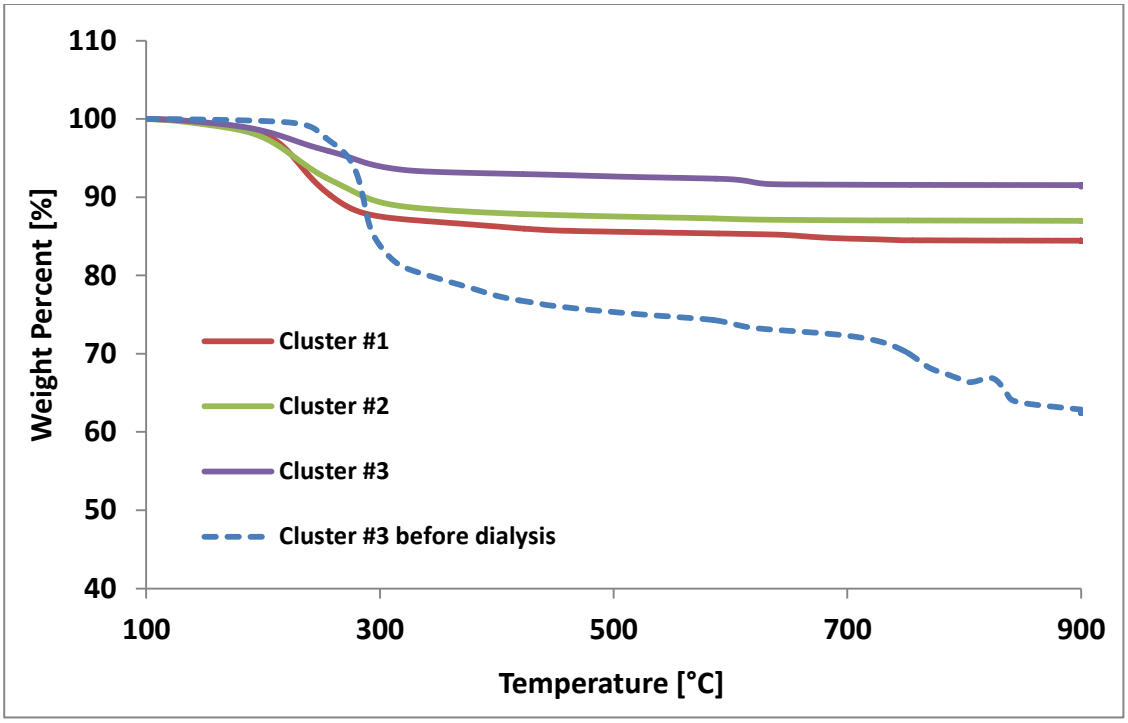

Figure 6.4 TGA measurements for citrate-coated iron oxide nanoclusters before and after dialysis.

During the synthesis of citrate-coated iron oxide nanoclusters with a diameter of 40 nm, we explored the possibility of controlling the size of citrate-coated iron oxide nanoclusters by varying the reaction conditions. First, we kept the amount of the iron chloride and total volume of the reaction in the flask constant, to ensure a similar environment for the oxidation of Fe (II) and Fe (III). Changes in the citric acid concentration with their corresponding products are shown in Table 6.1. By adjusting the amount of citrate, the individual NP size can be controlled. The TEM images (Figure 6.2) show the change in size of the individual NPs. As the amount of citric acid decreased from 1 to 0.05 g, the individual sizes of the synthesized NPs increased from 5 nm to 8 nm, because the citrate ions strongly affects the nucleation and growth rate of Fe_3O_4 particles.

The higher concentration of citrate ion makes smaller particles size due to the formation of a large number of seed nuclei, which results in high particle concentration and smaller particles.[16] The size of the primary particle clusters can be controlled from about 25 to about 60 nm by increasing the amount of ammonium hydroxide while fixing other parameters.[4] For example, the increase in the amounts of ammonium yydroxide of 5, 10, 15 mL leads to the clusters with average sizes of 25, 42, 60 nm, respectively. The above influence of base concentration on the size of the synthesized NPs was determined employing the DLS experiments. This size control of the nanoclusters may be the result of the alkalinity differences, because stronger alkalinity could accelerate the hydrolysis of $FeCl_3$ and $FeCl_2$, which subsequently promotes the formation of larger nanoclusters. The growth of the iron oxide clusters follows two-stage growth model that the primary nanocrystals nucleate first in a supersaturated solution and then they aggregate into larger clusters.[17]

To evaluate the magnetic properties of iron oxide NPs in response to an external field application, SQUID magnetometer was employed at 300 K by cycling the field between -40 and 40 kOe. Figure 6.5 shows that all the iron oxide NPs are superparamagnetic at room temperature. For the Cluster #3 with mean diameter of 8 nm primary particles, the specific saturation magnetization (σ_s) is 79.1 emu/g Fe. This value is fairly high compared to the value of bulk magnetite materials (92 emu/g).[18] In addition, the relative large size of Cluster #2 with mean diameter of 7 nm primary particles has a somewhat lower saturation magnetization (67.7 emu/g Fe). As the size of the iron oxide NPs is reduced to 5 nm, saturated magnetization decreases to 53.2 emu/g Fe. This

magnetization results show that lower citrate concentration favors the formation of magnetite particles with higher crystallinity. This difference in magnetization could be due to the existence of a magnetic inert layer on the surface of the magnetic particles. Because of the surface effect, as the sizes of particle gets smaller, the effective magnetic volume becomes smaller and the saturation magnetization decreases. Different values of magnetization may be obtained by varying the conditions of the iron oxide hydrolysis, as was observed by other research groups.[2b, c]

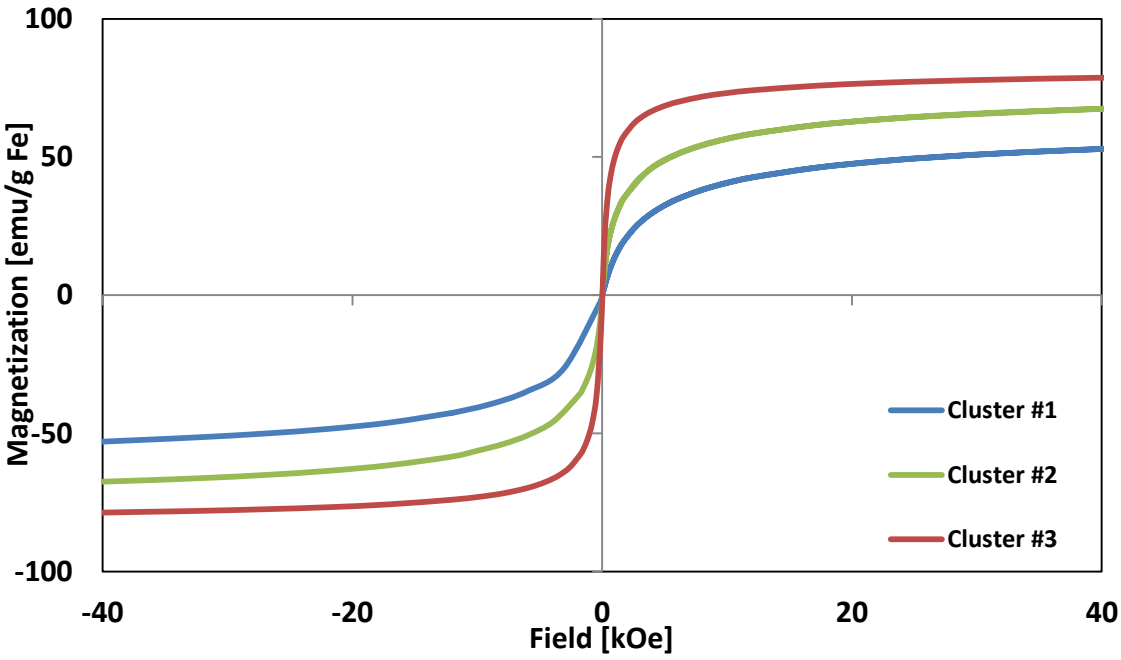

Figure 6.5 Magnetization (M) of iron oxide nanoparticles coated with citrate molecule in emu/g Fe vs. magnetic field (H) at 300 K.

6.3.2 Magneto-motive force for nanoclusters versus primary individual nanoparticles

Iron oxide nanoparticles with smaller than 20 nm diameter generally exhibit superparamagnetic properties with high magnetic susceptibility.[19] The relationship between magneto-motive force Fm and magnetic field H is given by [1, 20]

$$F_m = -\mu_0 V_P M_P \nabla H \qquad (1)$$

where V_p and M_P are the volume and saturation magnetization of the nanoparticles in a given field (H) and μ_0 is the permeability of free space.[7a] The increase in particle volume, $V_{p,}$ raises Fm and thus causes the greater motion of a particle in a magnetic field [21] which can enhance signals in magneto-motive imaging. The superparamagnetism, which is the nanocrystal's magnetic spin alignment, is only observed for magnetic domains smaller than 20 nm. Due to this, V_p (and thus F_m) is limited for a single nanocrystal of iron oxide.[22] We overcome this limitation of V_p and thus Fm by forming ~40 nm clusters of sub-10 nm primary nanocrystals. This ensures that bigger nanocluster remains superparamagnetic as desired for biomedical applications. As the particle motion is opposed by the gel matrix due to the drag force acting between the particle surface, a smaller surface area to volume ratio would lead to more motion. This is because the force causing the motion is a body force, due to the magnetic field while the force opposing the motion is the drag force which is proportional to the particle surface area. Therefore, the larger being larger undergo a larger displacement, leading to a higher signal perceived by the ultrasound measurement. The saturation magnetization, M_p, remains the same for the clusters as for the individual primary particles becasue there is no magnetic coupling

between the neighboring particles despite the small inter-particle spacing.[1d, 8] However, per unit volume basis, there is some loss in magnetization due to the porosity of the cluster. The clusters being stabilized by citrate have a higher iron oxide loading relative to particles stabilized by other, high–molecular-weight polymers; and thus are advantageous in increasing $F_{m,}$ due to the higher magnetization per unit particle mass. Therefore the clusters described in this paper have the ability to give a much better signal for pMMUS imaging than before.

6.3.3 pMMUS signal enhancement by utilizing larger individual primary nanoparticles into large clusters.

The sensitivity of pMMUS imaging is proportional to the magneto-motive force acting on magnetic nanoparticles. The magneto-motive force (F_{mz}) is proportional to the magnetic susceptibility of nanoparticles, geometry and composition of the nanoparticles. Assuming the magnetic field acts in z-direction only, the magneto-motive force (F_{mz}) acting on each magnetic nanoparticle can be expressed as,

$$F_{mz} = \frac{V_{np}\chi_{np}f_m}{\mu_0} B_z \frac{\partial B_z}{\partial z} \qquad (2)$$

where B_z is z-direction induced magnetic field, μ_0 is the permeability constant, and V_{np}, χ_{np} and f_m represent total volume of nanoparticle, its magnetic susceptibility and the volume fraction of the magnetic material in the nanoparticle, respectively.

Equation 2 indicates that the magneto-motive force (F_{mz}) is proportional to the magnetic susceptibility of nanoparticles, geometry and composition of the nanoparticles. Clearly, magnetic nanoparticles with larger susceptibility, which depends on the primary

particle size and volume fraction of magnetic materials, can exhibit larger magneto-motive force. Therefore, as the nanoclusters consisting of larger primary particles generate larger displacements and higher pMMUS signal, it leads to enhanced pMMUS imaging.

Another important parameter to enhance the pMMUS signal is the saturation magnetization of the nanoclusters. In the case of iron-oxide nanoparticles (or nanoclusters), increasing the size of nanocrystals can increase the saturation magnetization of them and thus enhance pMMUS signal. Therefore, the nanoclusters composed of larger primary nanoparticles can enhance the pMMUS signal through two different mechanisms: (i) their enhanced saturation magnetization and the the increased volume of the magnetic agents due to formation of clusters. The second mechanism is due to the fact that the driving force for motion is a body force due to magnetic field, while the force opposing the motion is the drag force which is proportional to the particle surface area. Therefore the larger clusters produce larger displacements leading to higher ultrasound signals.

To demonstrate the signal enhancement by using the larger nanoclusters composed of larger primary nanoparticles, we imaged three magnetic inclusions, which contain same concentration of the magnetic agents of different types. The signal was normalized with respect to magneto-motive force for the purpose of comparison among the different.[4] The pMMUS measurements were repeated for 10 different locations within each inclusion. Table 6.2 represents the pMMUS signal detected within inclusions

containing different types of magnetic nanoclusters. As the sizes of nanoclusters were between 32 nm and 42 nm, this does not affect the signal change drastically.

Our results of Table 6.2 indicate that the magnetic nanoclusters with a higher saturation magnetization show more enhancement in pMMUS signal. The signal enhancement from Cluster #1 to Cluster #3 apprears to be the results of both size and magnetization variation. However, the size in Cluster #2 was dominated by significant increase in its saturation magnetization and therefore signals enhancement was still detectable. The background noise (i.e. the non-desired vibration detected in non-magnetic background) was detected as 5 μm. Therefore the signal-to-noise ratio (SNR) of magnetic inclusions containing Cluster #1, Cluster #2, and Cluster #3 (defined as $20\log(\frac{mean\ displacement}{noise})$ were measured as 21.13 dB, 22.67 dB and 24.29 dB (Table 6.2). The significant SNR enhancement by using larger magnetic nanoclusters with superior magnetization (Cluster #3) can play an important role to further expand the ability of pMMUS imaging to detect lower concentration of iron (Fe) and at farther distance from magnetic excitation source.

Table 6.2 Summary of pMMUS measurements using different synthesized cit-coated nanoclusters.

Sample	Mean magnetically induced displacement (μm)	Standard deviation of magnetically induced displacement (μm)	pMMUS SNR (dB)
Cluester #1	57	4	21.13
Cluester #2	68	4	22.67
Cluester #3	82	6	24.29

6.4 CONCLUSIONS

In summary, coprecipitation method of Fe(II) and Fe(III) chlorides was used to synthesize highly water-dispersible magnetite nanoclusters with citrate as a stabilizer. The size of citrate-coated iron oxide nanoclusters can be easily controlled within a range of ~40 nm. The iron oxide nanoclusters are composed of primary magnetite nanocrystals with sizes of 3–10 nm, which allow not only superparamagnetism but also high magnetization of 53–79 emu/g Fe. The concentration of citrate ligand can be varied to make larger primary nanoparticles with higher saturation magnetization. The citrate-coated iron oxide nanoclusters have a high saturated magnetization, which enhances their response from external magnetic field. The clusters being stabilized by citrate have a higher iron oxide loading relative to the nanoparticles stabilized by the high molecular weight polymers. The citrate-based nanoclusters are therefore advantageous for the present pMMUS application, with the increased specific saturation magnetization and the

increased overall magnetic force. Moreover, the presence of the citrate groups on the surface of iron oxide nanoparticles enables the nanoclusters to have not only excellent dispersion stability in water, but also low cytotoxicity and good biocompatibility. Such nanoclusters are therefore excellent candidates for bio-applications in various fields such as cell imaging and censoring to find biomarkers.

6.5 REFERENCES

1. (a) Gupta, A. K.; Gupta, M., Synthesis and surface engineering of iron oxide nanoparticles for biomedical applications. *Biomaterials* **2005,** *26*, 3995–4021; (b) Oh, J.; Feldman, M. D.; Kim, J.; Condit, C.; Emelianov, S.; Milner, T. E., Detection of magnetic nanoparticles in tissue using magneto-motive ultrasound. *Nanotechnology* **2006,** *17* (16), 4183-4190; (c) Safarik, I.; Safarikova, M., Magnetic nanoparticles and biosciences. *Monatsh. Chem.* **2002,** *133*, 737–759.; (d) Ma, L. L.; Feldman, M. D.; Tam, J. M.; Paranjape, A. S.; Cheruku, K. K.; Larson, T. A.; Tam, J. O.; Ingram, D. R.; Paramita, V.; Villard, J. W.; Clarke, G. D.; Jenkins, J. T.; Asmis, R.; Sokolov, K.; Chandrasekar, B.; Milner, T. E.; Johnston, K. P., Small multifunctional nanoclusters (Nanoroses) for targeted cellular imaging and therapy. *ACS Nano* **2009,** *3*, 2686-2696; (e) Na, H. B.; Song, I. C.; Hyeon, T., Inorganic Nanoparticles for MRI Contrast Agents. *Adv. Mater.* **2009,** *21*, 2133; (f) Lee, J. H.; Huh, Y. M.; Jun, Y. W.; Seo, J. W.; Jang, J. T.; Song, H. T.; Kim, S.; Cho, E. J.; Yoon, H. G.; Suh, J. S.; and Cheon, J., Artificially engineered magnetic nanoparticles for ultra-sensitive molecular imaging. *Nature Medicine* **2007,** *13*, 95-99.

2. (a) Massart, R., Preparation of aqueous magnetic liquids in alkaline and acidic media. *IEEE Trans. Magn.* **1981,** *17*, 1247-1248; (b) Massart, R.; Dubois, E.; Cabuil, V.; Hasmonay, E., Preparation and properties of monodisperse magnetic fluids. *Journal of*

Magnetism and Magnetic Materials **1995,** *149*, 1-5; (c) Sahoo, Y.; Goodarzi, A.; Swihart, M. T.; Ohulchanskyy, T. Y.; Kaur, N.; Furlani, E. P.; Prasad, P. N., Aqueous ferrofluid of magnetite nanoparticles: fluorescence labeling and magnetophoretic control. *J. Phys. Chem. B* **2005,** *109*, 3879–3885; (d) Berret, J.-F.; Schonbeck, N.; Gazeau, F.; El Kharrat, D.; Sandre, O.; Vacher, A.; Airiau, M., Controlled clustering of superparamagnetic nanoparticles using block copolymers: design of new contrast agents for magnetic resonance imaging. *J. Am. Chem. Soc.* **2006,** *128*, 1755-1761.

3. (a) Liu, J.; Sun, Z.; Deng, Y.; Zou, Y.; Li, C.; Guo, X.; Xiong, L.; Gao, Y.; Li, F.; , a. Z., D., HighlyWater-Dispersible Biocompatible Magnetite Particles with Low Cytotoxicity Stabilized by Citrate Groups. *Angew. Chem. Int. Ed.* **2009,** *48*, 1-6; (b) Ge, J.; Hu, Y.; Biasini, M.; Beyermann, W. P.; Yin, Y., Superparamagnetic magnetite colloidal nanocrystal clusters. *Angew. Chem. Int. Ed.* **2007,** *46*, 4342-4345; (c) Ge, J.; Hu, Y.; Biasini, M.; Dong, C.; Guo, J.; Beyermann, W. P.; Yin, Y., One-step synthesis of highly water-soluble magnetite colloidal nanocrystals. *Chemistry-A European Journal* **2007,** *13* (25), 7153-7161; (d) Liang, X.; Wang, X.; Zhuang, J.; Chen, Y.; Wang, D.; and Li, Y., Synthesis of Nearly Monodisperse Iron Oxide and Oxyhydroxide Nanocrystals. *Adv. Funct. Mater.* **2005,** *16*, 1805-1813; (e) Wei, Q.; and Wei, A., Optical Imaging with Dynamic Contrast Agents. *Chem. Eur. J.* **2011,** *17*, 1080-1091; (f) Mehrmohammadi, M.; Oh, J.; Ma, L.; Yantsen, E.; Larson, T.; Mallidi, S.; Park, S.; Johnston, K. P.; Sokolov, K.; Milner, T. In *Imaging of iron oxide nanoparticles using magneto-motive ultrasound*, 2007 IEEE International Ultrasonics Symposium, 2007; pp 652–655.

4. Mehrmohammadi, M.; Yoon, K. Y.; Qu, M.; Johnston, K.; Emelianov, S. Y., Enhanced pulsed magneto-motive ultrasound imaging using superparamagnetic nanoclusters. *Nanotechnology* **2011,** *22*, 045502.

5. (a) Mehrmohammadi, M.; Oh, J.; Mallidi, S.; Emelianov, S. Y., Pulsed magneto-motive ultrasound imaging using ultrasmall magnetic nanoprobes. *Mol Imaging* **2011,** *10* (2), 102-10; (b) Mehrmohammadi, M.; Oh, J.; Aglyamov, S. R.; Karpiouk, A. B.;

Emelianov, S. Y., Pulsed magneto-acoustic imaging. *Conf Proc IEEE Eng Med Biol Soc* **2009,** *2009*, 4771-4.

6. (a) Yoon, K. Y.; Kotsmar, C.; Ingram, D. R.; Huh, C.; Bryant, S. L.; Milner, T. E.; Johnston, K. P., Stabilization of Superparamagnetic Iron Oxide Nanoclusters in Concentrated Brine with Cross-Linked Polymer Shells. *Langmuir* **2011,** *27*, 10962-10969; (b) Kotsmar, C.; Yoon, K. Y.; Ingram, D. R.; Ryoo, S. Y.; Barth, J.; Shao, S.; Prodanovic´, M.; Milner, T.; Bryant, S. L.; Huh, C.; Johnston, k. P., Stable Citrate-Coated Iron Oxide Superparamagnetic Nanoclusters at High Salinity. *Ind. Eng. Chem. Res.* **2010,** *49*, 12435–12443.

7. (a) Ditsch, A.; Laibinis, P. E.; Wang, D. I. C.; Hatton, T. A., Controlled Clustering and Enhanced Stability of Polymer-Coated Magnetic Nanoparticles. *Langmuir* **2005,** *21* (13), 6006-6018; (b) Lyon, J. L.; Fleming, D. A.; Stone, M. B.; Schiffer, P.; Williams, M. E., Synthesis of Fe oxide core/Au shell nanoparticles by iterative hydroxylamine seeding. *Nano Letters* **2004,** *4*, 719-723.; (c) Campelj, S.; Makovec, D.; Drofenik, M., Preparation and properties of water-based magnetic fluids. *J. Phys.: Condens. Matter* **2008,** *20*, 204101-204105.; (d) Hui, C.; Shen, C.; Yang, T.; Bao, L.; Tian, J.; Ding, H.; Li, C.; Gao, H.-J., Large-scale Fe3O4 nanoparticles soluble in water synthesized by a facile method. *J. Phys. Chem. C* **2008,** *112*, 11336–11339.

8. Ditsch, A. P.; Lindemann, S.; Laibnis, P. E.; Wang, D. I. C.; Hatton, T. A., High-gradient magnetic separation of magnetic nanoclusters. *Ind. Eng. Chem. Res.* **2005,** *44*, 6824-6836.

9. Berret, J.-F., Stoichiometry of Electrostatic Complexes Determined by Light Scattering. *Macromolecules* **2007,** *40*, 4260-4266.

10. Frankamp, B. L.; Uzun, O.; Ilhan, F.; Boal, A. K.; , a. R., V. M. , Recognition-Mediated Assembly of Nanoparticles into Micellar Structures with Diblock Copolymers. *J. Am. Chem. Soc.* **2002,** *124*, 892–893.

11. Ryoo, W.; Webber, S. E.; Johnston, K. P., Water-in-Carbon Dioxide Microemulsions with Methylated Branched Hydrocarbon Surfactants. *Ind. Eng. Chem. Res.* **2003,** *42*, 6348-6358.

12. Tam, J. M.; Murthy, A. K.; Ingram, D. R.; Nguyen, R.; Sokolov, K. V.; P., J. K., Kinetic assembly of near-IR active gold nanoclusters using weakly adsorbing polymers to control size. *Langmuir* **2010,** *26*, 8988-8999.

13. Mehrmohammadi, M.; Ma, L. L.; Qu, M.; Romanoviscz, D.; Johnston, K. P.; Sokolov, K. V.; and Emelianov, S. Y., Pulsed magneto-motive ultrasound imaging to detect intracellular accumulation of magnetic nanoparticles. *Nanotechnology* **2011,** *22*, 41510.

14. (a) Lubinski, M. A.; Emelianov, S. Y.; O'Donnell, M., Speckle tracking methods for ultrasonic elasticity imaging using short-time correlation. *IEEE Transactions on Ultrasonics, Ferroelectrics, and Frequency Control* **1999,** *46* (1), 82-96; (b) Park, S.; Aglyamov, S. R.; Emelianov, S. Y., Elasticity imaging using conventional and high-frame rate ultrasound imaging: Experimental study. *Ultrasonics, Ferroelectrics and Frequency Control, IEEE Transactions on* **2007,** *54* (11), 2246-2256.

15. Hiemenz, P. C.; Rajagopalan, R.; Editors, *Principles of Colloid and Surface Chemistry, Third Edition, Revised and Expanded*. Marcel Dekker Inc.: New York, 1997; p 688 pp.

16. Shevchenko, E.; Talapin, D.; Kornowski, A. L.; Rogach, A.; Kormowski, A.; Haase, M.; Weller, H., Colloidal Synthesis and Self-Assembly of CoPt3 Nanocrystals. *J. Am. Chem. Soc.* **2002,** (124), 11480.

17. Libert, S.; Gorshkov, V.; Goia, D.; Matijević, E.; and Privman, V., Model of Controlled Synthesis of Uniform Colloid Particles:Cadmium Sulfide. *Langmuir* **2003,** *19*, 10679-10683.

18. Sondjaja, R.; Hatton, A. T.; Tam, M. K. C., Clustering of magnetic nanoparticles using a double hydrophilic block copolymer, poly(ethylene oxide)-b-poly(acrylic acid). *J. Magn. Magn. Mat.* **2009,** *321*, 2393-2397.

19. (a) Wu, W.; He, Q.; Jiang, C., Magnetic iron oxide nanoparticles: synthesis and surface functionalization strategies. *Nanoscale Research Letters* **2008,** *3*, 397-415; (b) Lu, A.-H.; Salabas, E. L.; Schueth, F., Magnetic nanoparticles: synthesis, protection, functionalization and application. *Angew. Chem. Int. Ed.* **2007,** *46*, 1222-1244; (c) Huber, D. L., Synthesis, properties, and applications of iron nanoparticles. *Small* **2005,** *1* (5), 482-501.

20. Gerber, R.; Birss, R. R., *High Gradient Magnetic Separation*. Research Studies Press: London, 1983.

21. Moeser, G. D.; Roach, K. A.; Green, W. H.; Laibinis, P. E.; Hatton, T. A., High-gradient magnetic separation of coated magnetic nanoparticles. *AIChE Journal* **2004,** *50*, 2835-2848.

22. Yavuz, C. T.; Mayo, J. T.; Yu, W. W.; Prakash, A.; Falkner, J. C.; Yean, S.; Cong, L.; Shipley, H. J.; Kan, A.; Tomson, M.; Natelson, D.; Colvin, V. L., Low-field magnetic separation of monodisperse Fe_3O_4 nanocrystals. *Science* **2006,** *314*, 964-967.

Chapter 7: Conclusions and Recommendations

7.1 CONCLUSIONS

The main objective of this thesis research was to develop reliable and efficient ways to apply surface coatings to nanoparticles, so that the particles can withstand harsh environments (such as oil reservoirs with high salinity, high-hardness brine) while carrying out their desired function at the target location. While extensive research has been carried out to develop optimal surface coatings for nanoparticles in biological and medical applications, these results are not readily transferable for oil-reservoir applications because (i) the reservoir fluids are generally at much harsher conditions as mentioned above; (ii) the length scale and time scale for the oil-reservoir applications are orders of magnitude larger than those for the biomedical applications; and (iii) the nanoparticles may be adsorbed on the rock surfaces and lost during the delivery to the target locations. For the above reasons, the development of the surface coating was approached with an entirely new set of constraints and sub-objectives. To this end, the effects of different molecular structures and molecular weighst of the coating polymers on (i) the robustness of polymer coating attachment to the nanoparticle surface; (ii) the nanoparticle dispersion stability in brines of varying composition; and (iii) the nanoparticle's interfacial activity at the oil/water interface, were systematically investigated. This thesis research, therefore, provided an efficient protocol to synthesize polymer stabilized superparamagnetic nanoclusters that can be delivered to oil-water

interfaces in petroleum reservoirs, so that they can serve as a diagnostic source for magneto-acoustic tomography. Also, the superparamagnetic properties and colloidal properties in the presence of high salt concentrations could be highly useful in developing various other applications. Similarly, iron oxide nanoclusters targeted to cellular interfaces related to a pathological condition, can serve as a diagnostic source for magneto-optic tomographic imaging modalities.

The conclusions from the thesis research are briefly summarized below; further details are provided in the following sub-sections.

1. Carboxylic acid groups in copolymers were reacted with diamines to create a thin, crosslinked polymer films around nanoclusters, to attempt to lower the tendency of polymer detachment under harsh oil-reservoir conditions.
2. Citrate with its two carboxylic ions was bound to be a good coating ligand, as those ions carryout not only function of attachment to the nanocluster but also the crosslinking job.
3. By adjusting the relative mole fractions of the hydrophilic (PAA) and hydrophobic (PBA) ligands of a coating polymer, the interfacial activity of the nanoparticles with iron oxide cores could be adjusted.
4. Dispersions of graphene oxide nanoplatelets were formed in water at pH 2 to 10. Also, oil-in-water emulsions stabilized with graphene oxide nanoplatelets remained partially stable for one year.

5. By controlling the primary nanoparticle diameter, cluster size during synthesis, pMMUS signal enhancement was shown with Iron oxide nanoclusters made out of larger primary nanoparticles with larger magnetization.

7.1.1 Stabilization of Superparamagnetic Iron Oxide Nanoclusters in Concentrated Brine with Crosslinked Polymer Shells

Coating of iron oxide particles with poly(acrylic acid) (PAA) or (PSS-*alt*-MA) during synthesis resulted in sub-100 nm nanoclusters, which were stable even in 8 wt% NaCl at pH 8. This robust stability may be attributed to the cross-linked PSS-alt-MA stabilizer on the nanoparticle surface that provides not only the electrostatic repulsion but also entropic steric repulsion. In addition, cross-linking of PAA at various cross-link densities led to a coating with a polymer surface concentration of 12% that did not desorb even for iron oxide concentrations down to 0.014 wt%. Without cross-linking, over half of the polymer desorbed from the particle surfaces at these dilute conditions. The superparamagnetic nanoclusters with cross-linked PAA were characterized using SQUID, TEM, DLS, TGA, and zeta potential measurements. The incorporation of the cross-linking agent, 1,6-hexanediamine, enhances the hydrophobicity and thus the interfacial activity of the clusters at the oil-water interface. In this general and highly flexible approach, iron oxide nanoparticles may be formed with an adsorbed polymer stabilizer, which is then permanently bound to the surface via cross-linking. This cross-linking approach offers important benefits for the formation of inexpensive coatings on

nanoparticles for large scale applications including magnetomotive imaging of subsurface reservoirs.

7.1.2 Stable Citrate Coated Iron Oxide Superparamagnetic Nanoclusters at High Salinity

The formation of ~100 nm nanoclusters with adsorbed citrate ions provides colloidal stabilization even for salinities up to 4 wt% (680 mM). With the large cluster size and relatively thin shell layer, the magnetic fraction is high, which is important for increasing the magnetization per unit particle volume. Therefore, the large volume of the superparamagnetic nanoclusters relative to the primary particles is a novel approach for increasing the magnetic force for subsurface and other applications.

The strongly negative surface charge of the nanoparticles measured by zeta potentials indicates strongly adsorbed citrate ions on the nanoparticle surface, which provides strong electrostatic stabilization in aqueous media encountered in subsurface reservoirs. The citrate-stabilized iron oxide nanoparticle dispersions were stable for at least 2 months with high salt concentrations of 680 mM at pH 6 and pH 8. Transport experiments with citrate-stabilized iron oxide nanoparticle dispersions showed that the particles exhibit low retention in negatively charged sandstone and limestone, due to their surface coating and small cluster size.

7.1.3 Effect of adsorbed amphiphilic copolymers on the interfacial activity of superparamagnetic nanoclusters and emulsification of oil in water

After we developed methods to synthesize stable dispersions of small, about 100 nm superparamagnetic iron oxide nanoclusters with high magnetization and controllable sizes, we tackled the task of additionally increasing the interfacial activity of the particles. The surfaces were designed so that the particles can be easily adsorbed to the oil/water interface. Therefore, a series of amphiphilic PAA-*b*-PBA or PAA-*co*-PBA copolymers were used to stabilize iron oxide nanoclusters, which were synthesized by a coprecipitation method. The copolymers that were employed to stabilize iron oxide nanoclusters induced large reductions in the interfacial tension (high surface pressures) at the dodecane-water interface. The thin copolymer shells on the iron oxide surface played an important role in reducing the interfacial tension at the oil-water interface. Large surface pressures were achieved at lower nanoparticle concentrations than for homopolymer-stabilized nanoparticles.1 Amphiphilic block copolymer shells on iron oxide nanoparticles with 26 PBA units promote high interfacial activity, resulting in high emulsification efficiency and unusually small oil droplet sizes (~12.1 μm in water at 24 hours) at low nanocluster concentrations (~0.27 wt% w/w). The ability to achieve strong adsorption of amphiphilic copolymer-stabilized nanoclusters at the oil/water interface with high surface pressures is expected to find utility in a wide range of practical applications including magnetic imaging in oil reservoirs and in enhanced oil recovery.

7.1.4 Graphene Oxide Nanoplatelet Dispersions in Concentrated NaCl and Stabilization of Oil/Water Emulsion

Dispersion of graphene oxide nanoplatelets was achieved in water over pH 2-10 and salinity up to 5 wt.% NaCl. Oil-in-water emulsions with graphene oxide nanoplatelets (GON) were formed at various concentrations as low as 0.001 wt%. The GON-stabilized emulsions remained partially stable for one year. The stability of GON-stabilized emulsion at high salinity (up to 5 wt.% NaCl) is believed to be due to the high anion density at the GON edges, which are most likely in the water phase and provide electrostatic stabilization, and to the steric separation of the oil droplets. Important potential advantages for subsurface GON applications are that GON offers extremely large surface area per mass, while providing aqueous dispersion stability and emulsification of water and oil.

7.1.5 Control of primary nanoparticles in water dispersible iron oxide nanoclusters and their applications in pulsed magneto-motive ultrasound (MMUS) imaging

Highly water-dispersible magnetite nanoclusters with citrate ion as a stabilizer were synthesized by the coprecipitation method. The synthesized iron oxide particles with low molecular weight ligand were found to be very stable in aqueous media. We developed ways to control the primary nanoparticle diameter, cluster size during this synthesis by simply varying the concentration of citrate ion. We were able to synthesize clusters of magnetic nanoparticles to achieve both larger magnetization of 53–79 emu/g Fe and improved colloidal stability. Iron oxide nanoclusters made of larger primary

nanoparticles with larger magnetization offer the potential of signal enhancement in magnetomotive ultrasound.

7.2 RECOMMENDATIONS

To develop a novel method for magnetic-nanoparticle-enhanced imaging of oil displacement in reservoirs, fundamental studies of the particle's magnetic properties to design the best magnetic contrast agents are essential. The future work should be focused on developing an integrated program to develop paramagnetic nanoparticles that have not only the robust dispersion stability, minimal retention on rock surface, and large interfacial activity (as we attempted here), but also the high magnetization and the mass production capability at low cost. For example, we need to achieve high magnetic susceptibilities and to understand the relationship between susceptibilities and particle structure. It is recommended that the study of magnetite nanoparticles from iron chlorides be expanded for various core sizes to manipulate the magnetic moment and susceptibility, both with and hopefully without polymer coatings As the nanoparticles for practical reservoir application will be clusters of primary particles, we need to examine a range of synthetic techniques in water (i) to quantify the cluster morphologies as a function of primary particle size; (ii) particle volume fraction in the cluster (iii) spacing between primary particles in the cluster; and (iv) fractal dimension from looser clusters to fully solid particles. We need to optimize the increase in susceptibility with particle size, until the size limit is reached where poor crystallinity or grain boundaries or anisotropy weaken susceptibilities, or with increased size, dispersion stability is lost through

magnetic interactions or particle rock interactions. To carry out the above study effectively, the particle morphology needs to be quantified by DLS, TEM, and XRD; and relate to the magnetic susceptibility, to understand how to maximize susceptibility. We also need to determine the extent to which the coatings modify the magnetic properties. In addition, some of the specific items that have not been adequately studied in this thesis are discussed below.

7.2.1 Effect of volume fraction of the particle dispersions and comparisons with solid powders

The effect of the particle volume fraction in the aqueous dispersions on the susceptibility needs to be quantified, and compared with the results for solid powders. The effective medium theory or some other modeling techniques needs to be employed to understand the relationship between the two. Furthermore, we need to figure out why susceptibilities of dispersions are sometimes higher than those of particles, and utilize this knowledge to achieve even higher susceptibilities. A much larger number of magnetic measurements are reported in the literature for powders relative to dispersions[2]. Thus it is critical to understand how to utilize the pure-powder data to deduce the susceptibility for the dispersions.

7.2.2 Frequency dependence of susceptibility

The desired frequency for electromagnetic water flood imaging application is below 100 Hz. For most of the particle sizes of interest, the imaginary component of

susceptibility will be negligible at frequencies below 100 Hz. Through collaboration with Rice university lab, we have already begun studying the dynamics of magnetization by comparing multiple frequencies, DC measurement with VSM, AC measurement with an AC SQUID and AC susceptibility meter (operating frequency of ~700 Hz).

7.2.3 Temperature dependence of susceptibility

Through collaboration with Rice university lab, we have already begun studying the temperature dependence of magnetization by comparing magnetic permeability at multiple temperatures. As expected there is a reduction in magnetic permeability as temperature is increased. The VSM instrument from Micro sense Inc. will be able to measure magnetic properties at elevated temperatures up to 800 °C.

7.3 REFERENCES

1. Saleh, N.; Sarbu, T.; Sirk, K.; Lowry, G. V.; Matyjaszewski, K.; Tilton, R. D., Oil-in-Water Emulsions Stabilized by Highly Charged Polyelectrolyte-Grafted Silica Nanoparticles. *Langmuir* **2005,** *21*, 9873-9878.

2. Yin, H. M.; and Sun, L. Z., Effective magnetic permeability of composites containing chain-structured particles. *Acta Materialia* **2006,** *54*, 2317–2323.

Appendix 1: Effect of adsorbed amphiphilic copolymers on the interfacial activity of superparamagnetic nanoclusters and emulsification of oil in water

Derivation of the interfacial surface area per nanoparticle in an emulsion, *A*

Surface area of one oil droplet, $A_d = 4\pi R^2$, where R is radius of oil droplet

Effective area taken up by one nanoparticle, $A_p = \frac{\pi a^2}{\eta}$, where a is radius of nanoparticle

and η is nanoparticle 2-dimensional packing fraction on an oil droplet

Number of nanoparticles adsorbed on one oil droplet, $N_p = \frac{A_d}{A_p} = \frac{4R^2\eta}{a^2}$

Total surface area of all oil droplets in emulsion phase, $A_E = A_d \cdot N_d$, where N_d is number of oil droplets in emulsion

Total number of nanoparticles in emulsion, $N_{pE} = N_p \cdot N_d$

Interfacial surface area per nanoparticle, $A = \frac{A_E}{N_{pE}} = \frac{A_d}{N_p} = \frac{\pi a^2}{\eta}$ (Eq. 2 in chapter 4)

Derivation of the nanoparticle 2-dimensional packing fraction on an oil droplet, *η*

Total mass of nanoparticles in emulsion, $M = M_{sp} \cdot N_p \cdot N_d$, where M_{sp} is mass of one nanoparticle and N_p is number of nanoparticles adsorbed on one oil droplet

$M_{sp} = \frac{4}{3}\pi a^3 \rho_p$, where ρ_p is density of nanoparticle

Effective volume of an oil droplet in emulsion phase, $V_d = \frac{\left(\frac{4}{3}\pi R^3\right)}{\phi_c}$, where ϕ_c is the packing fraction of oil droplets in emulsion phase (assumed to be 0.74 for ideal close packing of spheres)

$N_d = \frac{V_{EP}}{V_d} = \frac{3V_{EP}\phi_c}{4\pi R^3}$, where V_{EP} is volume of emulsion phase

Combining, $M = \frac{4V_{EP}\phi_c a\rho_p\eta}{R}$

Thus, $\eta = \frac{MR}{4V_{EP}\phi_c a\rho_p}$ (Eq. 3 in chapter 4)

Bibliography

Adkins, S. S., D. Gohil, et al. (2007). "Water-in-carbon dioxide emulsions stabilized with hydrophobic silica particles." Physical Chemistry Chemical Physics **9**(48): 6333-6343.

Alargova, R. G., D. S. Warhadpande, et al. (2004). "Foam Superstabilization by Polymer Microrods." Langmuir **20**: 10371.

Arbab, A. S., L. A. Bashaw, et al. (2003). "Characterization of biophysical and metabolic properties of cells labeled with superparamagnetic iron oxide nanoparticles and transfection agent for cellular MR imaging." Radiology **229**: 838-846.

Arkles, B. (1977). "Tailoring surfaces with silanes." Chem. Tech. **7**: 766-770.

Aveyard, R., J. H. Clint, et al. (2003). "Aspects of the stabilisation of emulsions by solid particles: Effects of line tension and monolayer curvature energy." Phys. Chem. Chem. Phys. **5**: 2398–2409.

Bacri, J., R. Perzynski, et al. (1990). J. Magn. Magn. Mater. **85**: 27.

Bee, A., R. Massart, et al. (1995). "Synthesis of very fine maghemite particles." Journal of Magnetism and Magnetic Materials **149**: 6-9.

Berkowitz, A. E., J. A. Lahut, et al. (1975). "Spin Pinning at Ferrite-Organic Interfaces." Phys.Rev.Lett. **34**(10): 594–597.

Berret, J.-F. (2007). "Stoichiometry of Electrostatic Complexes Determined by Light Scattering." Macromolecules **40**: 4260-4266.

Berret, J.-F., N. Schonbeck, et al. (2006). "Controlled clustering of superparamagnetic nanoparticles using block copolymers: design of new contrast agents for magnetic resonance imaging." J. Am. Chem. Soc. **128**: 1755-1761.

Biesheuvel, P. M. (2004). "Ionizable polyelectrolyte brushes: Brush height and electrosteric interaction." J. Colloid Interface Sci. **275**: 97–106.

Binks, B. P. (2002). "Particles as surfactants similarities and differences." Current Opinion in Colloid and Interface Science **7**: 21-41.

Binks, B. P. (2004). "Silica Particle-Stabilized Emulsions of Silicone Oil and Water: Aspects of Emulsification." Langmuir **20**: 1130-1137.

Binks, B. P. and M. Kirkland (2002). "Interfacial structure of solid-stabilised emulsions studied by scanning electron microscopy." Phys. Chem. Chem. Phys. **4**: 3727-3733.

Binks, B. P., M. Kirkland, et al. (2008). "Origin of stabilisation of aqueous foams in nanoparticle–surfactant mixtures." Soft Matter **4**: 2373–2382.

Binks, B. P. and S. O. Lumsdon (2000). "Transitional phase inversion of solid-stabilized emulsions using particle mixtures." Langmuir **16**: 3748-3756.

Binks, B. P. and J. A. Rodrigues (2007). "Enhanced stabilization of emulsions due to surfactant-induced nanoparticle flocculation." Langmuir **23**: 7436-7439.

Bucak, S., D. A. Jones, et al. (2003). "Protein separations using colloidal magnetic nanoparticles." Biotechnol. nProg. **19**: 477-484.

Campelj, S., D. Makovec, et al. (2008). "Preparation and properties of water-based magnetic fluids." J. Phys.: Condens. Matter **20**: 204101-204105.

Chanteau, B., J. Fresnais, et al. (2009). "Electrosteric enhanced stability of functional sub-10 nm cerium and iron oxide particles in cell culture medium." Langmuir **25**(16): 9064-9070.

Chapman, D. L. (1913). Philos. Mag. **25**: 475.

Chen, D.-H. and S.-H. Huang (2004). "Fast separation of bromelain by polyacrylic acid-bound iron oxide magnetic nanoparticles." Process Biochemistry **39**: 2207-2211.

Chen, X., S. S. Adkins, et al. (2010). "Interfacial tension and the behavior of microemulsions and macroemulsions of water and carbon dioxide with a branched hydrocarbon nonionic surfactant." J. of Supercritical Fluids **55**: 712–723.

Cote, L. J., F. Kim, et al. (2009). "Langmuir-Blodgett Assembly of Graphite Oxide Single Layers." J. AM. CHEM. SOC. **131**: 1043-1049.

Cote, L. J., J. kim, et al. (2011). "Graphene oxide as surfactant sheets." Pure Appl. Chem. **83**(1): 95-110.

De Palma, R., S. Peeters, et al. (2007). "Silane Ligand Exchange to Make Hydrophobic Nanoparticles Water-Dispersible." Chem. Mater. **19**: 1821-1831.

Derjaguin, B. V. (1940). Trans. Faraday Sot.,(36): 203.

Dickson, J. L., B. P. Binks, et al. (2004). "Stabilization of carbon dioxide-in-water emulsions with silica nanoparticles." Langmuir **20**(19): 7976-7983.

Ditsch, A., P. E. Laibinis, et al. (2005). "Controlled Clustering and Enhanced Stability of Polymer-Coated Magnetic Nanoparticles." Langmuir **21**(13): 6006-6018.

Ditsch, A. P., S. Lindemann, et al. (2005). "High-gradient magnetic separation of magnetic nanoclusters." Ind. Eng. Chem. Res. **44**: 6824-6836.

Dresco, P. A., V. S. Zaitsev, et al. (1999). "Preparation and Properties of Magnetite and Polymer Magnetite Nanoparticles." Langmuir **15**: 1945-1951.

Dreyer, D. R., S. Park, et al. (2010). "The Chemistry of Graphene Oxide." Chem. Soc. Rev. **39**: 228-240.

Du, K., E. Glogowski, et al. (2010). "Adsorption Energy of Nano- and Microparticles at Liquid-Liquid Interfaces." Langmuir **26**(15): 12518-12522.

Elimelech, M. (1994). "Particle deposition on ideal collectors from dilute flowing suspensions: Mathematical formulation, numerical solution, and simulations." Sep. Technol. **4**: 186–212.

Espinosa, D. A., F. M. Caldelas, et al. (2010). "Nanoparticle-Stabilized Supercritical CO2 Foams for Potential Mobility Control Applications." Proceeding of SPE129925, presented at SPE/DOE Symp. Improved Oil Recovery, Tulsa, OK., Apr. 26-28, 2010.

Esser-Kahn, A. P., S. A. Odom, et al. (2011). "Triggered Release from Polymer Capsules." Macromolecules **44**: 5539–5553.

Euliss, L. E., S. G. Grancharov, et al. (2003). "Cooperative assembly of magnetic nanoparticles and block copolypeptides in aqueous media." nano Letters **3**: 1489-1493.

Frankamp, B. L., O. Uzun, et al. (2002). "Recognition-Mediated Assembly of Nanoparticles into Micellar Structures with Diblock Copolymers." J. Am. Chem. Soc. **124**: 892–893.

Fritz, G., V. Schadler, et al. (2002). "Electrosteric Stabilization of Colloidal Dispersions." Langmuir **18**: 6381-6390.

Ge, J., Y. Hu, et al. (2007). "Superparamagnetic magnetite colloidal nanocrystal clusters." Angew. Chem. Int. Ed. **46**: 4342-4345.

Ge, J., Y. Hu, et al. (2007). "One-step synthesis of highly water-soluble magnetite colloidal nanocrystals." Chemistry-A European Journal **13**(25): 7153-7161.

Gerber, R. and R. R. Birss (1983). High Gradient Magnetic Separation. London, Research Studies Press.

Golas, P. L., G. V. Lowry, et al. (2010). "Comparative Study of Polymeric Stabilizers for Magnetite Nanoparticles Using ATRP." Langmuir **26**: 16890–16900.

Golemanov, K., S. Tcholakova, et al. (2006). "Latex-Particle-Stabilized Emulsions of Anti-Bancroft Type." Langmuir **22**: 4968-4977.

Golomb, D., S. Pennell, et al. (2007). "Ocean sequestration of carbon dioxide: modeling of the deep ocean release of a dense emulsion of liquid CO2-in-water stabilized by pulverised limestone particles." Environ. Sci. Technol. **41**: 4698-4704.

Gouy, G. (1910). J. Physique **9**: 457.

Gu, B., T. L. Mehlhorn, et al. (1996). "Competitive adsorption, displacement, and transport of organic matter on iron oxide: I. Competitive adsorption." Geochimica et Cosmochimica Acta **60**(11): 1943-1950.

Gudarzi, M. M. and F. Sharif (2011). "Self assembly of graphene oxide at the liquid–liquid interface: A new route to the fabrication of graphene based composites." Soft Matter **7**: 3432-3440.

Guo, P., H. Song, et al. (2010). "Hollow graphene oxide spheres self-assembled by W/O emulsion." J. Mater. Chem. **20**: 4867-4874.

Gupta, A. K. and M. Gupta (2005). "Synthesis and surface engineering of iron oxide nanoparticles for biomedical applications." Biomaterials **26**: 3995–4021.

Herrera, A. P., C. Barrera, et al. (2008). "Synthesis and functionalization of magnetite nanoparticles with aminopropylsilane and carboxymethyldextran." J. Mater. Chem. **18**: 3650-3654.

Hiemenz, P. C., R. Rajagopalan, et al. (1997). Principles of Colloid and Surface Chemistry, Third Edition, Revised and Expanded. New York, Marcel Dekker Inc.

Hong, R. Y., T. T. Pan, et al. (2007). "Graft polymerization synthesis and application of magnetic Fe3O4/polyacrylic acid composite nanoparticles." J. Appl. Polym. Sci. **106**: 1439-1447.

Horozov, T. S. (2008). "Foams and foam films stabilised by solid particles." Current Opinion in Colloid & Interface Science **13**: 134-140.

Horozov, T. S. and B. P. Binks (2006). "Particle-Stabilized Emulsions: A Bilayer or a Bridging Monolayer?" Angew. Chem. Int. Ed. **45**: 773-776.

Huang, H., T. Kowalewski, et al. (1997). "Hydrogel-coated glassy nanospheres: a novel method for the synthesis of shell cross-linked knedels." J. Am. Chem. Soc. **119**: 11635-11659.

Huber, D. L. (2005). "Synthesis, properties, and applications of iron nanoparticles." Small **1**(5): 482-501.

Hui, C., C. Shen, et al. (2008). "Large-scale Fe3O4 nanoparticles soluble in water synthesized by a facile method." J. Phys. Chem. C **112**: 11336–11339.

Hummers Jr, W. S. and R. E. Offeman (1958). J. Am. Chem. Soc. **80**: 1339.

Hunter, T. N., R. J. Pugh, et al. (2008). "The role of particles in stabilising foams and emulsions." Advances in Colloid and Interface Science **137**: 57-81.

Imperiali, L., K. Liao, et al. (2012). "Interfacial Rheology and Structure of Tiled Graphene Oxide Sheets." Langmuir **28**: 7990-8000.

Ingram, D. R., C. Kotsmar, et al. (2010). "Superparamagnetic nanoclusters coated with oleic acid bilayers for stabilization of emulsions of water and oil at low loncentration." J. Colloid Interface Sci. **351**: 225-232.

Ishimuro, Y. and K. Ueberreiter (1980). "The surface tension of poly(acrylic acid) in aqueous solution." Coll. Polym. Sci. **258**: 928-931.

Isojima, T., M. Lattuada, et al. (2008). "Reversible Clustering of pH- and Temperature-Responsive Janus Magnetic Nanoparticles." ACS Nano **2**(9): 1799-1806.

Jacquin, M., P. Muller, et al. (2007). "Chemical analysis and aqueous solution properties of charged amphiphilic block copolymers PBA-b-PAA synthesized by MADIX®." Journal of Colloid and Interface Science **316**: 897–911.

Ju, B., T. Fan, et al. (2006). "Enhanced oil recovery by flooding with hydrophilic nanoparticles." China Particuology **4**: 41-46.

Kang, Y. S., S. Risbud, et al. (1996). "Synthesis and characterization of nanometer-size Fe3O4 and gamma-Fe2O3 particles." Chem. Mater. **8**: 2209-2211.

Kawano, T., Y. Niidome, et al. (2009). "PNIPAM Gel-Coated Gold Nanorods for Targeted Delivery Responding to a Near-Infrared Laser." Bioconjugate Chem. **20**: 209–212.

Kim, B.-S., J.-M. Qiu, et al. (2005). "Magnetomicelles: composite nanostructures from magnetic nanoparticles and cross-linked amphiphilic block copolymers." Nano Letters **5**: 1987-1991.

Kim, B.-S. and A. Taton (2007). "Multicomponent Nanoparticles via Self-Assembly with Cross-Linked Block Copolymer Surfactants." Langmuir **23**: 2198-2202.

kim, F., L. J. Cote, et al. (2010). "Graphene Oxide: Surface Activity and Two-Dimensional Assembly." adv. Mater. **22**: 1954-1958.

Kim, H. J., T. Phenrat, et al. (2008). Environ. Sci. Technol. **43**: 3824-3830.

Kim, J., L. J. Cote, et al. (2010). "Graphene Oxide Sheets at Interfaces." J. Am. Chem. Soc. **132**: 8180-8186

Kotsmar, C., K. Y. Yoon, et al. (2010). "Stable Citrate-Coated Iron Oxide Superparamagnetic Nanoclusters at High Salinity." Ind. Eng. Chem. Res. **49**: 12435–12443.

Kretzschmar, R. and H. Sticher (1997). "Transport of humic-coated iron oxide colloids in a sandy soil: Influence of Ca2+and trace metals." Environ. Sci. Technol. **31**: 3497–3504.

Kuranov, R., A. McElroy, et al. "Gas-cell referenced swept source phase sensitive optical coherence tomography." submitted to Optical Technology Letters.

Lan, Q., C. Liu, et al. (2007). "Synthesis of bilayer oleic acid-coated Fe3O4 nanoparticles and their application in pH-responsive Pickering emulsions." J. Colloid Interface Sci. **310**: 260-269.

Lattuada, M. and T. A. Hatton (2007). "Preparation and Controlled Self-Assembly of Janus Magnetic Nanoparticles." Journal of the American Chemical Society **129**(42): 12878-12889.

Lee, H., M. K. Yu, et al. (2007). "Thermally cross-linked superparamagnetic iron oxide nanoparticles: synthesis and application as a dual imaging probe for cancer in vivo." J.Am. Chem. Soc. 129: 12739-12745.

Lee, J. H., Y. M. Huh, et al. (2007). "Artificially engineered magnetic nanoparticles for ultra-sensitive molecular imaging." Nature Medicine **13**: 95-99.

Li, D. and R. B. and Kaner (2008). "Graphene-based Materials." Science **320**: 1170-1171

Li, D., M. B. Mu¨ller, et al. (2008). "Processable aqueous dispersions of graphene nanosheets." Nature Nanotech. **3**: 101-105.

Liang, X., X. Wang, et al. (2005). "Synthesis of Nearly Monodisperse Iron Oxide and Oxyhydroxide Nanocrystals." Adv. Funct. Mater. **16**: 1805-1813.

Liao, M.-H. and D.-H. Chen (2002). "Preparation and characterization of a novel magnetic nano-adsorbent." J. Mater. Chem. **12**: 3654-3659.

Libert, S., V. Gorshkov, et al. (2003). "Model of Controlled Synthesis of Uniform Colloid Particles:Cadmium Sulfide." Langmuir **19**: 10679-10683.

Lin, C.-L., C.-F. Lee, et al. (2005). "Preparation and properties of poly(acrylic acid) oligomer stabilized superparamagnetic ferrofluid." J. Colloid Interf. Sci. **291**: 411-420.

Lin, Y., H. Skaff, et al. (2003). "Nanoparticle Assembly and Transport at Liquid-Liquid Interfaces." Science **299**: 226-229.

Liu, D., P. R. Johnson, et al. (1995). "Colloid deposition dynamics in flow-through porous media: Role of electrolyte concentration." Environ. Sci. Technol. **29**: 2963–2973.

Liu, J., Z. Sun, et al. (2009). "HighlyWater-Dispersible Biocompatible Magnetite Particles with Low Cytotoxicity Stabilized by Citrate Groups." Angew. Chem. Int. Ed. **48**: 1-6.

Lu, A.-H., E. L. Salabas, et al. (2007). "Magnetic nanoparticles: synthesis, protection, functionalization and application." Angew. Chem. Int. Ed. **46**: 1222-1244.

Lubinski, M. A., S. Y. Emelianov, et al. (1999). "Speckle tracking methods for ultrasonic elasticity imaging using short-time correlation." IEEE Transactions on Ultrasonics, Ferroelectrics, and Frequency Control **46**(1): 82-96.

Lyon, J. L., D. A. Fleming, et al. (2004). "Synthesis of Fe oxide core/Au shell nanoparticles by iterative hydroxylamine seeding." Nano Letters **4**: 719-723.

Ma, H., M. Luo, et al. (2008). "Influences of surfactant and nanoparticle assembly on effective interfacial tensions." Physical Chemistry Chemical Physics **10**: 2207-2213.

Ma, L. L., M. D. Feldman, et al. (2009). "Small multifunctional nanoclusters (Nanoroses) for targeted cellular imaging and therapy." ACS Nano **3**: 2686-2696.

Mak, S.-Y. and D.-H. Chen (2005). "Binding and sulfonation of poly(acrylic acid) on iron oxide nanoparticles: a novel, magnetic, strong acid cation nano-adsorbent." Macromol. Rapid. Commun. **26**: 1567-1571.

Massart, R. (1981). "Preparation of aqueous magnetic liquids in alkaline and acidic media." IEEE Trans. Magn. **17**: 1247-1248.

Massart, R., E. Dubois, et al. (1995). "Preparation and Properties of Monodisperse Magnetic Fluids." Journal of Magnetizm and Magnetic Materials **149**: 1-5.

Masschaele, K., B. J. Park, et al. (2010). "Finite Ion-Size Effects Dominate the Interaction between Charged Colloidal Particles at an Oil-Water Interface." Physical Review Letters **105**: 048303.

Matteucci, M. E., J. C. Paguio, et al. (2008). "Flocculated amorphous nanoparticles for highly supersaturated solutions." Pharmaceutical Research **25**(11): 2477-2487.

Mehrmohammadi, M., L. L. Ma, et al. (2011). "Pulsed magneto-motive ultrasound imaging to detect intracellular accumulation of magnetic nanoparticles." Nanotechnology **22**: 41510.

Mehrmohammadi, M., J. Oh, et al. (2009). "Pulsed magneto-acoustic imaging." Conf Proc IEEE Eng Med Biol Soc **2009**: 4771-4774.

Mehrmohammadi, M., J. Oh, et al. (2007). Imaging of iron oxide nanoparticles using magneto-motive ultrasound. 2007 IEEE International Ultrasonics Symposium.

Mehrmohammadi, M., J. Oh, et al. (2011). "Pulsed magneto-motive ultrasound imaging using ultrasmall magnetic nanoprobes." Mol Imaging **10**(2): 102-110.

Mehrmohammadi, M., K. Y. Yoon, et al. (2011). "Enhanced pulsed magneto-motive ultrasound imaging using superparamagnetic nanoclusters." Nanotechnology **22**: 045502.

Melle, S., M. Lask, et al. (2005). "Pickering emulsions with controllable stability." Langmuir **21**: 2158-2162.

Moeser, G. D., K. A. Roach, et al. (2002). "Water-based magnetic fluids as extractants for synthetic organic compounds." Ind. Eng. Chem. Res. **41**: 4739-4749.

Moeser, G. D., K. A. Roach, et al. (2004). "High-gradient magnetic separation of coated magnetic nanoparticles." AIChE Journal **50**: 2835-2848.

Na, H. B., I. C. Song, et al. (2009). "Inorganic Nanoparticles for MRI Contrast Agents." Adv. Mater. **21**: 2133.

Nyer, E. K. and D. B. Vance (2001). "Nano-scale iron for dehalogenation." Ground Water Monit. Rem. **21**: 41–46.

Oh, J., M. D. Feldman, et al. (2006). "Detection of magnetic nanoparticles in tissue using magneto-motive ultrasound." Nanotechnology **17**(16): 4183-4190.

Ohshima, H. (1995). "Electrophoretic mobility of soft particles." Colloids Surfaces A: Physicochem. Eng. Aspects **103**: 249-255.

Ohshima, H. and K. and Makino (1996). "Electrophoretic mobility of a particle covered with a partially Electrophoretic mobility of a particle covered with a partially." Colloids Surfaces A: Physicochem. Eng. Aspects **109**: 71-75.

Park, S., S. R. Aglyamov, et al. (2007). "Elasticity imaging using conventional and high-frame rate ultrasound imaging: Experimental study." Ultrasonics, Ferroelectrics and Frequency Control, IEEE Transactions on **54**(11): 2246-2256.

Park, S., J. An, et al. (2008). "Aqueous Suspension and Characterization of Chemically Modified Graphene Sheets." Chem. Mater. **20**(21): 6592-6594.

Peppas, N. A., P. Bures, et al. (2000). "Hydrogels in pharmaceutical formulations." European Journal of Pharmaceutics and Biopharmaceutics **50**: 27-46.

Pham, T. T. H., C. Cao, et al. (2008). "Application of citrate-stabilized gold-coated ferric oxide composite nanoparticles for biological separations." J. Magn. Magn. Mat. **320**: 2049–2055.

Phenrat, T., N. Saleh, et al. (2008). "Stabilization of aqueous nanoscale zerovalent iron dispersions by anionic polyelectrolytes: adsorbed anionic polyelectrolyte layer properties and their effect on aggregation and sedimentation." J. Nanopart. Res. **10**: 795-814.

Philipse, A. P., M. P. B. van Bruggen, et al. (1994). "Magnetic silica dispersions: preparation and stability of surface-modified silica particles with a magnetic core." Langmuir **10**: 92-99.

Pincus, P. (1991). "Colloid stabilization with grafted polyelectrolytes." Macromolecules **24**: 2912–2919.

Prakash, A., H. Zhu, et al. (2009). "Bylayers as Phase Transfer Agents for Nanocrystals Prepared in Nonpolar Solvents." ACS Nano **3**: 2139-2146.

Prodanovic, M., S. Ryoo, et al. (2010). "Effects of magnetic field on the motion of multiphase fluids containing paramagnetic particles in porous media." 17th SPE Improved Oil Recovery Symposium Tulsa, OK **SPE 129850**.

Reith, D., B. Muller, et al. (2002). "How does the chain extension of poly „acrylic acid… scale in aqueous solution? A combined study with light scattering and computer simulation." Journal of Chemical Physics **116**: 9100-9106.

Rodriguez, E., M. R. Roberts, et al. (2009). "Enhanced migration of surface-treated nanoparticles in sedimentary rocks." SPE Annual Technical Conference and Exhibition, New Orleans, LA, USA **SPE 124418**.

Rosen, M. J. "Surfactants and Interfacial Phenomena; Wiley-Interscience: New York, 2002.".

Ryoo, S., A. R. Rahmani, et al. (2010). "Theoretical and experimental investigation of the motion of multiphase fluids containing paramagnetic nanoparticles in porous media." SPE Annual Meeting, Florence, Italy **SPE 134879**.

Ryoo, W., S. E. Webber, et al. (2003). "Water-in-Carbon Dioxide Microemulsions with Methylated Branched Hydrocarbon Surfactants." Ind. Eng. Chem. Res. **42**: 6348-6358.

Safarik, I. and M. Safarikova (2002). "Magnetic nanoparticles and biosciences." Monatsh. Chem. **133**: 737–759.

Sahoo, Y., A. Goodarzi, et al. (2005). "Aqueous ferrofluid of magnetite nanoparticles: fluorescence labeling and magnetophoretic control." J. Phys. Chem. B **109**: 3879–3885.

Saigal, T., H. C. Dong, et al. (2010). "Pickering Emulsions Stabilized by Nanoparticles with Thermally Responsive Grafted Polymer Brushes." Langmuir **26**(19): 15200-15209.

Saleh, N., H.-J. Kim, et al. (2008). "Ionic strength and composition affect the mobility of surface-modified Fe^0 nanoparticles in water-saturated sand columns." Environ. Sci. Technol. **42**: 3349-3355.

Saleh, N., T. Phenrat, et al. (2005). "Adsorbed Triblock Copolymers Deliver Reactive Iron Nanoparticles to the Oil/Water Interface." Nano Letters **5**(12): 2489-2494.

Saleh, N., T. Sarbu, et al. (2005). "Oil-in-Water Emulsions Stabilized by Highly Charged Polyelectrolyte-Grafted Silica Nanoparticles." Langmuir **21**: 9873-9878.

Santra, S., C. Kaittanis, et al. (2009). "Drug/dye-loaded, multifunctional iron oxide nanoparticles for combined targeted cancer therapy and dual optical/magnetic resonance imaging." Small **5**(16): 1862-1868.

Satarkar, N. S., D. Biswal, et al. (2010). "Hydrogel nanocomposites: a review of applications as remote controlled biomaterials." Soft Matter **6**: 2364–2371.

Schwartz, H., Y. Harel, et al. (2001). "Surface Behavior and Buckling of Silver Interfacial Colloid Films." Langmuir **17**: 3884-3892.

Sehgal, A., Y. Lalatonne, et al. (2005). "Precipitation-redispersion of cerium oxide nanoparticles with poly(acrylic acid): towards stable dispersions." Langmuir **21**: 9359-9364.

Shen, L., A. Stachowiak, et al. (2000). "Polymerization of olefin-terminated surfactant bilayers on magnetic fluid nanoparticles." Langmuir **16**: 9907-9911.

Shevchenko, E., D. Talapin, et al. (2002). "Colloidal Synthesis and Self-Assembly of CoPt3 Nanocrystals." J. Am. Chem. Soc.(124): 11480.

Sondjaja, R., A. T. Hatton, et al. (2009). "Clustering of magnetic nanoparticles using a double hydrophilic block copolymer, poly(ethylene oxide)-b-poly(acrylic acid)." J. Magn. Magn. Mat. **321**: 2393-2397.

Stankovich, S., R. D. Piner, et al. (2006). "Stable aqueous dispersions of graphitic nanoplatelets via the reduction of exfoliated graphite oxide in the presence of poly(sodium 4-styrenesulfonate)." J. Mater. Chem. **16**: 155-158.

Stankovich, S., R. D. Piner, et al. (2006). "Synthesis and exfoliation of isocyanate-treated graphene oxide nanoplatelets." carbon **44**: 3342-3347.

Stern (1924). Z. Electrochem. **30**: 508.

Stocco, A., W. Drenckhan, et al. (2009). "Particle-stabilised foams: an interfacial study." Soft Matter **5**: 2215–2222.

Sun, B., M.-J. Sun, et al. (2010). "Conjugated Polymer Fluorescence Probe for Intracellular Imaging of Magnetic Nanoparticles." Macromolecules **43**: 10348–10354.

Tam, J. M., A. K. Murthy, et al. (2010). "Kinetic assembly of near-IR active gold nanoclusters using weakly adsorbing polymers to control size." Langmuir **26**: 8988-8999.

Tcholakova, S., N. D. Denkov, et al. (2008). "Comparison of solid particles, globular proteins and surfactants as emulsifiers." Phys. Chem. Chem. Phys. **10**: 1608–1627.

Turner, J. L., D. Pan, et al. (2005). "Synthesis of gadolinium-labeled shell-crosslinked nanoparticles for magnetic resonance imaging application" Adv. Funct. Mater. **15**: 1248-1254.

Vervey, E. J. W. and J. T. G. and Overbeek "Theory ofthe Stability of Lyophobic Colloids.Elsevier, Amsterdam, New York, 1948."

Vignati, E. and R. and Piazza (2003). "Pickering Emulsions: Interfacial Tension, Colloidal Layer Morphology, and Trapped-Particle Motion." Langmuir **19**: 6650-6656.

Wan, S., Y. Zheng, et al. (2005). "Fe3O4 Nanoparticles coated with homopolymers of glycerol mono(meth)acrylate and their block copolymers." J. Mater. Chem. **15**: 3424-3430.

Wang, W., Z. Zhou, et al. (2003). "Effect of charged colloidal particles on adsorption of surfactants at oil–water interface." Journal of Colloid and Interface Science **274**: 625–630.

Wang, Y.-X. J., S. M. Hussain, et al. (2001). "Superparamagnetic iron oxide contrast agents: physicochemical characteristics and applications in MR imaging." Eur. Radiol. **11**: 2319-2331.

Wege, H. A., S. Kim, et al. (2008). "Long-Term Stabilization of Foams and Emulsions with In-Situ Formed Microparticles from Hydrophobic Cellulose." Langmuir **24**: 9245-9253.

Wei, Q. and A. and Wei (2011). "Optical Imaging with Dynamic Contrast Agents." Chem. Eur. J. **17**: 1080-1091.

Worthen, A. J., H. G. Bagaria, et al. (2012). "Nanoparticle-Stabilized Carbon Dioxide-in-Water Foams with Fine Texture." Journal of Colloid and Interface Science **391**: 142-151.

Wu, W., Q. He, et al. (2008). "Magnetic iron oxide nanoparticles: synthesis and surface functionalization strategies." Nanoscale Research Letters **3**: 397-415.

Wunderbaldinger, P., L. Josephson, et al. (2002). "Crosslinked iron oxide (CLIO): a new platform for the development of targeted MR contrast agents." Acad. Radiol. **Suppl 2**(S): 304-306.

Yavuz, C. T., J. T. Mayo, et al. (2006). "Low-field magnetic separation of monodisperse Fe3O4 nanocrystals." Science **314**: 964-967.

Yoon, K. Y., C. Kotsmar, et al. (2011). "Stabilization of Superparamagnetic Iron Oxide Nanoclusters in Concentrated Brine with Cross-Linked Polymer Shells." Langmuir **27**: 10962-10969.

Yoon, K. Y., Z. Li, et al. (2012). "Effect of Adsorbed Amphiphilic Copolymers on the Interfacial Activity of Superparamagnetic Nanoclusters and the Emulsification of Oil in Water." Macromolecules **45**: 5157-5166.

Yu, H., C. Kotsmar, et al. (2010). "Transport and retention of aqueous dispersions of paramagnetic nanoparticles in reservoir rocks." 17th SPE Improved Oil Recovery Symposium Tulsa, OK **SPE 129887**.

Yu, W., W., E. Chang, et al. (2007). "Forming Biocompatible and Nonaggregated Nanocrystals in Water Using Amphiphilic Polymers." Journal of American Chemical Society **129**: 2871-2879.

Zhang, T., D. Davidson, et al. (2010). "Nanoparticle-Stabilized Emulsions for Applications in Enhanced Oil Recovery." Proceeding of SPE 129885, presented at SPE/DOE Symp. Improved Oil Recovery, Tulsa, OK., Apr. 26-28, 2010.

Zhang, T., J. Ge, et al. (2007). "A general approach for transferring hydrophobic nanocrystals into water." Nano Letters **7**(10): 3203-3207.

Zheng, W., F. Gao, et al. (2005). "Magnetic polymer nanospheres with high and uniform magnetite content." J. Magn. Magn. Mater. **288**: 403-410.

Zhou, J., X. Qiao, et al. (2011). "Magnetic Pickering Emulsions Stabilized by Fe3O4 Nanoparticles." Langmuir **27**: 3308–3316.

.